Physics of Dense Matter
Fall 2005

Omar Benhar
INFN and Department of Physics.
Università "La Sapienza". I-00185 Roma, Italy

December 16, 2005

Contents

Introduction

The typical density of terrestrial macroscopic objects, i.e. the ratio of their mass to volume, does not exceed $\rho \sim 20$ g/cm^3. As a consequence, their structure is mainly dictated by electromagnetic interactions.

At much higher density, in the region $\rho \geq 10^4$ g/cm^3, the picture changes dramatically: the role of electromagnetic interactions becomes negligible and the structure of matter is mainly determined by quantum effects and nuclear interactions.

In the 1920s a star called Sirius B, a binary companion to the star Sirius, was found to be a highly compact object, of mass $\sim 0.75 - 0.95\ M_\odot$ ($M_\odot = 1.989 \times 10^{33}$ g denotes the mass of the sun) and size comparable to that of a planet[1]. Its density was estimated to reach millions of g/cm^3. Sirius B is now known to belong to a class of stellar objects called white dwarfs.

The effort to understand the structure of the white dwarfs triggered the first studies of physics of dense matter. More recently, these investigations have been considerably extended, to describe the physical properties of different types of dense matter of astrophysical and cosmological relevance.

Of particular relevance is the understanding of the structure of matter in the interior of neutron stars, whose existence was predicted right after the discovery of the neutron. Due to the large densities involved, up to $\sim 10^{15}$ g/cm^3, the theoretical description of neutron star matter must take into account the full complexity of the dynamcs of strong interactions, including the forces acting at nuclear and hadronic level, as well as the possible occurrence of a core of deconfined quark matter.

In this notes, we will discuss the properties of matter at densities $10^4 \lesssim \rho \lesssim 10^{15}$ g/cm^3, typical of white dwarfs and neutron stars. We will mostly focus on the region of $\rho > \rho_0$, where $\rho_0 = 2.67 \times 10^{14}$ g/cm^3 is the the central density of atomic nuclei, i.e. the largest density observed on earth under ordinary conditions.

[1]In his book *The Internal Constitution of the Stars*, published in 1926, Sir Arthur Eddington wrote: "we have a star of mass about equal to the sun and radius much less than Uranus".

Chapter 1

Equilibrium of white dwarfs

1.1 Stellar structure and evolution

The formation of a star is believed to be set off by the contraction of a self-gravitating hydrogen cloud. As the density increases, the temperature also increases, and eventually becomes high enough to ignite the chain of nuclear fusion reactions turning hydrogen into helium:

$$\begin{aligned}
p + p &\rightarrow {}^2\mathrm{H} + e^+ + \nu + 0.4 \text{ MeV} \ , \\
e^+ + e^- &\rightarrow \gamma + 1.0 \text{ MeV} \ , \\
{}^2\mathrm{H} + p &\rightarrow {}^3\mathrm{He} + \gamma + 5.5 \text{ MeV} \ , \\
{}^3\mathrm{He} +^3 \mathrm{He} &\rightarrow {}^4\mathrm{He} + 2p + 26.7 \text{ MeV} \ .
\end{aligned}$$

Note that the above reactions are all exothermic, and energy is released in form of kinetic energy of the produced particles (1 MeV $= 1.6021917 \times 10^{-6}$ erg). Equilibrium is reached as soon as gravitational attraction is balanced by matter pressure.

When the nuclear fuel is exhausted[1] the core stops producing heat, the internal pressure cannot be sustained and the contraction produced by gravitational attraction resumes. If the mass of the helium core is large enough its contraction, associated with a further increase of the temperature, can then lead to the ignition of new fusion reactions, resulting in the appearance of heavier nuclei (carbon, oxygen . . .). Depending on its intial mass, the sequence of epochs of gravitational contraction and nucleosynthesis can take place several times during the lifetime of the star. The endpoint of this process is the formation of a core made of iron as, ^{56}Fe being the most stable nuclear species, further exothermic fusion reactions are no longer possible.

[1]For example, in our sun, which has been already burnig for 5×10^9 years, hydrogen will been exhausted in 5×10^9 more years.

The outcome of the star evolution process depends primarily on the initial mass M_0. A white dwarf is formed when $M_0 < 4\ M_\odot$, while for $M_0 > 4\ M_\odot$ the star evolves into either a neutron star or a black hole.

For $M_0 < 4\ M_\odot$ the star does not reach the temperature required to ignite the fusion reactions turning carbon and oxygen into heavier elements (the ignition temperatures of the reactions taking place in a massive star are listed in Table 1.1). Nucleosynthesis stops at this stage and the pressure needed to balace gravitational attraction can no longer be produced burning nuclear fuel.

Nuclear fuel	Main products	Temperature [°K]	Density [g/cm^3]	Duration [yrs]
H	He	6×10^7	5	7×10^6
He	C, O	2×10^8	700	5×10^5
C	O, Ne, Mg	9×10^8	2×10^5	600
Ne	O, Mg, Si	1.7×10^9	4×10^5	1
O	Si, S	2.3×10^9	10^7	0.5
Si	Fe	4×10^9	3×10^7	0.0025

Table 1.1: Stages of nucleosynthesis for a star of mass $\sim 25\ M_\odot$

Equilibrium of white dwarfs is due to the pressure generated by the electrons. Being spin 1/2 particles, electrons obey Pauli's exclusion principle. As a consequence, even at zero temperature they carry nonvanishing momentum and produce a pressure, called *degeneracy* pressure, balancing gravitational attraction. Stability of the white dwarfs is the *macroscopic* manifestation of a purely quantum mechanical effect.

Typical values of mass and radius of a white dwarf are $M \sim 1\ M_\odot$ and $R \sim 5 \times 10^3$ km (to be compared to the solar radius $R_\odot = 6.960 \times 10^5$ km), corresponding to an average density $\sim 10^6$ g/cm^3. In 1931, Chandrasekhar was able to demonstrate the existence of a limiting white dwarf mass $M_c = 1.44\ M_\odot$. As we will see in Section 1.4, beyond this value white dwarfs become unstable against gravitational collapse.

Let us now consider the case of more massive stars, having $M_0 > 4\ M_\odot$, where nuclear fusion reactions continue and heavier elements are produced. With the appearance of the iron core neutrinos begin to appear through the process

$$^{56}\text{Ni} \rightarrow ^{56}\text{Fe} + 2e^+ + 2\nu_e \ . \tag{1.1}$$

The produced neutrinos do not interact appreciably with the surrounding matter, and leave the core of the star carrying away energy. Hence, during this stage both gravity and neutrino emission contribute to the collapse of the system, which becomes very fast due to the action of different mechanisms. The most efficient are:

- *neutronization*, i.e. electron capture by protons through the weak interaction process

  $$e^- + p \rightarrow n + \nu_e \ , \tag{1.2}$$

  whose main effect is the disappearance of electrons, leading in turn to a decrease of the pressure;

- *iron photodisintegration*

  $$\gamma +^{56}\text{Fe} \rightarrow 13\ ^4\text{He} + 4n \ , \tag{1.3}$$

  which, being an endothermal reaction, decreases the energy of the system, thus enhancing its contraction.

Due to the combined action of gravity and the above mechanisms, as soon as the mass exceeeds the Chandrasekhar limit the core collapses, within a time of the order of a fraction of a second, until it reaches the typical density of atomic nuclei, $\sim 10^{14}$ g/cm^3 or $\sim$ 100 million tons per cubic centimeter.

At this stage, the core of the star behaves as an atomic nucleus of macroscopic size, and becomes almost incompressible. The gravitational collapse stops and the core undergoes a bounce, producing a blast that ejects the star envelope into interstellar space. Most of the elements heavier than iron are created in this process.

The final outcome of this sequence of events, leading to the appearance of a *supernova* may be, in some cases, the birth of a rapidly rotating neutron star that can be observed many years later as a radio pulsar.

Neutron stars are the most interesting compact stars. Their structure and stability critically depend on the composition and the equation of state of the form of matter prevailing in the interior. Moreover, as the densities reached in neutron stars is much larger than the typical density of white dwarfs, the effects of general relativity cannot be neglected.

Before discussing some of the complex issues involved in the theoretical description of neutron star matter, in the rest of this Chapter we will focus on the simpler but instructive case of white dwarfs.

1.2 The degenerate electron gas

Let us consider a system of noninteracting electrons uniformly distributed in a cubic box of volume $V = \mathrm{L}^3$. If the temperature is sufficiently low, so that thermal energies can be neglected, the lowest quantum levels are occupied by two electrons, one for each spin state. Both electrons have the same energy, i.e. they are *degenerate*. This configuration corresponds to the ground state of the system. A gas of noninteracting electrons in its ground state is said to be *fully degenerate*. At higher temperature, the thermal energy can excite electrons to higher energy states, leaving some of the lower lying levels not fully degenerate.

As the electrons are uniformly distributed, their wave functions must exhibit translational invariance. They are eigenfunctions of the generator of space translation, i.e. the momentum operator, and can be written in the form

$$\psi_{\mathbf{p}\sigma}(\mathbf{r}) = \phi_{\mathbf{p}}(\mathbf{r})\chi_\sigma \ , \tag{1.4}$$

where χ_σ is a two-component Pauli spinor and

$$\phi_{\mathbf{p}}(\mathbf{r}) = \sqrt{\frac{1}{V}}\, \mathrm{e}^{i\mathbf{p}\cdot\mathbf{r}} \ , \tag{1.5}$$

satisfies periodic boundary conditions (x, y and z denote the components of the vector $\mathbf{r}$, specifying the electron position)

$$\phi_{\mathbf{p}}(x, y, z) = \phi_{\mathbf{p}}(x + n_x L, y + n_y L, z + n_z L) \ , \tag{1.6}$$

with $n_x, n_y, n_z = 0, \pm 1, \pm 2, \ldots$. The above equation obviously implies the relations ($\mathbf{p} \equiv (p_x, p_y, p_z)$)

$$p_x = \frac{2\pi n_x}{L}, \quad p_y = \frac{2\pi n_y}{L}, \quad p_z = \frac{2\pi n_z}{L} \ , \tag{1.7}$$

which in turn determine the momentum eigenvalues.

Each quantum state is associated with an eigenvalue of the momentum $\mathbf{p}$, i.e. with a specific triplet of integers (n_x, n_y, n_z). The corresponding energy eigenvalue is ($p^2 = |\mathbf{p}|^2 = p_x^2 + p_y^2 + p_z^2$)

$$\epsilon_p = \frac{p^2}{2m_e} = \left(\frac{2\pi}{L}\right)^2 \frac{1}{2m_e} \left(n_x^2 + n_y^2 + n_z^2\right) \ , \tag{1.8}$$

m_e being the electron mass ($m_e = 9.11 \times 10^{-28}$ g, or 0.51 MeV). The highest energy reached, called the Fermi Energy of the system, is denoted by ϵ_F, and the associated momentum, the Fermi momentum, is $p_F = \sqrt{2m_e\epsilon_F}$.

The number of quantum states with energy less or equal to ϵ_F can be easily calculated. Since each triplet (n_x, n_y, n_z) corresponds to a point in a cubic lattice with unit lattice spacing, the number of momentum eigenstates is equal to the number of lattice points within a sphere of radius $R = p_F L/(2\pi)$. The number of electrons in the system can then be obtained from (note: the factor 2 takes into account spin degeneracy, i.e. the fact that there are two electrons with opposite spin projections sitting in each momentum eigenstate)

$$N = 2 \ \frac{4\pi}{3} \ R^3 = V \ \frac{p_F^3}{3\pi^2} \ , \tag{1.9}$$

and the electron number density, i.e. the number of electrons per unit volume, is given by

$$n_e = \frac{N}{V} = \frac{p_F^3}{3\pi^2} \ . \tag{1.10}$$

The total ground state energy can be easily evaluated from

$$E = 2 \sum_{p<p_F} \frac{p^2}{2m_e} \tag{1.11}$$

replacing (use (1.7) again and take the limit of large L, corresponding to vanishingly small level spacing)

$$\sum_{p<p_F} \to \frac{V}{(2\pi^3)} \int_{p<p_F} d^3p \tag{1.12}$$

to obtain

$$E = 2 \ \frac{V}{(2\pi)^3} \ 4\pi \ \int_0^{p_F} p^2 dp \ \frac{p^2}{2m_e} \ . \tag{1.13}$$

The resulting energy density is

$$\epsilon = \frac{E}{V} = \frac{1}{(2\pi)^3} \ 4\pi \ \frac{p_F^5}{5m_e} \ . \tag{1.14}$$

From Eq. (1.10) it follows that the Fermi energy can be written in terms of the number density according to

$$\epsilon_F = \frac{p_F^2}{2m_e} = \frac{(3\pi^2 n_e)^{2/3}}{2m_e} \ . \tag{1.15}$$

The above equation can be used to define a density n_0 such that for $n_e \gg n_0$ the electron gas at given temperature T is fully degenerate. Full degeneracy is realized when the thermal energy K_BT (K_B is the Boltzman constant: $K_B = 1.38 \times 10^{-16}$ erg/°K, or 0.826×10^{-4} eV/°K) is much smaller than the Fermi energy ϵ_F, i.e. when

$$n_e \gg n_0 = \frac{1}{3\pi^2}\left(2m_e\ K_BT\right)^{3/2} \ . \tag{1.16}$$

For an ordinary star at the stage of hydrogen burning, like the Sun, the interior temperature is $\sim 10^7$ °K (yielding $K_BT \sim 10^3$ eV), and the corresponding value of n_0 is $\sim 10^{26}$ cm^{-3}. If we assume that the electrons come from a fully ionized hydrogen gas, the *matter* density of the proton-electron plasma is

$$\rho = (m_p + m_e)\ n_0 \sim 200 \text{ g/cm}^3 \ , \tag{1.17}$$

m_p being the proton mass ($m_p = 1.67 \times 10^{-24}$ g). This density is high for most stars in the early stage of hydrogen burning, while for ageing stars that have developed a substantial helium core the density (m_n denotes the neutron mass: $m_n \approx m_p$).

$$\rho = (m_p + m_n + m_e)\ n_0 \sim 400 \text{ g/cm}^3 \tag{1.18}$$

can be largely exceeded within the core. For example, white dwarfs have core densities of the order of 10^7 g/cm^3. As a consequence, in the study of their structure thermal energies can be safely neglected, the primary role being played by the degeneracy energy $p^2/2m_e$.

The pressure P of the electron gas, i.e. the force per unit area on the walls of the box, is defined in kinetic theory as the rate of momentum transferred by the electrons colliding on a surface of unit area. The pressure generated on the wall of the box lying on the yz plane by electrons moving with momentum p_x and velocity v_x parallel to the x axis is

$$P(p_x) = \frac{1}{L^2}\frac{dp_x}{dt} = \frac{1}{L^2}\ (2p_x)\ \left(\frac{1}{2}n_e v_x L^2\right) = \frac{N}{V} p_x v_x \ . \tag{1.19}$$

In the above equation, the first terms in round brackets is the momentum transfer associated with the reflection of one electron off the box wall, while the second term is the electron flux, i.e. the number of electrons hitting the wall over the time dt (the factor 1/2 accounts for the fact that half of the electrons go the wrong way). The total pressure can therefore be obtained from

$$P = 2\frac{1}{N}\sum_{p_x < p_F} P(p_x) = 2\int_{p\leq p_F}\frac{d^3p}{(2\pi)^3}\ p_x\ v_x \ . \tag{1.20}$$

Since the system is isotropic

$$p_x v_x = \frac{1}{3}\,(p_x v_x + p_y v_y + p_z v_z) = \frac{1}{3}\,(\mathbf{p}\cdot\mathbf{v}) = \frac{1}{3}\,(pv)\ , \tag{1.21}$$

and Eq. (1.20) can be rewritten (use $v = (\partial\epsilon_p/\partial p) = p/m_e$)

$$P = \frac{2}{3}\,\frac{1}{(2\pi)^3}\,4\pi\int_0^{p_F} p^2 dp\ (pv)\ = \frac{1}{(2\pi)^3}\,4\pi\,\frac{2p_F^5}{15m_e}\ . \tag{1.22}$$

Note that the above result can also be obtained from the standard thermodynamical definition of pressure

$$P = -\left(\frac{\partial E}{\partial V}\right)_N\ , \tag{1.23}$$

using E given by eq.(1.13) and $(\partial p_F/\partial V)_N = -p_F/(3V)$.

Equation (1.22) shows that the pressure of a degenerate Fermi gas decreases linearly as the mass of the constituent particle increases. For example, the pressure of an electron gas at number density n_e is $\sim$ 2000 times larger than the pressure of a gas of protons or neutrons at the same number density.

So far, we have been assuming that the electrons in the degenerate gas be nonrelativistic. However, the properties of the system depend primarily on the distribution of quantum states, which is dictated by translation invariance only, and is not affected by this assumption. Releasing the nonrelativivstic approximation simply amounts to replace the nonrelativistic energy with its relativistic counterpart:

$$\frac{p^2}{2m_e} \to \sqrt{p^2 + m_e^2} - m_e\ . \tag{1.24}$$

The transition from the nonrelativistic regime to the relativistic regime occurs when the electron energy becomes comparable to the electron rest mass, m_e. It is therefore possible to define a density n_c such that at $n_e \ll n_c$ the system is nonrelativistic, while $n_e \gg n_c$ corresponds to the relativistic regime. The value of n_c can be found requiring that the Fermi energy at $n_e = n_c$ be equal to m_e. The resulting expression is

$$n_c = \frac{2^{3/2}}{3\pi^2}\,m_e^3 \sim 10^{30}\ \mathrm{cm}^{-3}\ . \tag{1.25}$$

The energy density of a fully degenerate gas of relativistic electrons can be obtained from (compare to Eqs. (1.13) and (1.14))

$$\epsilon = 2\,\frac{1}{(2\pi^3)}\,4\pi\int_0^{p_F} p^2 dp\ \left[\sqrt{p^2+m_e^2} - m_e\right]\ , \tag{1.26}$$

while the equation for the pressure reads (compare to Eq. (1.22) and use again $v = \partial\epsilon_p/\partial p$ with relativistic ϵ_p)

$$P = \frac{2}{3} \frac{1}{(2\pi)^3} 4\pi \int_0^{p_F} p^2 dp \left(p \frac{\partial \epsilon_p}{\partial p} \right) . \tag{1.27}$$

Carrying out the integrations involved in eqs.(1.26) and (1.27) we find:

$$\epsilon = \frac{\pi m_e}{\lambda_e^3} \left[t \left(2t^2 + 1\right) \sqrt{t^2+1} - \log\left(t + \sqrt{t^2+1} \right) - \frac{8}{3} t^3 \right] , \tag{1.28}$$

where the last term in square brakets is the contribution resulting from the subtraction of the electron rest mass in Eq. (1.26), and

$$P = \frac{\pi m_e}{\lambda_e^3} \left[\frac{1}{3} t \left(2t^2 - 3\right) \sqrt{t^2+1} + \log\left(t + \sqrt{t^2+1} \right) \right] . \tag{1.29}$$

In the above equations, $\lambda_e = 2\pi/m_e$ is the electron Compton wavelength and (see Eq. (1.15))

$$t = \frac{p_F}{m_e} = \frac{\left(3\pi^2 n_e\right)^{1/3}}{m_e} . \tag{1.30}$$

Equations (1.28) and (1.29) give the energy density and pressure of a fully degenerate electron gas as a function of the dimensionless variable t, which can in turn be written in terms of the number density n_e according to Eq. (1.30).

1.3 Equation of state of the degenerate Fermi gas

The *equation of state* describes the relationship between the pressure of the system (P) and its matter density (ρ), related to the electron number density n_e by the equation

$$\rho = \frac{m_p}{Y_e} n_e , \tag{1.31}$$

where Y_e is the number of electrons per nucleon in the system. For a pure metarial $Y_e = Z/A$, Z and A being the atomic number and the nuclear mass number, respectively. For example, for a fully ionized helium plasma $Y_e = 0.5$, whereas for a plasma of iron nuclei $Y_e = 26/56 = 0.464$.

The equation of state of a fully degenerate electron gas (see Eq. (1.29)) takes a particularly simple form in the nonrelativistic limit (corresponding to

$t \ll 1$), as well as in the extreme relativistic limit (coresponding to $t \gg 1$). Using Eq. (1.27) we find (compare to Eq. (1.22))

$$P = \frac{8}{15} \frac{\pi}{\lambda_e^3 m_e^4} \left(\frac{3\pi^2 Y_e}{m_p} \right)^{5/3} \rho^{5/3} \tag{1.32}$$

for $e_F \ll m_e$ and

$$P = \frac{2}{3} \frac{\pi}{\lambda_e^3 m_e^3} \left(\frac{3\pi^2 Y_e}{m_p} \right)^{4/3} \rho^{4/3} \tag{1.33}$$

for $e_F \gg m_e$.

An equation of state of the form

$$P \propto \rho^\Gamma \ , \tag{1.34}$$

is said to be *polytropic*. The exponent Γ is called *adiabatic index*, whereas the quantity n, defined through

$$\Gamma = 1 + \frac{1}{n} \ , \tag{1.35}$$

goes under the name of *polytropic index*.

The adiabatic index, whose definition for a generic equation of state reads

$$\Gamma = \frac{d\,(\log P)}{d\,(\log \rho)} \ . \tag{1.36}$$

is related to the compressibility χ, characterizing the change of pressure with volume according to

$$\frac{1}{\chi} = -V \left(\frac{\partial P}{\partial V} \right)_N = \rho \left(\frac{\partial P}{\partial \rho} \right)_N \ , \tag{1.37}$$

through

$$\Gamma = \frac{1}{\chi P}. \tag{1.38}$$

The compressibility is in turn related to the speed of sound in matter, c_s, defined as

$$c_s = \left(\frac{\partial P}{\partial \rho} \right)^{1/2} = \frac{1}{\chi \rho} \ . \tag{1.39}$$

The magnitude of the adiabatic index reflects the so called *stiffnes* of the equation of state. Larger stiffness corresponds to more incompressible matter. As we will see in the following Sections, stiffness turns out to be critical in determining a number of stellar properties.

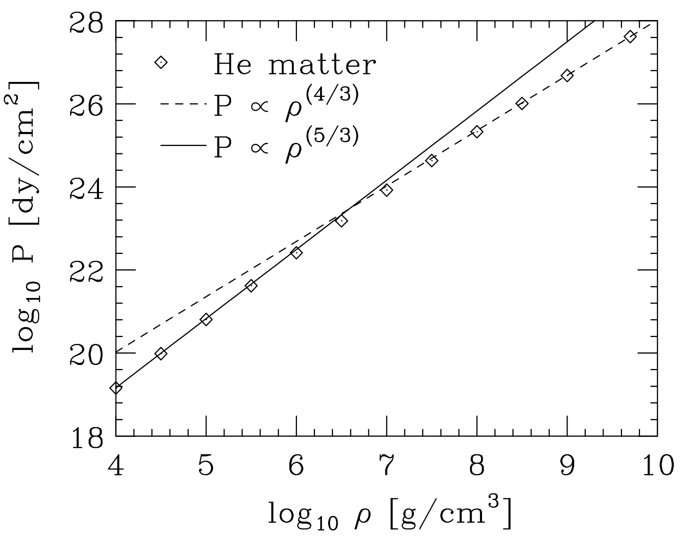

Figure 1.1: Equation of state of a fully ionized helium plasma at zero temperature (diamonds). The solid and dashed line correspond to the nonrelativistic and extreme relativistic limits, respectively. Note that the value of matter density corresponding to n_c defined in Eq. (1.25) corresponds to $\log_{10}\rho \sim 6.3$ g/cm^3.

1.4 Hydrostatic equilibrium of white dwarfs

Let us assume that white dwarfs consist of a plasma of fully ionized helium at zero temperature. The pressure of the system, P, is provided by the electrons, the contribution of the helium nuclei being negligible due to their large mass. For any given value of the matter density ρ, P can be computed from Eqs. (1.29) and (1.30) (in this case $Y_e = 0.5$, implying $n_e = \rho/2m_p$). The results of this calculation are shown by the diamonds in Fig. 1.1. For comparison, the nonrelativistic (Eq. (1.32)) and extreme relativistic (Eq. (1.33)) limits are also shown by the solid and dashed line, respectively.

In order to show the sensitivity of the equation of state to the value of Y_e, in Fig. 1.2 the equation of state of the fully ionized helium plasma ($Y_e = 0.5$) is compared to that of a hydrogen plasma ($Y_e = 1$).

The surface gravity of white dwarfs, GM/R (G is the gravitational constant), is small, of order $\sim 10^{-4}$. Hence, their structure can be studied neglecting the effects of general relativity and assuming that they consist of a spherically symmetric fluid in hydrostatic equilibrium.

Equilibrium requires that the gravitational force acting on an volume element at distance r from the center of the star, $F_G(r)$, be balanced by the

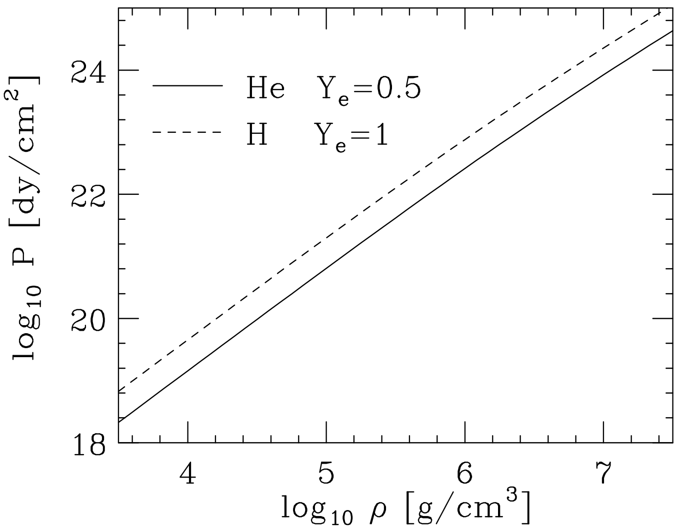

Figure 1.2: Comparison between the equations of state of a fully ionized plasma of helium (solid line) and hydrogen (dashed line) at zero temperature.

force produced by the spacial variation of the pressure. From

$$F_G(r) = -\ \rho(r)\ \frac{GM(r)}{r^2}\ , \tag{1.40}$$

with

$$M(r) = 4\pi \int_0^r dr'\ r'^2 \rho(r')\ , \tag{1.41}$$

it then follows the equilibrium equation

$$\frac{dP}{dr} = -\ \rho(r)\ \frac{GM(r)}{r^2}\ . \tag{1.42}$$

Given an equation of state, Eq. (1.42) can be integrated numerically for any value of the central density ρ_c to obtain the radius of the star, defined as the value $r = R$ corresponding to vanishing pressure, i.e. such that $P(R) = 0$. The mass can then be obtained from (see Eq. (1.41))

$$M = 4\pi \int_0^R dr\ r^2 \rho(r)\ . \tag{1.43}$$

The dependence of the mass of the star upon its central density, obtained from integration of Eq. (1.42) using the equation of state of a fully ionized helium plasma, is illustrated in Fig. 1.3. The figure shows that the mass increases as the central density increases, until a limiting value M $\sim$ 1.44

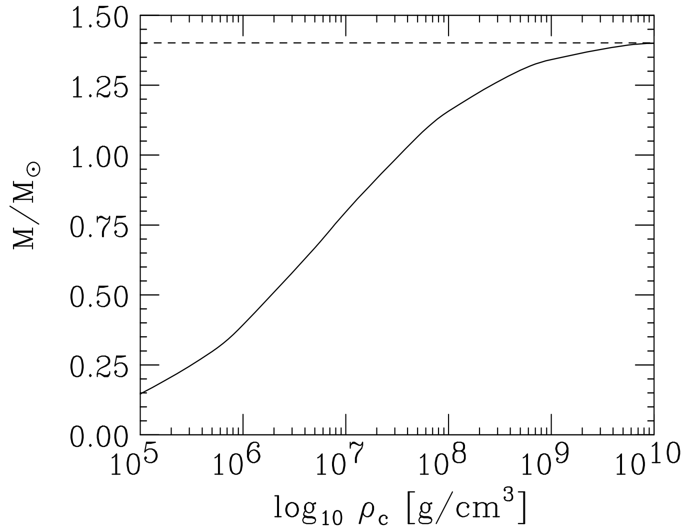

Figure 1.3: Dependence of the mass of a white dwarf upon its central density, obtained from the integration of Eq. (1.42) using the equation of state of a fully ionized helium plasma.

$M_\odot$ is reached at $\rho_0 \sim 10^{10}$ g/cm^3. The existence of this limiting mass was first pointed out by Chandrasekhar. However, as we will see in the following Sections, at $\rho \sim 10^8$ g/cm^3 the *neutronization* process sets in, and the validity of the description in terms of a helium plasma breaks down. At $\rho \geq 10^8$ g/cm^3, matter does not support pressure as effectively as predicted by the equation of state of the helium plasma. As a consequence, a more realistic estimate of the limiting mass, generally referred to as the *Chandrasekhar mass*, is given by the mass corresponding to a central density of 10^8 g/cm^3, i.e. ~ 1.2 $M_\odot$.

Chapter 2

The equation of state

The equation of state (EOS) is a nontrivial relation linking the thermodynamic variables specifying the state of a macroscopic physical system. The most popular example is Boyle's *ideal gas law*, stating that the pressure of a collection of N noninteracting, pointlike classical particles, enclosed in a volume V, grows linearly with the temperature T and the average particle density $n = N/V$.

The ideal gas law provides a good description of very dilute systems, in which interaction effects can be neglected. In general, the EOS can be written expanding the pressure, P, in powers of the density (from now on, we will use units such that $K_B = 1$) according to

$$P = nT \ \left[1 + nB(T) + n^2C(T) + \ldots\right] \ . \tag{2.1}$$

The coefficients appearing in the above series, called *virial expansion*, depend on temperature only and describe the departure from the ideal gas law arising from interactions.

The EOS carries a great deal of dynamical information and provides a link between measurable *macroscopic* quantities, such as pressure and temperature, and the forces acting between the constituents of the system at *microscopic* level.

2.1 The van der Waals fluid

This dynamical content of the EOS can be best illustrated using the van der Waals fluid as an example. This system consists of a collection of particles interacting through a potential featuring a strong repulsive core followed by a weaker attactive tail, as schematically illustrated in Fig.2.1.

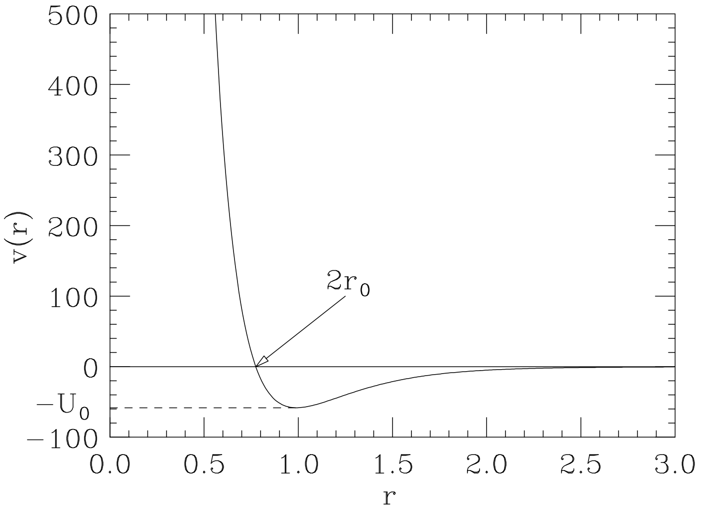

Figure 2.1: Behavior of the potential describing the interactions between constituents of a van der Waals fluid (both the interparticle distance r and $v(r)$ are given in arbitrary units).

The EOS of a van der Waals fluid is usually written in the form

$$P = \frac{nT}{1-nb} - an^2 \ , \tag{2.2}$$

where the two quantities a and b account for interaction effects. We will now show that a and b can be simply related to the potential $v(r)$.

The total energy of a system consisting of N nonrelativistic particles of mass m, enclosed in the volume V and interacting through the potential v, is

$$E = K + U \tag{2.3}$$

with

$$K = \sum_{i=1}^{N} \frac{p_i^2}{2m} \ , \tag{2.4}$$

and

$$U = \sum_{j>i=1}^{N} v(|\mathbf{r}_i - \mathbf{r}_j|) \ . \tag{2.5}$$

where $\mathbf{r}_i$ and $\mathbf{p}_i$ denote position and momentum of the i-th particle, respectively.

The free energy at temperature T can be obtained from

$$F = -T \log \int \mathrm{e}^{-\frac{E}{T}} \, d\Gamma \tag{2.6}$$

where $d\Gamma$ is the phase space volume element

$$d\Gamma = \prod_{i=1}^{N} d^3 r_i \prod_{i=1}^{N} \frac{d^3 p_i}{(2\pi)^3} \ . \tag{2.7}$$

Substitution of Eq. (2.3) in the right hand side of Eq. (2.6) leads to the factorization of the integral. For an ideal gas (IG), i.e. when $U = 0$, integration over the particle coordinates simply yields the result V^N and one finds

$$F_{IG} = -T \log V^N \int \prod_{i=1}^{N} \frac{d^3 p_i}{(2\pi)^3} \ \mathrm{e}^{-\frac{\mathrm{K}}{\mathrm{T}}} \ , \tag{2.8}$$

implying in turn

$$\begin{aligned} F &= F_{IG} - T \log \frac{1}{V^N} \int \prod_{i=1}^{N} d^3 r_i \ \mathrm{e}^{-\frac{\mathrm{U}}{\mathrm{T}}} \\ &= F_{IG} - T \log \left[\frac{1}{V^N} \int \prod_{i=1}^{N} d^3 r_i \left(\mathrm{e}^{-\frac{\mathrm{U}}{\mathrm{T}}} - 1 \right) + 1 \right] \ . \end{aligned} \tag{2.9}$$

We will now make the assumption that the system be so dilute that the probability of symultaneous collisions involving more than two particles be negligible. As the particles are identical, we can then rewrite the integral appearing in the second line of Eq. (2.9) as

$$\frac{N(N-1)}{2V^N} \int \prod_{i=1}^{N} d^3 r_i \left(\mathrm{e}^{-\frac{v_{12}}{\mathrm{T}}} - 1 \right) \ , \tag{2.10}$$

where $v_{ij} = v(|\mathbf{r}_i - \mathbf{r}_j|)$. The integrand only depends on the positions of particles 1 and 2, so that the remaining integrations, yielding a factor V^{N-2}, can be carried out right away. Moreover, as N is a large number $N(N-1) \approx N^2$, and Eq. (2.9) becomes

$$F = F_{IG} - T \log \left[\frac{1}{2} \left(\frac{N}{V} \right)^2 \int d^3 r_1 d^3 r_2 \left(\mathrm{e}^{-\frac{v_{12}}{\mathrm{T}}} - 1 \right) + 1 \right] \ . \tag{2.11}$$

In the low density limit, which is appropriate as we are dealing with a dilute system, the integral in the above equation, being proportional to $(N/V)^2$ is small. We can therefore use the result $\log(x+1) \approx x$ at $x \ll 1$ to obtain

$$F = F_{IG} - \frac{T}{2} \left(\frac{N}{V} \right)^2 \int d^3 r_1 d^3 r_2 \left(\mathrm{e}^{-\frac{v_{12}}{\mathrm{T}}} - 1 \right) \ . \tag{2.12}$$

The interaction potential depends on the relative coordinate only. Hence, defining

$$\mathbf{R_{12}} = \frac{1}{2}\left(\mathbf{r}_1 + \mathbf{r}_2\right) \quad , \quad \mathbf{r_{12}} = \mathbf{r}_1 - \mathbf{r}_2 \tag{2.13}$$

we can replace

$$\int d^3r_1 d^3r_2 \left(\mathrm{e}^{-\frac{v_{12}}{\mathrm{T}}} - 1\right) \to V \int d^3r_{12} \left(\mathrm{e}^{-\frac{v_{12}}{\mathrm{T}}} - 1\right) \tag{2.14}$$

to obtain

$$F = F_{IG} + \frac{N^2 T B(T)}{V} \ , \tag{2.15}$$

with

$$B(T) = \frac{1}{2} \int d^3r_{12} \left(1 - \mathrm{e}^{-\frac{v_{12}}{\mathrm{T}}}\right) \ . \tag{2.16}$$

Finally, from

$$P = -\left(\frac{\partial F}{\partial V}\right)_{N,T} \tag{2.17}$$

and

$$P_{IG} = \frac{N}{V}T \tag{2.18}$$

it follows that the EOS of a dilute gas can be written as a virial expansion, including terms of first and second order in the particle density N/V (compare to Eq. (2.1))

$$P = \frac{N}{V}T\left[1 + \frac{N}{V}B(T)\right] \ . \tag{2.19}$$

Let us now go back to the van der Waals fluid, and consider the expansion of the quantity $B(T)$ of Eq. (2.16) in powers of the ratio U_0/T, $U_0 > 0$ being the depth of the attractive part of the interparticle potential (see Fig. 2.1).

First, we split the integral in two parts according to (see Fig. 2.1)

$$B(T) = 2\pi \int_0^{2r_0} \left(1 - \mathrm{e}^{-\frac{v_{12}}{\mathrm{T}}}\right) r_{12}^2 dr_{12} + 2\pi \int_{2r_0}^{\infty} \left(1 - \mathrm{e}^{-\frac{v_{12}}{\mathrm{T}}}\right) r_{12}^2 dr_{12} \ . \tag{2.20}$$

At $0 \leq r_{12} \leq 2r_0$ the potential energy is positive and very large, implying that the exponential $\exp -v_{12}/T$ is small and can be neglected. As a consequence, we can define the quantity b as

$$b = 2\pi \int_0^{2r_0} \left(1 - \mathrm{e}^{-\frac{v_{12}}{\mathrm{T}}}\right) \approx \frac{16\pi}{3} r_0^3 \ . \tag{2.21}$$

Note that, if we interpret r_0 as the particle radius, b equals four times its volume.

Condider now the second integral in the right hand side of Eq. (2.20). For $U_0/T \ll 1$ the inequality $|v_{12}|/T \leq U_0/T$ implies

$$|v_{12}|/T \ll 1 \ , \tag{2.22}$$

and the integrand can be expanded in series of powers of v_{12}/T. Keeping the first nonvanishing term we obtain the result (recall that for $2r_0 \leq r_{12} \leq \infty$ v_{12} is always negative)

$$-\frac{2\pi}{T}\int_{2r_0}^{\infty} |v_{12}| r_{12}^2 dr_{12} = -\frac{a}{T} \ , \tag{2.23}$$

that defines the positive constant a. Collecting the two pieces together we can write

$$B(T) = b - \frac{a}{T} \ , \tag{2.24}$$

yielding (see Eq. (2.15))

$$F = F_{IG} + \frac{N^2}{V}(bT - a) \ . \tag{2.25}$$

To write the EOS in the form $P = P(N/V)$ we make use of the general expression of the free energy of the ideal gas

$$F_{IG} = -NT \log \frac{\mathrm{e}V}{N} + Nf(T) \ , \tag{2.26}$$

where $f(T)$ is a function of temperature only. Substitution into Eq. (2.25) leads to

$$F = Nf(T) - NT \log \frac{\mathrm{e}}{N} - NT\left(\log V - \frac{Nb}{V}\right) - \frac{N^2 a}{V} \ . \tag{2.27}$$

According with the hypotesis that the system be diluted, we now make the assumption that

$$Nb \ll V \ , \tag{2.28}$$

implying

$$\log(V - Nb) = \log V + \log\left(1 - \frac{Nb}{V}\right) \approx \log V - \frac{Nb}{V} \tag{2.29}$$

and

$$\begin{aligned} F &= Nf(T) - NT \log \frac{\mathrm{e}}{N}(V - Nb) - \frac{N^2 a}{V} \\ &= F_{IG} - NT \log\left(1 - \frac{Nb}{V}\right) - \frac{N^2 a}{V} \ . \end{aligned} \tag{2.30}$$

Note that the above equation yields the correct result, $F = F_{IG}$, in the limit of infinite dilution, corresponding to $V \to \infty$. On the other hand, it also implies that the system cannot be compressed indefinitely, as for $Nb/V > 1$ the argument of the logarithm becomes negative.

Knowing the free energy, we can finally obtain the pressure from Eq. (2.17), leading to

$$P = \frac{N}{V}T + NT\frac{Nb}{V(V-Nb)} - \left(\frac{N}{V}\right)^2 a = \frac{NT}{V-Nb} - \left(\frac{N}{V}\right)^2 a \ , \tag{2.31}$$

i.e. to Eq. (2.2) with $n = N/V$.

Equation (2.31) can also be rewritten in the form

$$\left[P + \left(\frac{N}{V}\right)^2 a\right](V - Nb) = NT \tag{2.32}$$

showing that (compare to the ideal gas EOS, $PV = NT$) the occurrence of interactions betwen the particles results in an increase of the pressure, driven by the constant a, and a decrease of the available volume, driven by the constant b (recall that $b \propto r_0^3$ can be related to the particle volume).

In spite of its simplicity, the van der Waals EOS provides a fairly accurate description of systems exhibiting a liquid-gas phase transition, like water (in this case the values of the parameters entering Eq. (2.31) are $a = 2 \times 10^{-48}$ J m^3 and $b = 6 \times 10^{-29}$ m^3).

Defining the quantities

$$P_c = \frac{a}{27b^2} \quad , \quad V_c = 3Nb \quad , \quad T_c = \frac{8a}{27b} \ , \tag{2.33}$$

and introducing the new adimensional variables

$$\widetilde{P} = \frac{P}{P_c} \quad , \quad \widetilde{V} = \frac{V}{V_c} \quad , \quad \widetilde{T} = \frac{T}{T_c} \ , \tag{2.34}$$

the van der Waals EOS can be rewritten in the form

$$\left(\widetilde{P} + \frac{3}{\widetilde{V}^2}\right)\left(\widetilde{V} - \frac{1}{3}\right) = \frac{8}{3}\widetilde{T} \ . \tag{2.35}$$

Note that the above relation is universal, as it does not explicitely depend on the constants a and b.

Figure 2.2 shows the relation between pressure in units of the critical pressure, $\widetilde{P}$, and density in units of the critical density, $\widetilde{n} = V_c/V$, for different values of $\widetilde{T}$. It appears that at $T < T_c$, i.e. $\widetilde{T} < 1$, the curves exhibit both

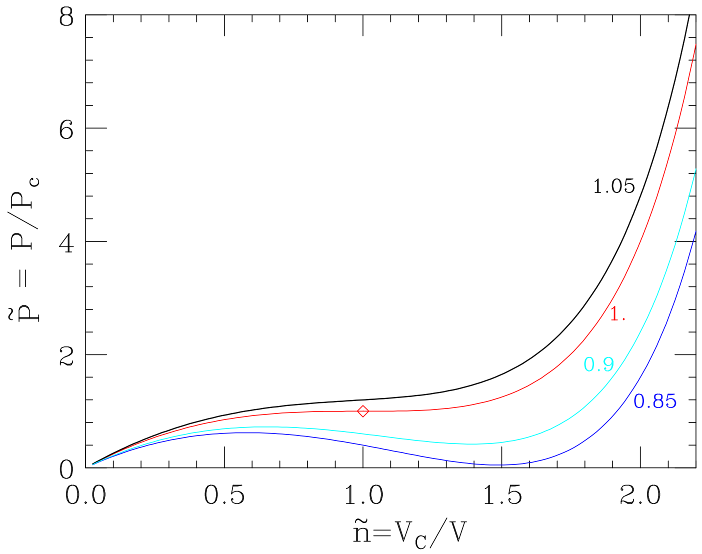

Figure 2.2: Behavior of the pressure (in units of the critical pressure) as a function of density (in units of the critical density) for a van der Waals fluid. The different curves are labelled according to the value of the ratio $\widetilde{T} = T/T_c$, T_c being the critical temperature. The diamond corresponds to the critical point $\widetilde{P} = \widetilde{V} = 1$.

a maximum and a minimum, whereas at $T > T_c$, i.e. $\widetilde{T} > 1$, $\widetilde{P}$ becomes a monotonically increasing function of $\widetilde{n}$. The curve corresponding to the critical temperature $T = T_c$ features a point of abscissa $\widetilde{n}_c$ such that

$$\left(\frac{\partial \widetilde{P}}{\partial \widetilde{n}} \right)_{\widetilde{n}=\widetilde{n}_c} = \left(\frac{\partial^2 \widetilde{P}}{\partial \widetilde{n}^2} \right)_{\widetilde{n}=\widetilde{n}_c} = 0 \ . \tag{2.36}$$

This point is called *critical point*. From Eqs. (2.35) and (2.36) it follows that $\widetilde{n}_c = 1$ and $\widetilde{P}(\widetilde{n}_c) = 1$.

As already pointed out, the van der Waals EOS describes a system exhibiting a liquid-gas phase transition. For $T > T_c$ the system is in the liquid phase at density $n > n_c$ ($n_c = N/V_c$) and in the gas phase at $n < n_c$. For $T < T_c$ there is a density region $n_1 < n < n_2$, with $n_1 < n_c$ and $n_2 > n_c$, in which the two phases cohexist. The values of n_1 and n_2 are determined by the requirements

$$P(n_1) = P(n_2) \tag{2.37}$$

and

$$P(n_1) \left(\frac{1}{n_2} - \frac{1}{n_1} \right) = - \int_{n_1}^{n_2} P(n) \, \frac{dn}{n^2} \ . \tag{2.38}$$

These features are best illustrated by the *phase diagram* of Fig. 2.3, showing the boundary of the regions corresponding to the different phases in the $(\widetilde{n}, \widetilde{T})$ plane.

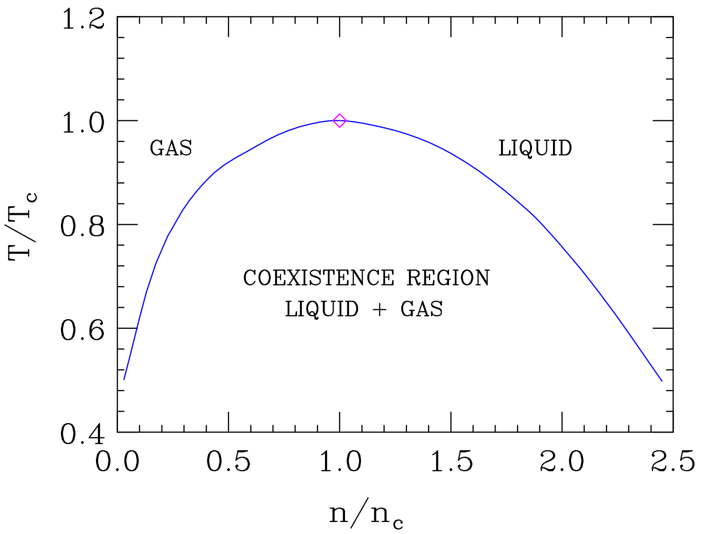

Figure 2.3: Phase diagram of a van der Waals fluid.

The example of the van der Waals fluid shows that the EOS contains information on the dynamics driving the interactions between the constituents of the system at microscopic level. The rather simple structure of the phase diagram of Fig. 2.3 reflects the simplicity of the potential represented in Fig. 2.1.

In the case of strongly interacting matter, the complexity of the underlying dynamics leads to a much richer structure, schematically illustrated in Fig. 2.4.

Under standard terrestrial conditions the elementary degrees of freedom of the fundamental theory of strong interactions (Quantum Chromo-Dynamics, or QCD) are confined within hadrons, and protons and neutrons cluster to form nuclei. At much larger density and/or temperature, however, the situation dramatically changes, and many different forms of matter are expected to become energrtically favoured. In the following sections we will discuss the structure of matter at large density and low temperature, relevant to the understanding of neutron star properties.

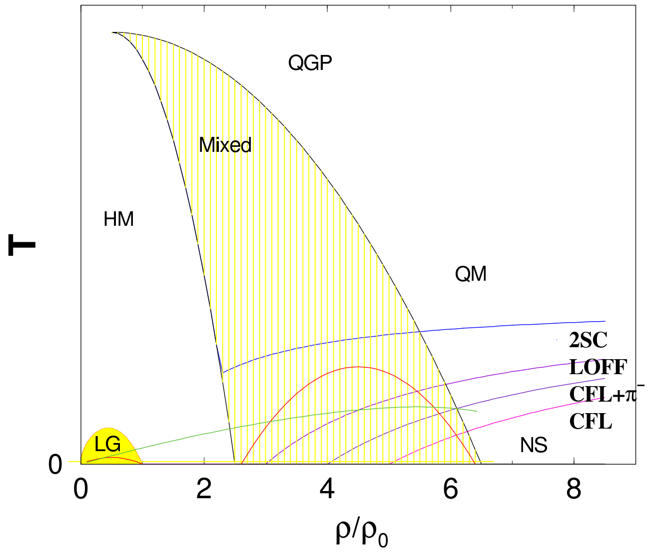

Figure 2.4: Temperature *vs* baryon density phase diagram of charge neutral strongly interacting matter in β-equilibrium. Hatched areas correspond to mixed phases of hadronic matter (HM) and quark matter (QM/QGP), as well as the nuclear liquid-gas (LG). The density is given in units of the central density of atomic nuclei.

Chapter 3

Matter at subnuclear densities

3.1 Overview of neutron star structure

The existence of compact astrophysical objects made of neutrons was predicted by Landau right after the discovery of the neutron, back in 1932. In 1934, Baade and Zwicky first suggested that a neutron star may be formed in the aftermath of a supernova explosion. Finally, in 1968 the newly observed pulsars, radio sources blinking on and off at a constant frequency, were identified with rotating neutron stars.

The results of a pioneering study, carried out in 1939 by Oppenheimer and Volkoff within the framework of general relativity, show that the mass of a star consisting of noninteracting neutrons cannot exceed $\sim 0.8\ M_\odot$. The fact that this maximum mass, the analogue of the Chandrasekhar mass of white dwarfs, turns out to be much smaller that the observed neutron star masses (typically $\sim 1.4\ M_\odot$) clearly shows that neutron star equilibrium requires a pressure other than the degeneracy pressure, whose origin has to be traced back to the nature of hadronic interactions.

Unfortunately, the need of including dynamical effects in the EOS is confronted with the complexity of the fundamental theory of strong interactions. As a consequence, all available description of the EOS of neutron star matter are obtained within models, based on the theoretical knowledge of the underlying dynamics and constrained, as much as possible, by empirical data.

The internal structure of a neutron star, schematically illustrated in Fig. 3.1, is believed to feature a sequence of layers of different composition.

The properties of matter in the outer crust, corresponding to densities ranging from $\sim 10^7$ g/cm^3 to the neutron drip density $\rho_d = 4 \times 10^{11}$ g/cm^3, can be obtained directly from nuclear data. On the other hand, models of the EOS at $4 \times 10^{11} < \rho < 2 \times 10^{14}$ g/cm^3 are somewhat based on extrapolations

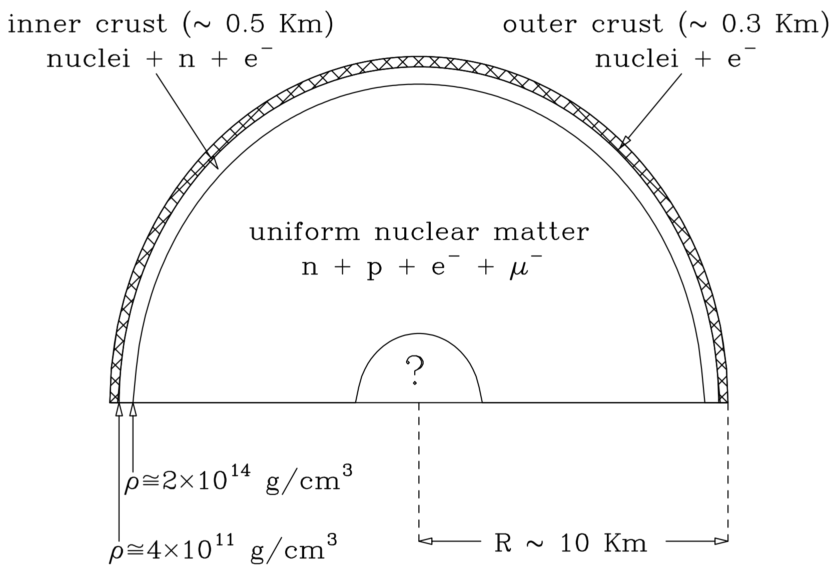

Figure 3.1: Schematic illustration of a neutron star cross section. Note that the equilibrium density of uniform nuclear matter corresponds to $\sim 2.7 \times 10^{14}$g/cm^3.

of the available empirical information, as the extremely neutron rich nuclei appearing in this density regime are not observed on earth.

The density of the neutron star core ranges between $\sim \rho_0$ ($= 2.67 \times 10^{14}$ g/cm^3) at the boundary with the inner crust, and a central value that can be as large as $1 \div 4 \times 10^{15}$ g/cm^3. All models of EOS based on hadronic degrees of freedom predict that in the density range $\rho_0 \lesssim \rho \lesssim 2\rho_0$ neutron star matter consists mainly of neutrons, with the admixture of a small number of protons, electrons and muons. At any given density the fraction of protons and leptons is determined by the requirements of equilibrium with respsect to β-decay and charge neutrality.

This picture may change significantly at larger density with the appearance of heavy strange baryons produced in weak interaction processes. For example, although the mass of the Σ^- exceeds the neutron mass by more than 250 MeV, the reaction $n+e^- \rightarrow \Sigma^- + \nu_e$ is energetically allowed as soon as the sum of the neutron and electron chemical potentials becomes equal to the Σ^- chemical potential.

Finally, as nucleons are known to be composite objects of size $\sim 0.5 - 1.0$ fm, corresponding to a density $\sim 10^{15}$ g/cm^3, it is expected that if the density in the neutron star core reaches this value matter undergoes a transition to a new phase, in which quarks are no longer clustered into nucleons or hadrons.

The theoretical description of matter in the outer and inner neutron star crust will be outlined in the following Sections, whereas the region corresponding to supranuclear density will be discussed in Chapter 4.

3.2 Outer crust

A solid is expected to form when the ratio of Coulomb energy to thermal energy becomes large, i.e. when

$$\Gamma = \frac{Z^2 e^2}{T r_L} \gg 1 \ , \tag{3.1}$$

with r_L defined through

$$n_I \frac{4\pi r_L^3}{3} = 1 \ , \tag{3.2}$$

n_I being the number density of ions. If the condition (3.1) is fulfilled Coulomb forces are weakly screened and become dominant, while the fluctuation of the ions is small compared to average ion spacing r_L. From (3.1) it follows that a solid is expected to form at temperature

$$T < T_m = \frac{Z^2 e^2}{r_L} \propto Z^2 e^2 n_I^{1/3} \ . \tag{3.3}$$

For example, in the case of ^{56}Fe at densities $\sim 10^7$ g/cm^3 solidification occurs at temperatures below 10^8 °K and Coulomb energy is minimized by a Body Centered Cubic (BCC) lattice. As the density further increases, r_L decreases, so that the condition for solidification continues to be fulfilled. However, as matter density advances into the density domain, 10^7 - 10^{11} g/cm^3, the large kinetic energy of the relativistic electrons shifts the energy balance, favouring inverse β-decay (i.e. electron capture) that leads to the appearance of new nuclear species through sequences like

$$Fe \to Ni \to Se \to Ge \ . \tag{3.4}$$

This process is called neutronization, because the resulting nuclide is always richer in neutron content than that initial one.

Before going on with the analysis of the neutronization process in the neutron star crust, we will duscuss a simple but instructive example, that will allows us to introduce some concepts and procedures to be used in the following Sections.

3.2.1 Inverse β-decay

Consider a gas of noninteracting protons and electrons at $T = 0$. The neutronization process is due to the occurrence of weak interactions turning protons into neutrons through

$$p + e^- \to n + \nu_e \ . \tag{3.5}$$

Assuming neutrinos to be massless and non interacting, the above process is energetically favorable as soon as the electron energy becomes equal to the neutron-proton mass difference

$$\Delta m = m_n - m_p = 939.565 - 938.272 = 1.293 \text{ MeV} \ . \tag{3.6}$$

As a consequence, the value of n_e at which inverse β-decay sets in can be estimated from

$$\sqrt{p_{F_e}^2 + m_e^2} = \Delta m \ , \tag{3.7}$$

where (see Section 1.2)

$$p_{F_e} = (3\pi^2 n_e)^{1/3} \ , \tag{3.8}$$

leading to

$$n_e = \frac{1}{3\pi^2} \left(\Delta m^2 - m_e^2\right)^{3/2} \approx 7 \times 10^{30} \text{cm}^{-3} \ . \tag{3.9}$$

The corresponding mass density for a system having $Y_e \sim 0.5$, is $\rho \approx 2.4 \times 10^7$ g/cm^3.

Now we want to address the problem of determining the ground state of the system consisting of protons, electrons and neutrons, once equilibrium with respect to the inverse β-decay of Eq. (3.5) has been reached. All interactions, except the weak interaction, will be neglected. Note that process (3.5) conserves baryon number N_B (i.e. the baryon number density n_B) and electric charge.

For any given value of n_B, the ground state is found by minimization of the total energy density of the systems, $\epsilon(n_p, n_n, n_e)$, n_p and n_n being the proton and neutron density, respectively, with the constraints $n_B = n_p + n_n$ (conservation of baryon number) and $n_p = n_e$ (charge neutrality).

Let us define the function

$$F(n_p, n_n, n_e) = \epsilon(n_p, n_n, n_e) + \lambda_B \left(n_B - n_p - n_n\right) + \lambda_Q \left(n_p - n_e\right) \ , \tag{3.10}$$

where ϵ is the energy density, while λ_B and λ_Q are Lagrange multipliers.

The minimum of F corrisponds to the values of n_p, n_n and n_e satisfying the conditions

$$\frac{\partial F}{\partial n_p} = \frac{\partial F}{\partial n_n} = 0 \quad , \quad \frac{\partial F}{\partial n_e} = 0 \tag{3.11}$$

as well as the aditional costraints

$$\frac{\partial F}{\partial \lambda_B} = \frac{\partial F}{\partial \lambda_Q} = 0 \ . \tag{3.12}$$

From the definition of chemical potential of the particles of species i ($i = p, n, e$)

$$\mu_i = \left(\frac{\partial E}{\partial N_i}\right)_V = \left(\frac{\partial \epsilon}{\partial n_i}\right)_V \tag{3.13}$$

it follows that Eqs. (3.11) imply

$$\mu_p - \lambda_B + \lambda_Q = 0 \quad , \quad \mu_n - \lambda_B = 0 \quad , \quad \mu_e - \lambda_Q = 0 \ , \tag{3.14}$$

leading to the condition of chemical equilibrium

$$\mu_n - \mu_p = \mu_e \ , \tag{3.15}$$

where, in the case of noninteracting particles at $T = 0$,

$$\begin{aligned} \mu_i &= \frac{\partial \epsilon}{\partial n_i} = \frac{2}{(2\pi)^3} \left(\frac{\partial p_{F_i}}{\partial n_i}\right) \frac{\partial}{\partial p_{F_i}} 4\pi \int_0^{p_{F_i}} p^2 \ dp \ \sqrt{p^2 + m_i^2} \\ &= \frac{8\pi}{(2\pi)^3} \left(\frac{\partial n_i}{\partial p_{F_i}}\right)^{-1} p_{F_i}^2 \ \sqrt{p_{F_i}^2 + m_i^2} = \sqrt{p_{F_i}^2 + m_i^2} \ . \end{aligned} \tag{3.16}$$

Defining now the proton and neutron fraction of the system as

$$x_p = \frac{n_p}{n_B} = \frac{n_p}{n_p + n_n} \quad , \quad x_n = \frac{n_n}{n_B} = 1 - x_p \tag{3.17}$$

we can rewrite

$$p_{F_p} = p_{F_e} = \left(3\pi^2 x_p n_B\right)^{1/3} \quad , \quad p_{F_n} = \left[3\pi^2 \left(1 - x_p\right) n_B\right]^{1/3} \ . \tag{3.18}$$

For fixed baryon density, use of the above definitions in Eq. (3.16) and substitution of the resulting chemical potentials into Eq. (3.15) leads to an equation in the single variable x_p. Hence, for any given n_B the requirements of chemical equilibrium and charge neutrality uniquely determine the fraction of protons in the system.

Once the value of x_p is known, the neutron, proton and electron number densities can be evaluated and the pressure

$$P = P_n + P_p + P_e \tag{3.19}$$

can be obtained using Eq. (1.27).

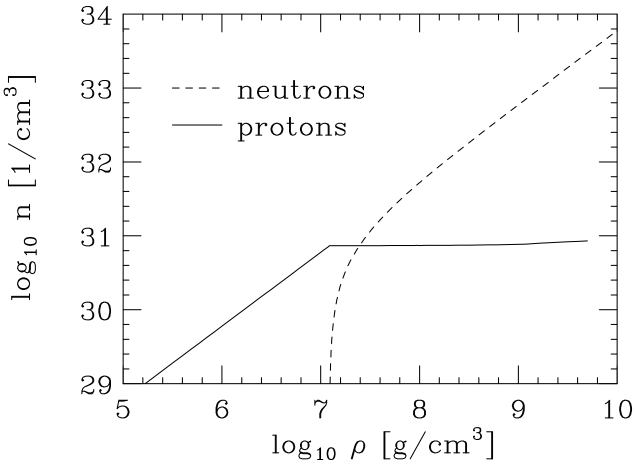

Figure 3.2: Number density of noninteracting protons and neutrons in β-equilibrium as a function of matter density.

Figure 3.2.1 shows the proton and neutron number densities, n_p and n_n (recall that $n_e = n_p$) as a function of matter density ρ. It can be seen that in the range $10^5 \leq \rho \leq 10^7$ g/cm^3 there are protons only and $\log n_p$ grows linearly with $\log \rho$. At $\rho \sim 10^7$ g/cm^3 neutronization sets in and the neutron number density begins to steeply increase. At $\rho > 10^7$ n_p stays nearly constant, while neutrons dominate.

The equation of state of the β-stable mixture is shown in the upper panel of Fig. 3.2.1. Its main feature is that pressure remains nearly constant as matter density increases by almost two orders of magnitude, in the range $10^7 \leq \rho \leq 10^9$ g/cm^3. The electron and neutron contributions to the pressure are shown in the lower panel of Fig. 3.2.1. Note that, since charge neutrality requires n_p=n_e, the proton pressure is smaller than the electron pressure by a factor $(m_p/m_e) \sim 2000$.

3.2.2 Neutronization

The description of β-stable matter in terms of a mixture of degenerate Fermi gases of neutrons, protons and electrons is strongly oversimplified. In reality, electron capture changes a nucleus with given charge Z and mass number A into a different nucleus with the same A and charge (Z$-$1). Moreover, the new nucleus may be metastable, so that two-step processes of the type

$$ {}^{56}_{26}\mathrm{Fe} \to {}^{56}_{25}\mathrm{Mn} \to {}^{56}_{24}\mathrm{Cr} \tag{3.20} $$

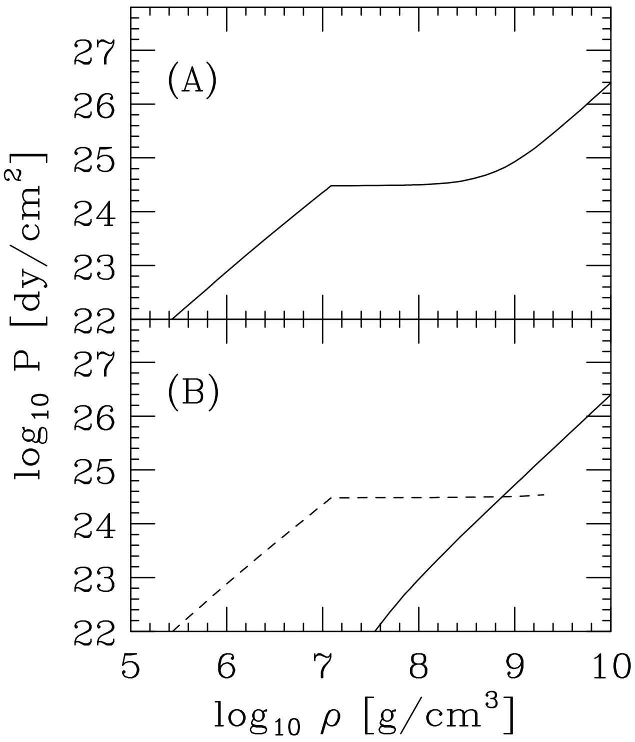

Figure 3.3: (A) Equation of state of a mixture of noninteracting neutrons, electrons and protons in β-equilibrium. (B) Density dependence of the neutron (solid line) and electron (dashed line) contributions to the pressure of β-stable matter.

can take place. In this case, chemical equilibrium is driven by the mass difference between neighboring nuclei rather than the neutron-proton chemical potential difference.

The measured nuclear charge distributions and masses, $\rho_{ch}(r)$ and $M(Z, A)$, exhibit two very important features

- The charge density is nearly constant within the nuclear volume, its value being roughly the same for all stable nuclei, and drops from $\sim$ 90 % to $\sim$ 10 % of the maximum over a distance $R_T \sim 2.5$ fm (1 fm $= 10\times10^{-13}$ cm), independent of A, called surface thickness (see Fig. 3.4). It can be parametrized in the form

$$\rho_{ch}(r) = \rho_0 \ \frac{1}{1 + \mathrm{e}^{(r-\mathrm{R})/\mathrm{D}}} \ , \tag{3.21}$$

where $\mathrm{R} = r_0 \mathrm{A}^{1/3}$, with $r_0 = 1.07$ fm, and $\mathrm{D} = 0.54$ fm. Note that the nuclear charge radius is proportional to $\mathrm{A}^{1/3}$, implying that the nuclear volume increases linearly with the mass number A.

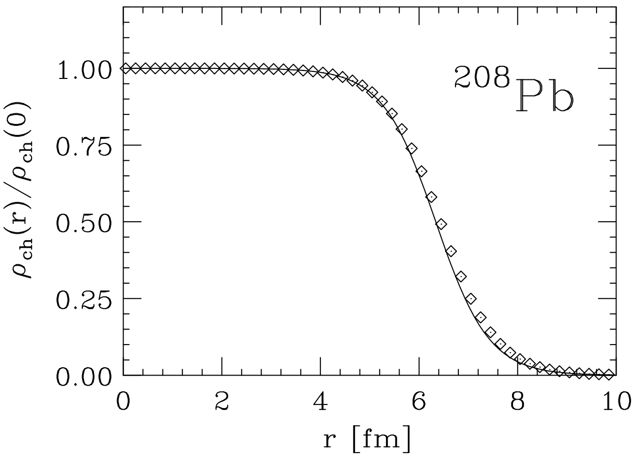

Figure 3.4: Nuclear charge distribution of ^{208}Pb, normalized to $Z/\rho(0)$ (Z = 82). The solid line has been obtained using the parametrization of Eq. (3.21), while the diamonds represent the results of a model independent analysis of electron scattering data.

- The (positive) binding energy per nucleon, defined as

$$\frac{B(\mathrm{Z},\mathrm{A})}{A} = \frac{1}{A}\left[\mathrm{Z}m_p + (\mathrm{A}-\mathrm{Z})m_n + \mathrm{Z}m_e - M(\mathrm{Z},\mathrm{A})\right] \ , \tag{3.22}$$

where $M(\mathrm{Z},\mathrm{A})$ is the measured nuclear mass, is almost constant for A$\geq$ 12 , its value being $\sim$ 8.5 MeV (see Fig. 3.5).

The A and Z dependence of $B(\mathrm{Z},\mathrm{A})$ can be parametrized according to the *semiempirical-mass formula*

$$\begin{aligned}\frac{B(\mathrm{Z},\mathrm{A})}{A} = \frac{1}{A}[\ a_{\mathrm{V}}\mathrm{A} \ &- \ a_{\mathrm{s}}\mathrm{A}^{2/3} - a_{\mathrm{c}}\frac{\mathrm{Z}^2}{\mathrm{A}^{1/3}} \\ &- \ a_{\mathrm{A}}\frac{(\mathrm{A}-2\mathrm{Z})^2}{4\mathrm{A}} + \lambda\ a_{\mathrm{p}}\frac{1}{\mathrm{A}^{1/2}}\ ] \ .\end{aligned} \tag{3.23}$$

The first term in square brackets, proportional to A, is called the *volume term* and describes the bulk energy of nuclear matter. The second term, proportional to the nuclear radius squared, is associated with the surface energy, while the third one accounts for the Coulomb repulsion between Z protons uniformly distributed within a sphere of radius R. The fourth term, that goes under the name of *symmetry energy* is required to describe the experimental observation that stable nuclei tend to have the same number of neutrons and protons. Moreover, even-even nuclei (i.e. nuclei having even

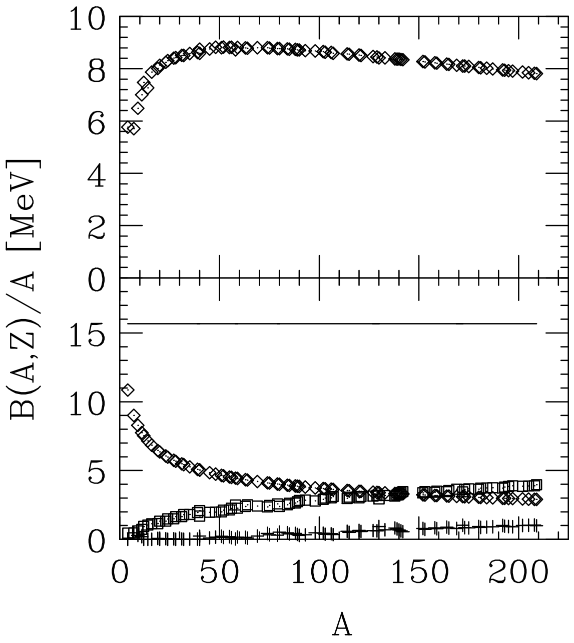

Figure 3.5: Upper panel: A-dependence of the binding energy per nucleon of stable nuclei, evaluated according to Eq. (3.23) with $a_{\rm V}$ = 15.67 MeV, $a_{\rm s}$ = 17.23 MeV, $a_{\rm c}$ = .714 MeV, $a_{\rm A}$ = 93.15 MeV and $a_{\rm p}$ = 11.2 MeV. Lower panel: the solid line shows the magnitude of the volume contribution to the binding energy per nucleon, whereas the A-dependence of the surface, coulomb and symmetry contributions are represented by diamonds, squares and crosses, respectively.

Z and even A $-$ Z) tend to be more stable than even-odd or odd-odd nuclei. This property is accounted for by the last term in the above equation, where λ -1, 0 and $+1$ for even-even, even-odd and odd-odd nuclei, respectively. Fig. 3.5 shows the different contributions to $B({\rm Z},{\rm A})/{\rm A}$, evaluated using Eq. (3.23).

The semi-empirical nuclear mass fomula of Eq. (3.23) can be used to obtain a qualitative description of the neutronization process. The total energy density of the system consisting of nuclei of mass number A and charge Z arranged in a lattice and surrounded by a degenerate electron gas is

$$\epsilon_T(n_B,{\rm A},{\rm Z}) = \epsilon_e + \left(\frac{n_B}{\rm A}\right)[M({\rm Z},{\rm A}) + \epsilon_L] \ , \tag{3.24}$$

where ϵ_e is the energy density of the electron gas, Eq. (1.26), n_B and $(n_B/{\rm A})$ denote the number densities of nucleons and nuclei, respectively, and ϵ_L is the electrostatic lattice energy per site. As a first approximation, the contribution of ϵ_L will be neglected.

At any given nucleon density n_B the equilibrium configuration corresponds to the values of A and Z that minimize $\epsilon_T(n_B, \mathrm{A}, \mathrm{Z})$, i.e. to A and Z such that

$$\left(\frac{\partial \epsilon_T}{\partial Z}\right)_{n_B} = 0 \ , \ \left(\frac{\partial \epsilon_T}{\partial A}\right)_{n_B} = 0 \ . \tag{3.25}$$

Combining the above relationships and using Eq. (3.23) one finds

$$\mathrm{Z} \simeq 3.54 \ A^{1/2}. \tag{3.26}$$

Once Z is known as a function of A, any of the two relationships (3.25) can be used to obtain A as a function of n_B. The mass number A turns out to be an increasing function of n_B, implying that Z also increases with n_B, but at a slower rate. Hence, nuclei become more massive and more and more neutron rich as the nucleon density increases.

The above discussion is obvioulsy still oversimplified. In reality, A and Z are *not* continuous variables and the total energy has to be minimized using the measured nuclear masses, rather than the parametrization of Eq. (3.23), and including the lattice energy, that can be written as

$$\epsilon_L = -K \ \frac{(\mathrm{Z}e)^2}{r_s} \tag{3.27}$$

where r_s is related to the number density of nuclei through $(4\pi/3)r_s^3 = (n_B/\mathrm{A})^{-1}$ and $K = 0.89593$ for a BCC lattice, yielding the lowest energy. At fixed nucleon number density n_B the total energy density can be written in the form

$$\epsilon_T(n_B, \mathrm{A}, \mathrm{Z}) = \epsilon_e + \left(\frac{n_B}{\mathrm{A}}\right) \left[M(\mathrm{Z}, \mathrm{A}) - 1.4442(\mathrm{Z}e)^2 \ \left(\frac{n_B}{\mathrm{A}}\right)^{1/3}\right] \ , \tag{3.28}$$

where, for matter density exceeding $\sim 10^6$ g/cm^3, the extreme relativistic limit of the energy density of an electron gas at number density n_e=Zn_B/A (see Section 1.2)

$$\epsilon_e = \frac{3}{4}\left(\mathrm{Z}\frac{n_B}{\mathrm{A}}\right)^{4/3} \ , \tag{3.29}$$

has to be used.

Collecting together the results of Eqs. (3.27)-(3.29) and expressing n_B in units of $n_{B_0} = 10^{-9}$ fm^{-3} (the number density corresponding to a matter density $\sim 10^6$ g/cm^3), the total *energy per nucleon*, ϵ_T/n_B, can be rewritten in units of MeV as

$$\frac{\epsilon_T}{n_B} = \frac{M(\mathrm{Z}, \mathrm{A})}{\mathrm{A}} + \frac{1}{\mathrm{A}^{4/3}} \ \left[0.4578 \ \mathrm{Z}^{4/3} - \frac{\mathrm{Z}^2}{480.74}\right] \ \left(\frac{n_B}{n_{B_0}}\right)^{1/3} \ . \tag{3.30}$$

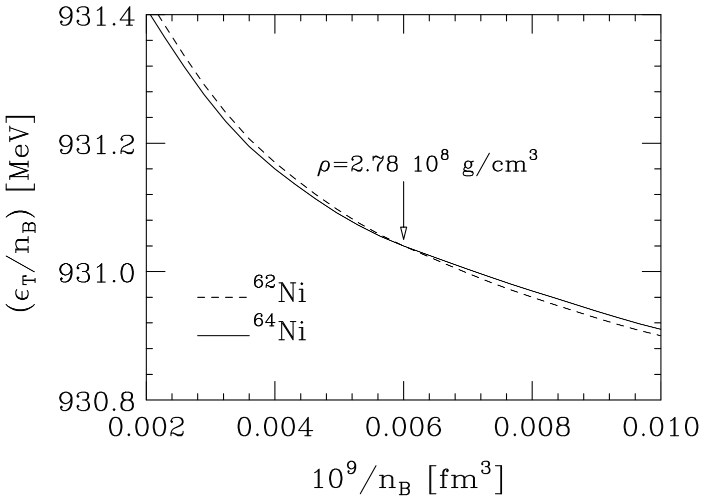

Figure 3.6: Total energy per nucleon of a BCC lattice of ^{62}Ni (dashed line) and ^{64}Ni (solid line) nuclei surrounded by an electron gas, evaluated using eq.(3.30) and plotted versus the inverse nucleon number density.

The average energy per nucleon in a nucleus is about 930 MeV. It can be conveniently written in units of MeV in the form $M(\mathrm{Z}, \mathrm{A})/\mathrm{A} = 930 + \Delta$. As long as we are dealing with nuclides that are not very different from the stable nuclides, the values of Δ are available in form of tables based on actual measurements or extrapolations of the experimental data.

In practice, ϵ_T/n_B of Eq. (3.30) is computed for a given nucleus (i.e. for given A and Z) as a function of n_B, and plotted versus $1/n_B$ (see Fig. 3.6). The curves corresponding to different nuclei are then compared and the nucleus corresponding to the minimum energy at given n_B can be easily identified. For example, the curves of Fig. 3.6 show the behavior of the energy per particle corresponding to ^{62}Ni and ^{64}Ni, having $\mathrm{A}-\mathrm{Z} = 34$ and 36, respectively. It is apparent that a first order phase transition is taking place around the point where the two curves cross one another. The exact densities at which the phase transition occurs and terminates can be obtained using Maxwell's double tangent construction. This method essentially amounts to drawing a straight line tangent to the convex curves corresponding to the two nuclides. In a first order phase transition the pressure remains constant as the density increases. Hence, as all points belonging to the tangent of Maxwell's construction correspond to the same pressure, the onset and termination of the phase transition are simply given by the points of tangency. As expected, at higher density the nucleus with the largest number of neutrons yields a lower energy.

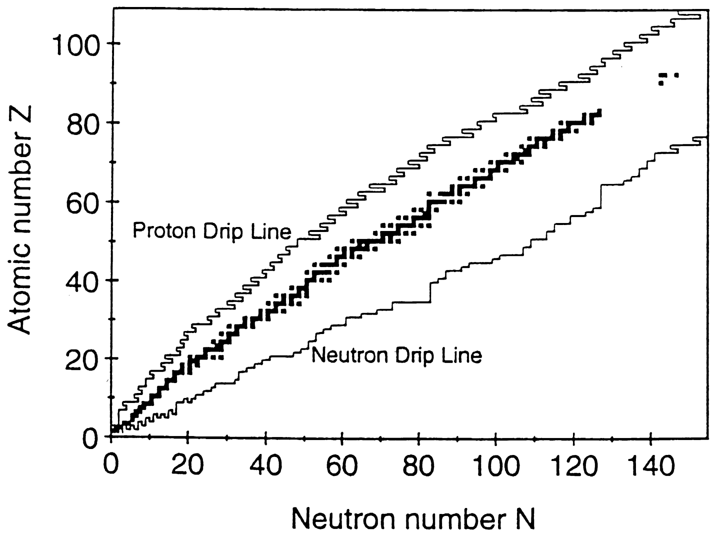

Figure 3.7: Chart of the nuclides. The black squares represent the stable nuclei as a function of Z and N=A−Z. The solid lines correspond to the estimated proton and neutron drip lines.

It has to be pointed out that there are limitations to the approach described in this section. Some of the nuclides entering the minimization procedure have ratios Z/A so different from those corresponding to stable nuclei (whose typical value of Z/A is ~ 0.5, as shown in Fig. 3.7) that the accuracy of the extrapolated masses may be questionable. Obviously, this problem becomes more and more important as the density increases. The study of nuclei far from stability, carried out with radioactive nuclear beams, is regarded as one of the highest priorities in nuclear physics research, and new dedicated experimental facilities are currently being planned both in the U.S. and in Europe.

Table 3.1 reports the sequence of nuclides corresponding to the ground state of matter at subnuclear density, as a function of matter density.

3.3 Inner crust

Table 3.1 shows that as the density increases the nuclides corresponding to the ground state of matter become more and more neutron rich. At $\rho \sim 4.3 \times 10^{11}$ g/cm^3 the ground state corresponds to a Coulomb lattice of ^{118}Kr nuclei, having proton to neutron ratio ~ 0.31 and a slighltly negative neutron chemical potential (i.e. neutron Fermi energy), surrounded by a degenerate electron gas with chemical potential $\mu_e \sim 26$ MeV. At larger

Nuclide	Z	N = A − Z	Z/A	Δ [MeV]	ρ_{max} [g/cm^3]
^{56}Fe	26	30	.4643	.1616	8.1×10^6
^{62}Ni	28	34	.4516	.1738	2.7×10^8
^{64}Ni	28	36	.4375	.2091	1.2×10^9
^{84}Se	34	50	.4048	.3494	8.2×10^9
^{82}Ge	32	50	.3902	.4515	2.1×10^{10}
^{84}Zn	30	54	.3750	.6232	4.8×10^{10}
^{78}Ni	28	50	.3590	.8011	1.6×10^{11}
^{76}Fe	26	50	.3421	1.1135	1.8×10^{11}
^{124}Mo	42	82	3387	1.2569	1.9×10^{11}
^{122}Zr	40	82	.3279	1.4581	2.7×10^{11}
^{120}Sr	38	82	.3166	1.6909	3.7×10^{11}
^{118}Kr	36	82	.3051	1.9579	4.3×10^{11}

Table 3.1: Sequence of nuclei corresponding to the ground state of matter and maximum density at which they occur. Nuclear masses are given by M(Z,A)/A = (930 + Δ) MeV.

densities a new regime sets in, since the neutrons created by electron capture occupy positive energy states and begin to *drip* out of the nuclei, filling the space between them.

At these densities the ground state corresponds to a mixture of two phases: matter consisting of neutron rich nuclei (phase I), with density $\rho_{\rm nuc}$, and a neutron gas of density $\rho_{\rm NG}$ (phase II).

The equilibrium conditions are

$$(\mu_n)_I = (\mu_n)_{II} = \mu_n \tag{3.31}$$

and

$$\mu_p = \mu_n - \mu_e \ , \tag{3.32}$$

where $(\mu_n)_I$ and $(\mu_n)_{II}$ denote the neutron chemical potential in the neutron gas and in the matter of nuclei, respectively.

The details of the ground state of matter in the neutron drip regime are specified by the densities ρ, $\rho_{\rm nuc}$ and $\rho_{\rm NG}$, the proton to neutron ratio of the matter in phase I and its surface, whose shape is dictated by the interplay between surface and Coulomb energies.

Recent studies suggest that at densities $4.3\times 10^{10} \lesssim \rho \lesssim .75\times 10^{14}$ g/cm^3 the matter in phase I is arranged in spheres immersed in electron and neutron gas, whereas at $.75\times 10^{14} \lesssim \rho \lesssim 1.2\times 10^{14}$ g/cm^3 the energetically favoured configurations exhibit more complicated structures, featuring rods of matter in phase I or alternating layers of matter in phase I and phase II. At $\rho \gtrsim 1.2\times 10^{14}$ g/cm^3 there is no separation between the phases, and the ground state of matter corresponds to a homogeneous fluid of neutrons, protons and electrons.

Chapter 4

The nuclear many-body problem

Understandig the properties of matter at densities comaparable to the central density of atomic nuclei ($\rho_0 \sim = 2.7 \times 10^{14}$ g/cm^3) is made difficult by *both* the complexity of the interactions *and* the approximations implied in the theoretical description of quantum mechanical many particle systems. The situation becomes even more problematic as we enter the region of *supranuclear* density, corresponding to $\rho > \rho_0$, as the available empirical information is scarce, and one has to unavoidably resort to a mixture of extrapolation and speculation.

The approach based on nonrelativistic quantum mechanics and phenomenological nuclear hamiltonians, while allowing for a rather satisfactory description of nuclear bound states and nucleon-nucleon scattering data, fails to fulfill the constraint of causality, as it leads to predict a speed of sound in matter that exceeds the speed of light at large density. On the other hand, the approach based on relativistic quantum field theory, while fulfilling the requirement of causality by construction, assumes a somewhat oversimplified dynamics, not constrained by nucleon-nucleon data. In addition, it is plagued by the uncertainty associated with the use of the mean field approximation, which is long known to fail in strongly correlated systems.

In this Chapter, after reviewing the phenomenological constraints on the EOS of cold nuclear matter, we will outline the current understanding of the nucleon-nucleon interaction and the nonrelativistic and relativistic approaches employed to study the structure of neutron star matter at nuclear and supernuclear density. As anticipated in Section 3.1, in this region a neutron star is believed to consist of a uniform fluid of neutrons, protons and electrons in β-equilibrium.

4.1 Constraints on the nuclear matter EOS

The body of data on nuclear masses can be used to constrain the density depencence predicted by theoretical models of uniform nuclear matter at zero temperature.

As we have seen in Section 3.2.2, the A-dependence of the nuclear binding energy is well described by the semiempirical formula (3.23). In the large A limit and neglecting the effect of Coulomb repulsion between protons, the only term surviving in the case $Z = A/2$ is the term linear in A. Hence, the coefficient a_V can be identified with the binding energy per particle of *symmetric nuclear matter*, an ideal uniform system consisting of equal number of protons and neutrons coupled by strong interactions only. The equilibrium density of such a system, n_0, can be inferred exploiting saturation of nuclear densities, i.e. the fact that the central density of atomic nuclei, measured by elastic electron-nucleus scattering, does not depend upon A for large A (see Fig. 4.1).

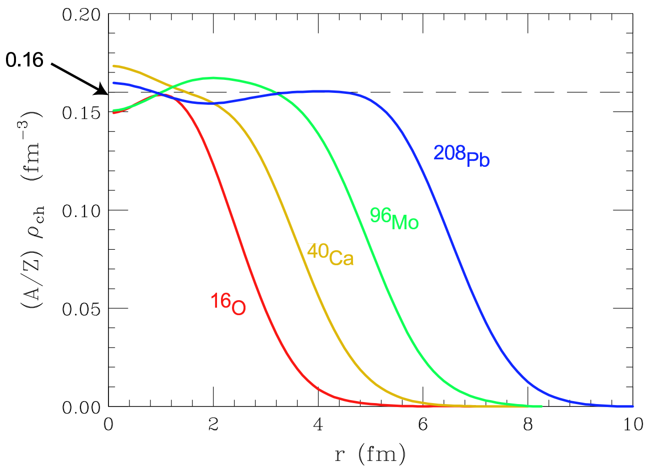

Figure 4.1: Saturation of central nuclear densities measured by elastic electron-nucleus scattering.

The empirical equilibrium properties of symmetric nuclear matter are

$$\left(\frac{E}{A}\right)_{n=n_0} = -16 \text{ MeV} \quad , \quad n_0 \sim .16 \text{ fm}^{-3} \ . \tag{4.1}$$

In the vicinity of the equilibrium density $e = E/A$ can be expanded according to

$$e(n) \approx e_0 + \frac{1}{2}\,\frac{K}{9}\,\frac{(n-n_0)^2}{n_0^2} \ , \tag{4.2}$$

where

$$K = 9\ n_0^2 \left(\frac{\partial^2 e}{\partial n^2} \right)_{n=n_0} = 9 \left(\frac{\partial P}{\partial n} \right)_{n=n_0} \tag{4.3}$$

is the (in)compressibility module, that can be extracted from the measured excitation energies of nuclear vibrational states. Due to the difficulties implied in the analysis of these experiments, however, empirical estimates of K have a rather large uncertainty, and range from $\sim$ 200 MeV (corresponding to more compressible nuclear matter, i.e. to a *soft* EOS) to $\sim$ 300 MeV (corresponding to a *stiff* EOS).

Unfortunately, the quadratic extrapolation of Eq. (4.2) cannot be expected to work far from equilibrium density. In fact, assuming a parabolic behavior of $e(n)$ at large n ($>> n_0$) leads to predict a speed of sound in matter, c_s, larger than the speed of light, i.e. (compare to Eq. (1.39))

$$c_s^2 = \frac{1}{n} \left(\frac{\partial P}{\partial e} \right) > 1\ , \tag{4.4}$$

regardless of the value of K.

Equation (4.4) shows that causality requires

$$\left(\frac{\partial P}{\partial \epsilon} \right) < 1\ , \tag{4.5}$$

ϵ being the energy-density. For a noniteracting Fermi gas $\epsilon \propto n^{4/3}$, implying (the equal sign corresponds to massless fermions)

$$P \leq \frac{\epsilon}{3}\ \ ,\ \ c_s \leq \frac{1}{3}\ . \tag{4.6}$$

In presence of interactions the above limits can be easily exceeded. For example, modeling the repulsion between nucleons in terms of a rigid core leads to predict infinite pressure at finite density.

The relation between microscopic dynamics and speed of sound in matter has been studied by Zel'dovich in th early 60s within the framework of relativistic quantum field theory.

Assuming that the energy density be related to number density through the power law

$$\epsilon = \frac{E}{V} = an^{\nu}\ , \tag{4.7}$$

energy per particle and pressure can be written

$$e = \frac{E}{N} = a\nu^{n-1}\ , \tag{4.8}$$

$$P = n^2 \left(\frac{\partial e}{\partial n} \right) = (n-1)an^{\nu} = (n-1)\epsilon \ . \tag{4.9}$$

From the above relations we easily see that that $\nu = 4/3$ corresponds to $P = \epsilon/3$ and that the limiting case $c_s = 1$, i.e. $(\partial P)/(\partial \epsilon) = 1$ is reached when $\nu = 2$. Powers higher than $\nu = 2$ are forbidden by causality.

In the model proposed by Zel'dovich matter consists of baryons interacting through exchange of a massive vector meson described by the lagrangian density

$$\mathcal{L}_V = -\frac{1}{4} F_{\mu\nu} F^{\mu\nu} - \frac{1}{2} \mu^2 A_\mu A^\mu \tag{4.10}$$

where $A^\mu \equiv (\phi, \mathbf{A})$ and μ is the meson mass. The corresponding field equation is

$$(\partial^\nu \partial_\nu + \mu^2) A_\mu = g J_\mu \ , \tag{4.11}$$

g being the coupling constant. In the simple case of a point source located at $\mathbf{x} = 0$

$$J_\mu \equiv (J_0, \mathbf{J}) \equiv (\delta(\mathbf{x}), 0) \tag{4.12}$$

and the solution of (4.11) is

$$\phi(\mathbf{x}') = g \ \frac{\mathrm{e}^{-\mu|\mathbf{x}' - \mathbf{x}|}}{|\mathbf{x}' - \mathbf{x}|} \quad , \quad \mathbf{A} = 0 \ . \tag{4.13}$$

Two charges at rest separated by a distance r repel each other with a force of magnitude

$$F = -g^2 \frac{d}{dr} \frac{\mathrm{e}^{-\mu r}}{r} \tag{4.14}$$

and the corresponding interaction energy is

$$g\phi = g^2 \frac{\mathrm{e}^{-\mu r}}{r} \ . \tag{4.15}$$

In the case of N particles of mass M, as the equation of motion (4.11) is linear, we can use the superposition principle and write the total energy as ($r_{ij} = |\mathbf{r}_i - \mathbf{r}_j|$)

$$E = NM + g^2 \sum_{j>i=1}^{N} \frac{\mathrm{e}^{-\mu r_{ij}}}{r_{ij}} \ . \tag{4.16}$$

Let us now make the further assumption that the average particle density be such that

$$\left(\frac{1}{n} \right)^{1/3} < \frac{1}{\mu} \ . \tag{4.17}$$

The above equation implies that the meson field changes slowly over distances comparable to the average particle separation. If this is the case we can use the mean field approximation and rewrite Eq. (4.16) in the form

$$e = \frac{E}{N} = M + \frac{g^2}{2} \int d^3r \frac{\mathrm{e}^{-\mu r}}{r} = m + 2\pi g^2 \frac{n}{\mu} \ . \tag{4.18}$$

The corresponding expression of the energy density and pressure read

$$\epsilon = ne = nM + 2\pi g^2 \frac{n^2}{\mu} \tag{4.19}$$

and

$$P = n^2 \left(\frac{\partial e}{\partial n} \right) = 2\pi g^2 \frac{n^2}{\mu} \ . \tag{4.20}$$

From the above equations it follows that, in the large n limit $P \to \epsilon$, inplying in turn $c_s \to 1$.

In conclusion, Zel'dovich model shows that the causality limit, corresponding to $\epsilon \propto n^2$, is indeed attained in a simple semirealistic theory, in which nucleons are assumed to interact through exchange of a vector meson.

4.2 The nucleon-nucleon interaction

The main features of the nucleon-nucleon (NN) interaction, inferred from the analysis of nuclear systematics, may be summarized as follows.

- The *saturation* of nuclear density (see Fig. 4.1), i.e. the fact that density in the interior of atomic nuclei is nearly constant and independent of the mass number A, tells us that nucleons cannot be packed together too tightly. Hence, at short distance the NN force must be repulsive. Assuming that the interaction can be described by a nonrelativistic potential v depending on the interparticle distance, $\mathbf{r}$, we can then write:

$$v(\mathbf{r}) > 0 \quad , \quad |\mathbf{r}| < r_c \ , \tag{4.21}$$

  r_c being the radius of the repulsive core.

- The fact that the nuclear binding energy per nucleon is roughly the same for all nuclei with A$\geq$ 20, its value being

$$\frac{B(\mathrm{Z},\mathrm{A})}{\mathrm{A}} \sim 8.5 \ \mathrm{MeV} \ , \tag{4.22}$$

  suggests that the NN interaction has a finite range r_0, i.e. that

$$v(\mathbf{r}) = 0 \quad , \quad |\mathbf{r}| > r_0 \ . \tag{4.23}$$

- The spectra of the so called *mirror nuclei*, i.e. pairs of nuclei having the same A and charges differing by one unit (implying that the number of protons in a nucleus is the same as the number of neutrons in its mirror companion), e.g. ${}^{15}_{7}$N (A = 15, Z = 7) and ${}^{15}_{8}$O (A = 15, Z = 8), exhibit striking similarities. The energies of the levels with the same parity and angular momentum are the same up to small electromagnetic corrections, showing that protons and neutrons have similar nuclear interactions, i.e. that nuclear forces are *charge symmetric*.

Charge symmetry is a manifestation of a more general property of the NN interaction, called *isotopic invariance*. Neglecting the small mass difference, proton and neutron can be viewed as two states of the same particle, the nucleon (N), described by the Dirac equation obtained from the lagrangiam density

$$\mathcal{L} = \overline{\psi}_N \left(i\gamma^\mu \partial_\mu - m \right) \psi_N \tag{4.24}$$

where

$$\psi_N = \begin{pmatrix} p \\ n \end{pmatrix} , \tag{4.25}$$

p and n being the four-spinors associated with the proton and the neutron, respectively. The lagrangian density (4.24) is invariant under the SU(2) global phase transformation

$$U = \mathrm{e}^{i\alpha_j \tau_j} , \tag{4.26}$$

where $\boldsymbol{\alpha}$ is a constant (i.e. independent of x) vector and the τ_j ($j = 1, 2, 3$) are Pauli matrices. The above equations show that the nucleon can be described as a doublet in isospin space. Proton and neutron correspond to isospin projections $+1/2$ and $-1/2$, respectively. Proton-proton and neutron-neutron pairs always have total isospin T=1 whereas a proton-neutron pair may have either $T = 0$ or $T = 1$. The two-nucleon isospin states $|T, T_3\rangle$ can be summarized as follows

$$\begin{aligned}
|1,1\rangle &= |pp\rangle \\
|1,0\rangle &= \frac{1}{\sqrt{2}} \left(|pn\rangle + |np\rangle \right) \\
|1,-1\rangle &= |nn\rangle \\
|0,0\rangle &= \frac{1}{\sqrt{2}} \left(|pn\rangle - |np\rangle \right) .
\end{aligned}$$

Isospin invariance implies that the interaction between two nucleons separated by a distance $r = |\mathbf{r}_1 - \mathbf{r}_2|$ and having total spin S depends on their total isospin T but not on T_3. For example, the potential $v(\mathbf{r})$ acting between two protons with spins coupled to $S = 0$ is the same as the potential acting between a proton and a neutron with spins and isospins coupled to $S = 0$ and $T = 1$.

4.3 The two-nucleon system

The details of the NN interaction can be best studied in the two-nucleon system. There is *only one* NN bound state, the nucleus of deuterium, or deuteron (^{2}H), consisting of a proton and a neutron coupled to total spin and isospin $S = 1$ and $T = 0$, respectively. This is clear manifestation of the fact that nuclear forces are *spin dependent*.

Another important piece of information can be inferred from the observation that the deuteron exhibits a nonvanishing electric quadrupole moment, implying that its charge distribution is not spherically symmetryc. Hence, the NN interaction is *noncentral*.

Besides the properties of the two-nucleon bound state, the large data base of phase shifts measured in NN scattering experiments ($\sim$ 4000 data points corresponding to energies up to 350 MeV in the lab frame) provides valuable additional information on the nature of NN forces.

The theoretical description of the NN interaction was first attempted by Yukawa in 1935. He made the hypotesis that nucleons interact through the exchange of a particle, whose mass μ can be related to the interaction range r_0 according to

$$r_0 \sim \frac{1}{\mu} \ . \tag{4.27}$$

Using $r_0 \sim 1$ fm, the above relation yields $\mu \sim 200$ MeV (1 fm $=$ 197.3 MeV).

Yukawa's idea has been successfully implemented identifying the exchanged particle with the π meson (or *pion*), discovered in 1947, whose mass is $m_\pi \sim$ 140 MeV. Experiments show that the pion is a spin zero pseudoscalar particle [1] (i.e. it has spin-parity 0^-) that comes in three charge states, denoted π^+, π^- and π^0. Hence, it can be regarded as an isospin T=1 triplet, the charge states being associated with isospin projections T_3=+ 1, 0 and -1, respectively.

The simplest π-nucleon coupling compatible with the observation that nuclear interactions conserve parity has the pseudoscalar form $ig\gamma^5\boldsymbol{\tau}$, where g is a coupling constant and $\boldsymbol{\tau}$ describes the isospin of the nucleon. With this

[1] The pion spin has been deduced from the balance of the reaction $\pi^+ + ^2\mathrm{H} \leftrightarrow p + p$, while its intrinsic parity was determined observing the π^- capture from the K shell of the deuterium atom, leading to the appearance of two neutrons: $\pi^- + d \to n + n$.

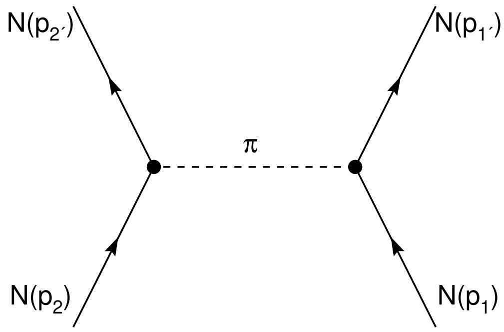

Figure 4.2: Feynman diagram describing the one-pion-exchange process between two nucleons. The corresponding amplitude is given by Eq. (4.28).

choice for the interaction vertex, the amplitude of the process depicted in Fig. 4.2 can readily be written, using standard Feynman's diagram techniques, as

$$\langle f|M|i\rangle = -ig^2 \ \frac{\bar{u}(p_2', s_2')\gamma_5 u(p_2, s_2)\bar{u}(p_1', s_1')\gamma_5 u(p_1, s_1)}{k^2 - m_\pi^2} \ \langle \boldsymbol{\tau}_1 \cdot \boldsymbol{\tau}_2 \rangle \ , \tag{4.28}$$

where $k = p_1' - p_1 = p_2 - p_2'$, $k^2 = k_\mu k^\mu = k_0^2 - |\vec{k}|^2$, $u(p, s)$ is the Dirac spinor associated with a nucleon of four momentum $p \equiv (\vec{p}, E)$ (E$=\sqrt{\mathbf{p}^2 + m^2}$) and spin projection s and

$$\langle \boldsymbol{\tau}_1 \cdot \boldsymbol{\tau}_2 \rangle = \eta_{2'}^\dagger \boldsymbol{\tau} \eta_2 \ \eta_{1'}^\dagger \boldsymbol{\tau} \eta_1 \ , \tag{4.29}$$

η_i being the two-component Pauli spinor describing the isospin state of particle i.

The calculation of the amplitude of Eq.(4.28) is described in Appendix B. In the nonrelativisti limit, Yukawa's theory leads to define a NN interaction potential that can be written in coordinate space as

$$\begin{aligned}
v_\pi &= \frac{g^2}{4m^2} \ (\boldsymbol{\tau}_1 \cdot \boldsymbol{\tau}_2)(\boldsymbol{\sigma}_1 \cdot \boldsymbol{\nabla})(\boldsymbol{\sigma}_2 \cdot \boldsymbol{\nabla}) \ \frac{e^{-m_\pi r}}{r} \\
&= \frac{g^2}{(4\pi)^2} \ \frac{m_\pi^3}{4m^2} \ \frac{1}{3}(\boldsymbol{\tau}_1 \cdot \boldsymbol{\tau}_2) \left\{ \left[(\boldsymbol{\sigma}_1 \cdot \boldsymbol{\sigma}_2) + S_{12} \left(1 + \frac{3}{x} + \frac{3}{x^2} \right) \right] \frac{e^{-x}}{x} \right. \\
&\qquad \left. - \ \frac{4\pi}{\mu^3} (\boldsymbol{\sigma}_1 \cdot \boldsymbol{\sigma}_2) \delta^{(3)}(\mathbf{r}) \right\} \ ,
\end{aligned} \tag{4.30}$$

where $x = m_\pi |\mathbf{r}|$ and

$$S_{12} = \frac{3}{r^2} (\boldsymbol{\sigma}_1 \cdot \mathbf{r})(\boldsymbol{\sigma}_2 \cdot \mathbf{r}) - (\boldsymbol{\sigma}_1 \cdot \boldsymbol{\sigma}_2) \ , \tag{4.31}$$

is reminiscent of the operator describing the noncentral interaction between two magnetic dipoles.

For $g^2/(4\pi) = 14$, the above potential provides an accurate description of the long range part ($|\mathbf{r}| > 1.5$ fm) of the NN interaction, as shown by the very good fit of the NN scattering phase shifts in states of high angular momentum. In these states, due to the strong centrifugal barrier, the probability of finding the two nucleons at small relative distances becomes in fact negligibly small.

At medium- and short-range other more complicated processes, involving the exchange of two or more pions (possibly interacting among themselves) or heavier particles (like the ρ and the ω mesons, whose masses are $m_\rho =$ 770 MeV and $m_\omega = 782$ MeV, respectively), have to be taken into account. Moreover, when their relative distance becomes very small ($|\mathbf{r}| \lesssim 0.5$ fm) nucleons, being composite and finite in size, are expected to overlap. In this regime, NN interactions should in principle be described in terms of interactions between nucleon constituents, i.e. quarks and gluons, as dictated by *quantum chromodynamics* (QCD), which is believed to be the fundamental theory of strong interactions.

Phenomenological potentials describing the *full* NN interaction are generally written as

$$v = \widetilde{v}_\pi + v_R \tag{4.32}$$

where $\widetilde{v}_\pi$ is the one pion exchange potential, defined by Eqs. (4.30) and (4.31), stripped of the δ-function contribution, whereas v_R describes the interaction at medium and short range. The spin-isospin dependence and the noncentral nature of the NN interactions can be properly described rewriting Eq. (4.32) in the form

$$v_{ij} = \sum_{ST} \left[v_{TS}(r_{ij}) + \delta_{S1} v_{tT}(r_{ij}) S_{12} \right] P_S \Pi_T \ , \tag{4.33}$$

S and T being the total spin and isospin of the interacting pair, respectively. In the above equation P_S ($S = 0, 1$) are the spin projection operators

$$P_0 = \frac{1}{4}\left(1 - \boldsymbol{\sigma}_1 \cdot \boldsymbol{\sigma}_2\right) \quad , \quad P_1 = \frac{1}{4}\left(3 + \boldsymbol{\sigma}_1 \cdot \boldsymbol{\sigma}_2\right) \ , \tag{4.34}$$

satisfying

$$P_0 + P_1 = 1 \ , \ P_S|S'\rangle = \delta_{SS'}|S'\rangle \ , \ P_S P_{S'} = P_S \delta_{SS'} \ , \tag{4.35}$$

and Π_T are the isospin projection operators that can be written as in Eq. (4.34) replacing $\boldsymbol{\sigma} \to \boldsymbol{\tau}$. The functions $v_{TS}(r_{ij})$ and $v_{Tt}(r_{ij})$ describe the radial dependence of the interaction in the different spin-isospin channels and reduce to the corresponding components of the one pion exchange potential at large r_{ij}. Their shapes are chosen in such a way as to reproduce the available NN data (deuteron binding energy, charge radius and quadrupole moment and the NN scattering phase shifts).

Substitution of Eq. (4.34) and the corresponding expressions for the isospin projection operators allows one to rewrite Eq. (4.33) in the form

$$v_{ij} = \sum_{n=1}^{6} v^{(n)}(r_{ij}) O_{ij}^{(n)} \ , \tag{4.36}$$

where

$$O_{ij}^{(n)} = 1,\ (\boldsymbol{\tau}_i \cdot \boldsymbol{\tau}_j),\ (\boldsymbol{\sigma}_i \cdot \boldsymbol{\sigma}_j),\ (\boldsymbol{\sigma}_i \cdot \boldsymbol{\sigma}_j)(\boldsymbol{\tau}_i \cdot \boldsymbol{\tau}_j),\ S_{ij},\ S_{ij}(\boldsymbol{\tau}_i \cdot \boldsymbol{\tau}_j) \tag{4.37}$$

and the $v^{(n)}(r_{ij})$ are linear combination of the $v_{TS}(r_{ij})$ and $v_{tT}(r_{ij})$. Note that the operatos defined in Eq. (4.37) form an algebra, as they satisfy the relation

$$O_{ij}^{(n)} O_{ij}^{(m)} = \sum_{\ell} K_{nm\ell} O_{ij}^{(\ell)} \ , \tag{4.38}$$

where the coefficients $K_{nm\ell}$ can be easily obtained from the properties of Pauli matrices. Equations (4.38) can be exploited to greatly simplify the calculation of nuclear observables based on the representation (4.36)-(4.37) of the NN potential.

The typical shape of the NN potential in the state of relative angular momentum $\ell = 0$ and total spin and isospin $S = 0$ and $T = 1$ is shown in Fig. 4.3. The short range repulsive core, to be ascribed to heavy meson exchange or to more complicated mechanisms involving nucleon constituents, is followed by an intermediate range attractive region, largely due to two-pion exchange processes. Finally, at large interparticle distance the one-pion-exchange mechanism dominates. Note the similarity with the van der Waals potential of Fig. 2.1.

4.4 Nonrelativistic many-body theory

Within nonrelativistic many-body theory (NMBT), nuclear systems are described as a collection of pointlike nucleons interacting through the hamiltonian

$$H = \sum_{i=1}^{A} \frac{\mathbf{p}_i^2}{2m} + \sum_{j>i=1}^{A} v_{ij} + \ldots \ , \tag{4.39}$$

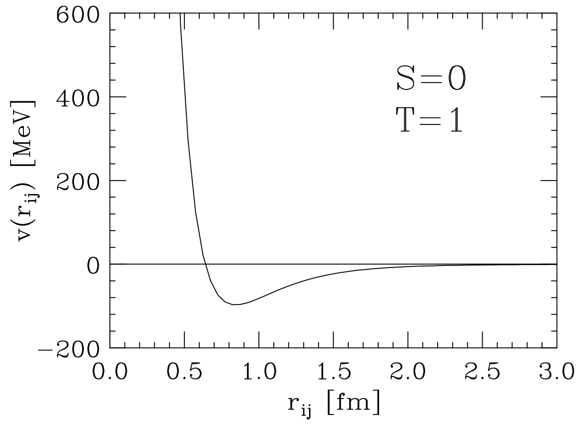

Figure 4.3: Radial dependence of the NN potential describing the interaction between two nucleons in the state of relative angular momentum $\ell = 0$, and total spin and isospin $S = 0$ and $T = 1$.

where $\mathbf{p}_i$ denotes the momentum carried by the i-th nucleon, v_{ij} is the two-body potential describing NN interactions the and the ellipsis refers to the possible existence of interactions involving more than two nucleons.

Unfortunately, solving the Schrödinger equation

$$H|\Psi_0\rangle = E_0|\Psi_0\rangle \tag{4.40}$$

for the ground state of a nucleus, using the hamiltonian (4.39) and the NN potential of Eqs.(4.36) and (4.37), is only possible for not too large A. The numerical solution is trivial for A=2 only. For A=3 Eq. (4.40) can still be solved using deterministic approaches, while for A>3 sthocastic methods, such as the Green Function Monte Carlo method, have to be employed. The results of these calculations will be briefly reviewed in the next Section.

4.4.1 The few-nucleon systems

The NN potential determined from the properties of the two-nucleon system can be used to solve Eq. (4.40) for $A > 2$. In the case $A = 3$ the problem can be still solved exactly, but the resulting ground state energy, E_0, turns out to be slightly different from the experimental value. For example, for ^3He one typically finds $E_0 = 7.6$ MeV, to be compared to $E_{exp} = 8.48$ MeV. In order to exactly reproduce E_{exp} one has to add to the nuclear hamiltonian a term containing three-nucleon interactions described by a potential V_{ijk}. The most important process leading to three nucleon interactions is the two-pion exchange associated with the excitation of a nucleon resonance in the intermediate state, depicted in Fig. 4.4.

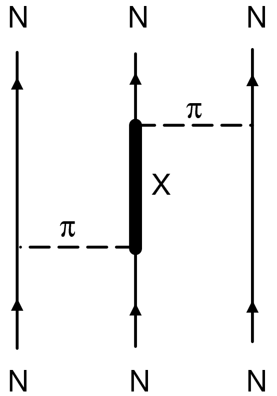

Figure 4.4: Diagrammatic representation of the process providing the main contribution to the three-nucleon interaction. The thick solid line corresponds to an excited state of the nucleon.

The three-nucleon potential is usually written in the form

$$V_{ijk} = V_{ijk}^{2\pi} + V_{ijk}^{N} \ , \tag{4.41}$$

where the first contribution takes into account the process of Fig. 4.4 while V_{ijk}^N is purely phenomenological. The two parameters entering the definition of the three-body potential are adjusted in such a way as to reproduce the properties of ${}^3H$ and $3He$. Note that the inclusion of V_{ijk} leads to a very small change of the total potential energy, the ratio $\langle v_{ij} \rangle / \langle V_{ijk} \rangle$ being ~ 2 %.

For $A > 3$ the Scrödinger equation is no longer exactly solvable. The ground state energy of nuclei having $A \geq 4$ can be estimated from Ritz principle, stating that the expectation value of the hamiltonian in the trial state $|\Psi_V\rangle$ satisfies

$$E_V = \frac{\langle \Psi_V | H | \Psi_V \rangle}{\langle \Psi_V | \Psi_V \rangle} \geq E_0 \ , \tag{4.42}$$

E_0 being the ground state energy. Obviously, the larger the overlap $\langle \Psi_0 | \Psi_V \rangle$ the closer E_V is to E_0.

In the variational approach based on Eq. (4.42) E_0 is estimated carrying out a functional minimization of E_V. The trial ground state is written in such a way as to reflect the structure of the nuclear interaction hamiltonian. For few nucleon systems it takes the form

$$|\Psi_V\rangle = (1 + U) \, |\Psi_P\rangle \ , \tag{4.43}$$

where

$$|\Psi_P\rangle = F | \Phi_A(J J_3 T T_3) \rangle \ . \tag{4.44}$$

In the above equations $|\Phi_A(JJ_3TT_3)\rangle$ is a shell model state, describing A independent particles coupled to total angular momentum J and total isospin T, with third components J_3 and T_3, while the operators U and F take into acount the correlation structure induced by the two- and three-nucleon potentials, respectively. The dominant correlation effects, associated with the NN potential v_{ij}, are described by the operator F, which is usually written

$$F = \mathcal{S} \prod_{j>i=1}^{A} f_{ij} \ , \tag{4.45}$$

where $\mathcal{S}$ is the symmetrization operator and (compare to Eq. (4.36))

$$f_{ij} = \sum_{n=1}^{6} f^{(n)}(r_{ij}) O_{ij}^{(n)} \ . \tag{4.46}$$

The shape of the radial correlation functions $f^{(n)}$ are determined by minimizing the expectation value E_V. In few nucleon systems this procedure is implemented choosing suitable analytical expressions involving few adjustable parameters.

The main features of the $f^{(n)}$ are dictated by the behaviour of the corresponding component of the potential v_{ij}. For example, due to the presence of the strong repulsive core $f^{(n)}(r) \ll 1$ at $r \lesssim 1$ fm. A typical set of radial correlation functions is shown in Fig. 4.5.

The main difficulty of the variational approach is the calculation of the expectation value E_V, involving an integration over $3A$ space coordinate as well as a sum over the spin-isospin degrees of freedom, which makes the dimensionality of the problem very difficult to handle for $A \geq 8$.

To understand this problem, let us write the variational state in the form

$$|\Psi_V\rangle = \sum_n \Psi_n(R) |n\rangle \ , \tag{4.47}$$

where the sum includes all possible spin-isospin states, labelled by the index n, and $R \equiv \{\mathbf{r}_1, \ldots, \mathbf{r}_A\}$ specifies the space configuration of the system. For example, in the case of ^3He ($J = T = 1/2$) one finds

$$\begin{aligned}
|1\rangle &= |\uparrow p \ \uparrow n \ \downarrow n \ \rangle \\
|2\rangle &= |\downarrow p \ \uparrow n \ \downarrow n \ \rangle \\
|3\rangle &= |\downarrow n \ \uparrow p \ \downarrow n \ \rangle \\
\ldots &= \ldots\ldots
\end{aligned} \tag{4.48}$$

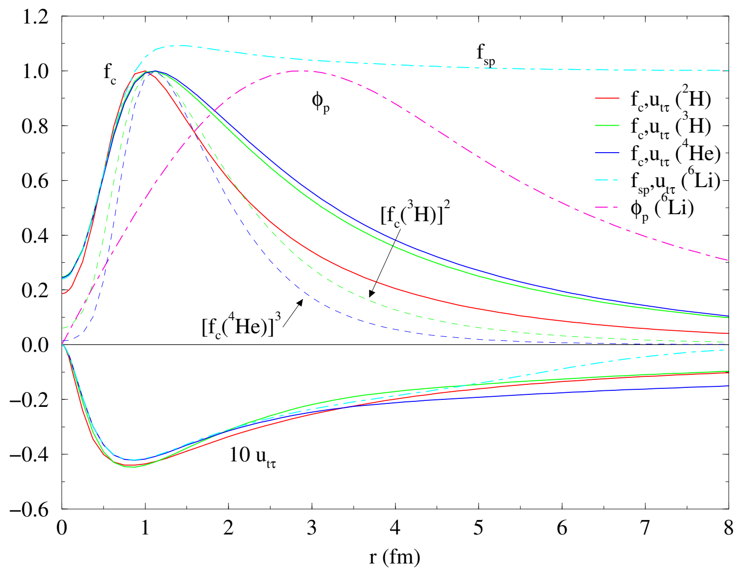

Figure 4.5: Correlation functions in few nucleon systems: the central and tensor-isospin components $f^{(1)}$ and $f^{(4)}$ are denoted by f_c and $u_{t\tau}$, respectively. The dashed lines show $f_c^2(^3\mathrm{H})$ and $f_c^3(^4\mathrm{He})$ to illustrate the large r behavior. The dot-dashed line marked ϕ_p shows the independent particle model wave function for ^{6}Li.

The possible spin states of A spin-1/2 particles are 2^A and, since Z of the A nucleons can be protons, there are $A!/Z!(A-Z)!$ isospin states. Hence, the sum over n in Eq. (4.47) involves

$$M = 2^A \, \frac{A!}{Z!(A-Z)!} \tag{4.49}$$

contributions.

In the representation of Eq. (4.47) the nuclear hamiltonian H is a $M \times M$ matrix whose elements depend upon R. To obtain E_V one has to evaluate the $M \times M$ integrals

$$\int dR \Psi_n^\dagger(R) H_{nm} \Psi_m(R) \ , \tag{4.50}$$

whose calculation is carried out using the Monte Carlo (MC) method.

The expectation value of any operator O in the state Ψ_V can be written in the form

$$\begin{aligned}\langle O\rangle &= \sum_{m,n}\int dR\left[\frac{\Psi_m^\dagger(R)O_{mn}(R)\Psi_n(R)}{P_{mn}(R)}\right]P_{mn}(R)\\ &= \sum_{m,n}\int dR\,\widetilde{O}_{mn}(R)P_{mn}(R)\ ,\end{aligned} \tag{4.51}$$

with

$$\widetilde{O}_{mn} = \frac{\Psi_m^\dagger(R)O_{mn}(R)\Psi_n(R)}{P_{mn}(R)}\ , \tag{4.52}$$

the probability distribution $P_{mn}(\mathbf{R})$ being given by

$$P_{mn}(R) = |\mathrm{Re}(\Psi_m^\dagger(R)\Psi_n(R))|\ . \tag{4.53}$$

Let $\{R_p\} \equiv \{R_1,\ldots,R_{N_c}\}$ be a set of N_c configurations drawn from the probability distribution of Eq. (4.51), i.e. such that the probability that a configuration $\widetilde{R}$ belongs to the set $\{R_p\}$ is proportional to $P_{mn}(R)$. It then follows that

$$\int dR\,\widetilde{O}_{mn}(R)P_{mn}(R) = \lim_{N_c\to\infty}\frac{1}{N_c}\sum_{p=1}^{N_c}\widetilde{O}_{mn}(R_p)\ . \tag{4.54}$$

The above procedure, called Variational Monte Carlo (VMC) method, allows one to obtain estimates of the ground state energy E_0 whose accuracy is limited by the statistical error associated with the use of a finite configuration set and by the uncertainty in the choice of the trial wave function. The second source of error can be removed using the Green Function Monte Carlo (GFMC) approach.

Let $\{|\Psi_m\rangle\}$ be the complete set of eigenstates of the nuclear hamiltonian, satisfying

$$H|\Psi_m\rangle = E_m|\Psi_m\rangle\ . \tag{4.55}$$

The trial variational wave function can obviously be expanded according to

$$|\Psi_V\rangle = \sum_n \beta_n\ |\Psi_m\rangle\ , \tag{4.56}$$

implying

$$\lim_{\tau\to\infty}\mathrm{e}^{-H\tau}|\Psi_V\rangle = \lim_{\tau\to\infty}\sum_n\beta_n\ \mathrm{e}^{-E_m\tau}|\Psi_m\rangle = \beta_0\ \mathrm{e}^{-E_0\tau}|\Psi_0\rangle\ . \tag{4.57}$$

Hence, evolution of the variational ground state to infinite imaginary time projects out the *true* ground state of the nuclear hamiltonian and allows one to extract the corresponding eigenvalue.

The calculation is carried out dividing the imaginary time interval τ in N steps of length $\Delta\tau = \tau/N$ to rewrite

$$e^{-H\tau} = \left(e^{-H\Delta\tau}\right)^N \ . \tag{4.58}$$

The state at imaginary time $(i+1)\Delta\tau$ is can be obtained from the one corresponding to $\tau = i\Delta\tau$ through the relation

$$|\Psi_V^{i+1}\rangle = e^{-H\Delta\tau}|\Psi_V^i\rangle \ , \tag{4.59}$$

that can be rewritten ($|RST\rangle$ specifies the configuration of the system in coordinate, spin and isospin space)

$$\langle R'S'T'|\Psi_V^{i+1}\rangle = \sum_{ST}\int dR\ \langle R'S'T'|e^{-H\Delta\tau}|RST\rangle\langle RST|\Psi_V^i\rangle \tag{4.60}$$

or

$$\Psi_{V,S'T'}^{i+1}(R) = \sum_{ST}\int dR\ G_{S'T',ST}(R',R)\Psi_{V,ST}^i(R) \ , \tag{4.61}$$

The Green's function appearing in the above equation, yielding the amplitude for the system to evolve from $|RST\rangle$ to $|R'S'T'\rangle$ during the imaginary time interval $\Delta\tau$, is defined as

$$G_{S'T',ST}(R',R) = \langle R'S'T'|e^{-H\Delta\tau}|RST\rangle \ . \tag{4.62}$$

The GFMC approach has been succesfully employed to describe the ground state and the low lying excited states of nuclei having A up to 8. The results of these calculations, summarized in Table 4.1 and Fig. 4.6, show that the nonrelativistic approach, based on a dynamics modeled to reproduce the properties of two- and three-nucleon systems, has a remarkable predictive power.

4.4.2 Nuclear matter

In the case of neutron stars, correponding to A $\sim 10^{57}$, the computational techniques described in Section 4.4.1 cannot be applied and approximations need to be made.

In the simplest scheme the complicated NN potential is replaced by a *mean field*. This amount to substituting

$$\sum_{j>i=1}^{A} v_{ij} \to \sum_{i=1}^{A} U_i \ , \tag{4.63}$$

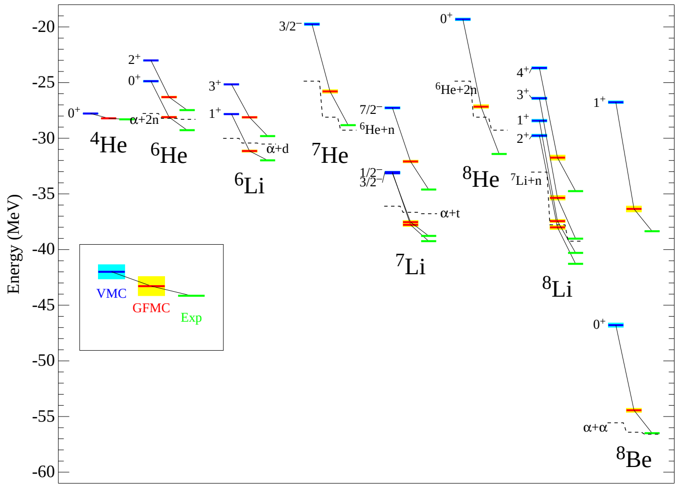

Figure 4.6: VMC and GFMC energies of nuclei with $A \leq 8$ compared to experiment.

in Eq. (4.39), witht the potential U chosen in such a way that the *single particle* hamiltonian

$$h_0 = \frac{p^2}{2m} + U \tag{4.64}$$

be diagonalizable. Within this framework the nuclear ground state wave function reduces to a Slater determinant, constructed using the A lowest energy eigenstates of h_0:

$$|\Psi_0\rangle = \frac{1}{\sqrt{A!}} \det\{\phi_i\} \ , \tag{4.65}$$

the ϕ_i's (i = 1, 2,. . ., A) being solutions of the Schrödinger equation

$$h_0|\phi_i\rangle = \epsilon_i|\phi_i\rangle \ , \tag{4.66}$$

and the corresponding ground state energy is given by

$$E_0 = \sum_{i=1}^{A} \epsilon_i \ . \tag{4.67}$$

This procedure is the basis of the nuclear shell model, that has been succesfully applied to explain many nuclear properties.

Matter in the neutron star interior, however, is a uniform, dense nuclear fluid, whose single particle wave functions are known to be plane waves, as dictated by translational invariace. Shell effects are not expected to play a

$^AZ(J^\pi;T)$	VMC (Ψ_T)	VMC (Ψ_V)	GFMC	Expt
^{2}H$(1^+;0)$	–2.2248(5)			–2.2246
^{3}H$((1/2)^+;1/2)$	–8.15(1)	–8.32(1)	–8.47(1)	–8.48
^{4}He$(0^+;0)$	–26.97(3)	–27.78(3)	–28.34(4)	–28.30
^{6}He$(0^+;1)$	–23.64(7)	–24.87(7)	–28.11(9)	–29.27
^{6}Li$(1^+;0)$	–27.10(7)	–27.83(5)	–31.15(11)	–31.99
^{7}He$((3/2)^-;3/2)$	–18.05(11)	–19.75(12)	–25.79(16)	–28.82
^{7}Li$((3/2)^-;1/2)$	–31.92(11)	–33.04(7)	–37.78(14)	–39.24
^{8}He$(0^+;2)$	–17.98(8)	–19.31(12)	–27.16(16)	–31.41
^{8}Li$(2^+;1)$	–28.00(14)	–29.76(13)	–38.01(19)	–41.28
^{8}Be$(0^+;0)$	–45.47(16)	–46.79(19)	–54.44(19)	–56.50

Table 4.1: Experimental and quantum Monte Carlo ground state energies of nuclei with A=2-8 in MeV. The columns marked VMC(Ψ_V) and GFMC show the VMC and GFMC results, respectively.

major role in such a system. On the other hand, strong correlations between nucleons induced by the NN potential, not taken into account within the mean field approximation, become more and more important as the density increases, and can not be disregarded.

Let us first consider symmetric nuclear matter, defined as a uniform extended system containing equal numbers of proton and neutrons which interact through strong interactions only. Neglecting, for the sake of simplicity, three-nucleon forces, the nuclear matter hamiltonian can be written as in Eq.(A.1) with v_{ij} denoting the NN potential. In absence of interactions, the wave function is a Slater determinant of single particle states

$$\varphi_{\mathbf{k}\sigma\tau}(\mathbf{r}) = \frac{1}{\sqrt{V}} \mathrm{e}^{\mathbf{k}\cdot\mathbf{r}} \ \chi_\sigma \eta_\tau \ , \tag{4.68}$$

where χ and η are the Pauli spinors describing spin and isospin, respectively, and $|\mathbf{k}| < k_F = (3\pi^2 n/2)^{1/3}$, n being the matter density.

The main problem associated with the application of many-body perturbation theory to nuclear matter is the presence of the strongly repulsive core in the NN potential (see Section 4.2 and Fig. 4.3), that makes the matrix elements

$$\langle \varphi_{\mathbf{k_{1'}}\sigma_{1'}\tau_{1'}} \varphi_{\mathbf{k_{2'}}\sigma_{2'}\tau_{2'}} | v_{12} | \varphi_{\mathbf{k}_1\sigma_1\tau_1} \varphi_{\mathbf{k}_2\sigma_2\tau_2} \rangle \tag{4.69}$$

very large or even divergent. As we will see, this difficulty can be circumvented either through a proper redefintion of the interaction potential or changing the basis of states describing the "unperturbed" system.

A. G-matrix perturbation theory

Within the first approach the hamiltonian is first split in two pieces as in Eq. (A.2) with

$$H_0 = \sum_{i=1}^{N} (K_i + U_i) \ , \tag{4.70}$$

where $K = -\boldsymbol{\nabla}^2/2m$ is the kinetic energy operator, and

$$H_1 = \sum_{j>i=1}^{N} v_{ij} - \sum_{i=1}^{N} U_i \ , \tag{4.71}$$

with the single particle potential generally chosen in such a way as to make the perturbative expansion rapidly convergent. The interaction hamiltonian H_1 is then treated perturbatively, summing up infinite set of diagrams to overcome the problems assciated with the calculation of the matrix elements (4.69). This procedure leads to the integral equation defining the G-matrix

$$G(W) = v - v \ \frac{Q}{W} \ G \ . \tag{4.72}$$

The G-matrix, as diagrammatically illustrated in Fig. 4.7, is the operator describing NN scattering in the nuclear medium. The quantity W appearing in Eq. (4.72) is the energy denominator associated with the propagator of the intermediate state, while the operator Q prevents scattering to states in the Fermi sea, forbidden by Pauli exclusion principle.

The state describing two interacting nucleons ψ_{ij} can be expressed in terms of G through the Bethe-Golstone equation

$$\psi_{ij} = \phi_{ij} - \frac{Q}{W} G \ \psi_{ij} \ , \tag{4.73}$$

where $\phi_{ij} = \varphi_i \varphi_j$, with $\varphi_i = \varphi_{\mathbf{k}_i \sigma_i \tau_i}$ given by Eq. (4.68), is the corresponding unperturbed state. From Eq. (4.73) it follows that the matrix elements of G between unperturbed states

$$\langle \phi_{i'j'} | G | \phi_{ij} \rangle = \langle \phi_{i'j'} | v | \psi_{ij} \rangle \tag{4.74}$$

are well behaved.

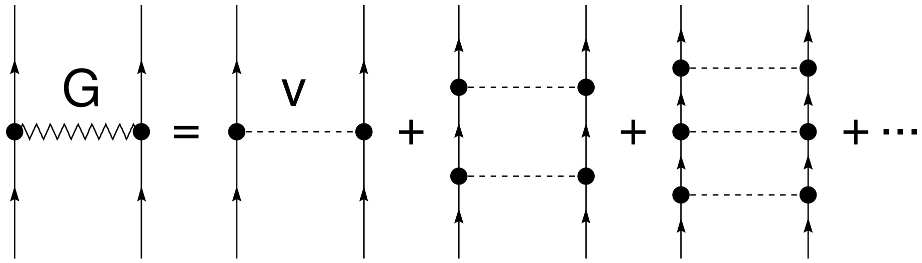

Figure 4.7: Diagrammatic representation of Eq. (4.72).

Although the expansion in powers of G is still not convergent, the terms in the perturbative series can be grouped in such a way as to obtain a convergent expansion in powers of the quantity

$$\kappa = n \sum_{ij} \int d^3r |\phi_{ij}(r) - \psi_{ij}(r)|^2 \ , \tag{4.75}$$

where the sum is extended to all states belonging to the Fermi sea. The definition shows that κ measures the average distortion of the two-nucleon wave function produced by NN forces.

Nuclear matter calculations carried out within G-matrix perturbation theory include contributions of order κ^3 to the energy per nucleon. The results show that the convergence strongly depends on the choice of the single particle potential U.

B. CBF perturbation theory

In the alternative approach, called Correlated Basis Functions (CBF) perturbation theory, the nonperturbative effects arising from the short range repulsive core of the interaction potential are incorporated in the basis functions. The unperturbed Fermi gas states $|n_0\rangle$ are replaced by the set of correlated states

$$|n\rangle = \frac{F|n_0\rangle}{\langle n_0|F^\dagger F|n_0\rangle^{1/2}} \ , \tag{4.76}$$

where F is the *correlation operator*, whose structure reflects the complexity of the NN potential. In most nuclaer matter applications F is written in the form

$$F = \mathcal{S} \prod_{j>i=1}^{A} f_{ij} \ , \tag{4.77}$$

where

$$f_{ij} = \sum_n f^{(n)}(r_{ij}) O_{ij}^{(n)} \ , \tag{4.78}$$

$\mathcal{S}$ is the operator that symmetrizes the product on its right hand side and the operators $O^{(n)}$ are defined in Eq. (4.38).

The correlated states (4.76) form a complete set but are *not* orthogonal to one another. However, they can be orthogonalized using standard techniques of many-body perturbation theory.

The radial shapes of the $f^{(n)}(r)$ are determined minimizing the expectation value $E_V = \langle 0|H|\rangle$. In nuclear matter, this procedure leads to a set of Euler-Lagrange equations, whose solutions satisfy the conditions

$$\lim_{r\to\infty} f^{(n)}(r) = \left\{ \begin{array}{ll} 1 & n = 1 \\ 0 & n > 1 \end{array} \right. \ . \tag{4.79}$$

The short range behaviour of the two-nucleon correlation finctions is such that the quantity

$$f_{ij}^\dagger H_{ij} f_{ij} = f_{ij}^\dagger \left(\frac{\mathbf{p}_i^2}{2m} + \frac{\mathbf{p}_j^2}{2m} + v_{ij} \right) f_{ij}, \tag{4.80}$$

which reduces to H_{ij} at large interparticel distances, is well behaved as $r \to 0$.

Once the correlated basis has been defined, the nuclear hamiltonian can be split in two pieces according to Eq. (A.2), where H_0 and H_1 are now defined as the diagonal and off diagonal part of H in the correlated basis, respectively. We can then write

$$\langle m|H_0|n\rangle = \delta_{mn} \langle m|H|n\rangle \tag{4.81}$$

$$\langle m|H_1|n\rangle = (1 - \delta_{mn}) \langle m|H|n\rangle \ . \tag{4.82}$$

If the two-body correlation function has been properly chosen, i.e. if E_V is close to the eigenvalue E_0, the correlated states have large overlaps with the true eigenstates of the nuclear hamiltonian and the matrix elements of H_1 are small. Hence, the perturbative expansion in powers of H_1 is expected to be rapidly convergent.

The explicit calculation of matrix elements of H between correlated states involves prohibitive difficulties, as it requires integrations over the coordinates of a huge number of particles. It is usually performed expanding the matrix element in a series whose terms represent the contributions of subsystems (clusters) containing an increasing number (2, 3, ..., A) of nucleons. The terms in the series can be classified according to their topological structure and summed up to all orders solving a set of coupled integral equations, called Fermi Hyper-Netted Chain (FHNC) equations.

4.5 Relativistic mean field theory

The theoretical approach described in the previous section is based on the assumption that the degrees of freedom associated with the carriers of the NN interaction can be eliminated in favor of a static NN potential. While this procedure appears to be most succesful at $\rho \sim \rho_0$, as matter density (and therefore the nucleon Fermi momentum) increases the relativistic propagation of the nucleons, as well as the retarded propagation of the virtual meson fields giving rise to nuclear forces, are expected to become more and more important.

In principle, relativistic quantum field theory provides a well defined theoretical framework in which relativistic effects can be taken into account in a fully consistent fashion. Due to the complexity and nonperturbative nature of the interaction, however, the *ab initio* approach to the nuclear many problem, based on the QCD lagrangian, involves prohibitive difficulties. In fact, even the structure of individual hadrons, like the proton or the π meson, is not yet understood at a fully quantitative level in terms of QCD degrees of freedom. Let alone the structure of highly condensed hadronic matter at supernuclear densities.

It has to be pointed out, however, that when dealing with condensed matter it is often convenient to replace the lagrangian describing the interactions between elementary constituents, be it solvable or not, with properly constructed *effective interactions*. For example, the properties of highly condensed systems bound by electromagnetic interactions are most successfully explained using effective interatomic potentials. In spite of the fact that the lagrangian of quantum electrodynamics is very well known and can be treated in perturbation theory, nobody in his right mind would ever use it to carry out explicit calculations in condensed matter physics.

The fact that most of the time nucleons in nuclear matter behave as individual particles interacting through boson exchange (see Lecture 3), suggests that the fundamental degrees of freedom of QCD, quarks and gluons, may indeed be replaced by nucleons and mesons, to be regarded as the degrees of freedom of an *effective* field theory.

In this section we will describe a simple model in which nulcear matter is viewed as a static uniform system of nucleons, described by Dirac spinors, interacting through exchange of a scalar and a vector meson, called σ and ω, respectively.

The basic ingredient of the σ-ω model is the lagrangian density

$$\mathcal{L} = \mathcal{L}_N + \mathcal{L}_B + \mathcal{L}_{int} \ , \tag{4.83}$$

where $\mathcal{L}_N$, $\mathcal{L}_B$ and $\mathcal{L}_{int}$ describe free nucleons and mesons and their interactions, respectively. The dynamics of the free nucleon field is dictated by the Dirac lagrangian of Eq. (4.24)

$$\mathcal{L}_N(x) = \overline{\psi}(x)\,(i\partial\!\!\!/ - m)\,\psi(x)\ , \tag{4.84}$$

where the nucleon field, denoted by $\psi(x)$, combines the two four-component Dirac spinors describing proton and neutron, as in Eq. (4.25). The meson lagrangian reads

$$\begin{aligned}\mathcal{L}_B(x) &= \mathcal{L}_\omega(x) + \mathcal{L}_\sigma(x) \\ &= -\frac{1}{4}F^{\mu\nu}(x)F_{\mu\nu}(x) + \frac{1}{2}m_\omega^2 V_\mu(x)V^\mu(x) \\ &+ \frac{1}{2}\partial_\mu\phi(x)\partial^\mu\phi(x) - \frac{1}{2}m_\sigma^2\phi(x)^2\end{aligned} \tag{4.85}$$

where

$$F_{\mu\nu}(x) = \partial_\mu V_\nu(x) - \partial_\nu V_\mu(x)\ , \tag{4.86}$$

$V_\mu(x)$ and $\sigma(x)$ are the vector and scalar meson fields, respectively, and m_ω and m_σ the corresponding masses.

In specifying the form of the interaction lagrangian we will require that, besides being a Lorentz scalar, $\mathcal{L}_{int}(x)$ give rise to a Yukawa-like meson exchange potential in the static limit. Hence, we write

$$\mathcal{L}_{int}(x) = g_\sigma\phi(x)\overline{\psi}(x)\psi(x) - g_\omega V_\mu(x)\overline{\psi}(x)\gamma^\mu\psi(x)\ , \tag{4.87}$$

where g_σ and g_ω are coupling constants and the choice of signs reflect the fact that the NN interaction contains both attractive and repulsive contributions.

The equations of motion for the fields follow from the Euler-Lagrange equations associated with the lagrangian density of Eq. (4.83). The meson fields satisfy

$$(\Box + m_\sigma^2)\phi(x) = g_\sigma\ \overline{\psi}(x)\psi(x) \tag{4.88}$$

and

$$(\Box + m_\omega^2)V_\mu(x) - \partial_\mu(\partial^\nu V_\nu) = g_\omega\ \overline{\psi}(x)\gamma_\mu\psi(x)\ , \tag{4.89}$$

while the evolution of the nucleon field is dictated by the equation

$$\left[(\partial\!\!\!/ - g_\omega\gamma_\mu V^\mu(x)) - (m - g_\sigma\phi(x))\right]\psi(x) = 0\ . \tag{4.90}$$

The above coupled equations are fully relativistic and Lorentz covariant. However, their solution involves prohibitive difficulties. Here we will restrict ourselves to the discussion of an approximation scheme widely used to solve Eqs. (4.88)-(4.90), known as *mean field* approximation, that essentially amounts to treat $\phi(x)$ and $V_\mu(x)$ as classical fields.

We replace the meson field with their mean values in the ground state of static and uniform nuclear matter

$$\phi(x) \to \langle\phi(x)\rangle \ , \quad V_\mu(x) \to \langle V_\mu(x)\rangle \ , \tag{4.91}$$

where $\langle\phi(x)\rangle$ and $\langle V_\mu(x)\rangle$ must be computed from the equations of motion. In static and uniform nuclear matter the baryon and scalar densities, $n_B = \psi^\dagger\psi$ and $n_s = \overline{\psi}\psi$, as well as the current $j_\mu = \overline{\psi}\gamma_\mu\psi$, are constants, independent of x. As a consequence, the mean values of the meson fields are also constants satisfying the relations

$$m_\sigma^2 \ \langle\phi\rangle = g_\sigma\langle\overline{\psi}\psi\rangle \tag{4.92}$$

$$m_\omega^2 \ \langle V_0\rangle = g_\omega\langle\psi^\dagger\psi\rangle \tag{4.93}$$

$$m_\omega^2 \ \langle V_i\rangle = g_\omega\langle\overline{\psi}\gamma_i\psi\rangle \ , \quad i = 1,2,3 \ . \tag{4.94}$$

The nucleon equation of motion, rewritten in terms of the mean values of the meson fields, reads

$$\left[(\partial\!\!\!/ - g_\omega\gamma_\mu\langle V^\mu\rangle) - (m - g_\sigma\langle\phi\rangle)\right]\psi(x) = 0 \ . \tag{4.95}$$

In static and uniform matter, the nucleon states must be eigenstates of the four-momentum operator, that can be written as

$$\psi_{\mathbf{k}}\mathrm{e}^{ikx} = \psi_{\mathbf{k}}\mathrm{e}^{ik_\mu x^\mu} = \psi_{\mathbf{k}}\mathrm{e}^{i(k_0 t - \mathbf{k}\cdot\mathbf{r})} \ , \tag{4.96}$$

the $\psi_{\mathbf{k}}$ being solutions of

$$\begin{aligned}&\left[(k\!\!\!/ - g_\omega\gamma_\mu\langle V^\mu\rangle) - (m - g_\sigma\langle\phi\rangle)\right]\psi_{\mathbf{k}} \\ &\qquad = \left[\gamma_\mu\left(k^\mu - g_\omega\langle V^\mu\rangle\right) - (m - g_\sigma\langle\phi\rangle)\right]\psi_{\mathbf{k}} = 0 \ .\end{aligned} \tag{4.97}$$

The above equation can be recast in a form reminiscent of the Dirac equation. Defining

$$K_\mu = k_\mu - g_\omega\langle V^\mu\rangle \tag{4.98}$$

$$m^* = m - g_\sigma\langle\phi\rangle \ , \tag{4.99}$$

we obtain

$$\left(K\!\!\!/ - m^*\right)\psi_{\mathbf{k}} = 0. \tag{4.100}$$

The corresponding energy eigenvalues can be found from

$$\begin{aligned}\left(K\!\!\!/ + m^*\right)\left(K\!\!\!/ - m^*\right) &= K\!\!\!/K\!\!\!/ - m^{*2} = K_\mu K_\nu\gamma^\mu\gamma^\nu - m^{*2} \\ &= K_\mu K_\nu\frac{\gamma^\mu\gamma^\nu + \gamma^\nu\gamma^\mu}{2} - m^{*2} \\ &= K_\mu K^\mu - m^{*2} \ ,\end{aligned} \tag{4.101}$$

implying

$$\left(K_\mu K^\mu - m^{*2}\right)\psi_{\mathbf{k}} = 0 \ , \tag{4.102}$$

leading to

$$\left(K_\mu K^\mu - m^{*2}\right) = 0 \tag{4.103}$$

and

$$\begin{aligned} K_0 &= E_{\mathbf{k}} = k_0 - g_\omega \langle V_0 \rangle = \sqrt{|\mathbf{K}|^2 + m^{*2}} \\ &= \sqrt{|\mathbf{k} - g_\omega \langle \mathbf{V} \rangle|^2 + (m - g_\sigma \langle \phi \rangle)^2} \ . \end{aligned} \tag{4.104}$$

It follows that the energy eigenvalues associated with nucleons and antinucleons can be written

$$e_{\mathbf{k}} = E_{\mathbf{k}} + g_\omega \langle V_0 \rangle \tag{4.105}$$

and

$$\overline{e}_{\mathbf{k}} = E_{\mathbf{k}} - g_\omega \langle V_0 \rangle \ , \tag{4.106}$$

respectively. The above equations give the nucleon (and antinucleon) energies in terms of the mean values of the meson fields, which are in turn defined in terms of the ground state expectation values of the nucleon densities and current, according to Eqs. (4.92)-(4.94).

The ground state expectation value of an operator $\overline{\psi}\Gamma\psi$ can be evaluated exploiting the fact that each nucleon state is specified by its momentum, $\mathbf{k}$, and spin-isospin projections. Denoting the average of $\overline{\psi}\Gamma\psi$ in a single particle state by $\langle\overline{\psi}\Gamma\psi\rangle_{\mathbf{k}\alpha}$, where the index α labels the spin-isospin state, we can write the ground state expectation value as

$$\langle\overline{\psi}\Gamma\psi\rangle = \sum_\alpha \int \frac{d^3k}{(2\pi)^3} \ \langle\overline{\psi}\Gamma\psi\rangle_{\mathbf{k}\alpha} \ \theta(e_F - e_{\mathbf{k}}) \ , \tag{4.107}$$

where the θ-function restricts the momentum integration to the region corresponding to energies lower than the Fermi energy e_F. To obtain the single particle average $\langle\overline{\psi}\gamma_\mu\psi\rangle_{\mathbf{k}\alpha}$, we use Eq. (4.100), implying

$$k_0 = \gamma_0 \left(\boldsymbol{\gamma} \cdot \mathbf{k} + g_\omega \gamma_\mu \langle V^\mu \rangle + m^*\right) \ . \tag{4.108}$$

The quantity defined by the above equation can be regarded as the single nucleon hamiltonian, whose eigenvalues are given by (compare to Eq. (4.105))

$$\langle k_0 \rangle_{\mathbf{k}\alpha} = \langle \psi^\dagger k_0 \psi \rangle_{\mathbf{k}\alpha} = E_{\mathbf{k}} + g_\omega \langle V_0 \rangle \ . \tag{4.109}$$

The ground state expectation value of the baryon density can be readily evaluated from Eqs. (4.108) and (4.109) noting that

$$\begin{aligned} \frac{\partial}{\partial \langle V_0 \rangle} \langle \psi^\dagger k_0 \psi \rangle_{\mathbf{k}\alpha} &= \frac{\partial}{\partial \langle V_0 \rangle} \left(E_{\mathbf{k}} + g_\omega \langle V_0 \rangle \right) = g_\omega \\ &= \langle \psi^\dagger \frac{\partial k_0}{\partial \langle V_0 \rangle} \psi \rangle_{\mathbf{k}\alpha} = g_\omega \langle \psi^\dagger \psi \rangle_{\mathbf{k}\alpha} \ , \end{aligned} \tag{4.110}$$

implying

$$\langle \psi^\dagger \psi \rangle_{\mathbf{k}\alpha} = 1 \ . \tag{4.111}$$

It follows that n_B can be obtained using Eq. (4.107), leading to

$$n_B = \langle \psi^\dagger \psi \rangle = \nu \int \frac{d^3k}{(2\pi)^3} \theta(e_F - e_{\mathbf{k}}) \ , \tag{4.112}$$

where ν is the degeneracy of the momentum eigenstate ($\nu = 2$ and 4 for pure neutron matter and symmetric nuclear matter, respectively).

The same procedure can be applied to calculate the ground state expectation value $\langle \overline{\psi} \gamma^i \psi \rangle$ ($i = 1, 2, 3$). Taking the derivative with respect to k_i we find

$$\begin{aligned} \frac{\partial}{\partial k_i} \langle \psi^\dagger k_0 \psi \rangle_{\mathbf{k}\alpha} &= \frac{\partial}{\partial k_i} \left(E_{\mathbf{k}} + g_\omega \langle V_0 \rangle \right) = \frac{\partial E_{\mathbf{k}}}{\partial k_i} \\ &= \langle \psi^\dagger \frac{\partial k_0}{\partial k_i} \psi \rangle_{\mathbf{k}\alpha} = \gamma^0 \langle \psi^\dagger \gamma^i \psi \rangle_{\mathbf{k}\alpha} = \langle \overline{\psi} \gamma^i \psi \rangle_{\mathbf{k}\alpha} \ , \end{aligned} \tag{4.113}$$

leading to

$$\begin{aligned} \langle \overline{\psi} \gamma^i \psi \rangle &= \nu \int \frac{d^3k}{(2\pi)^3} \left(\frac{\partial E_{\mathbf{k}}}{\partial k_i} \right) \ \theta(e_F - e_{\mathbf{k}}) \\ &= \nu \int \frac{dk_j dk_k}{(2\pi)^3} \int dE_{\mathbf{k}} \ \theta(e_F - e_{\mathbf{k}}) = 0 \ . \end{aligned} \tag{4.114}$$

The above result follows from the fact that, by definition, $e_{\mathbf{k}} \equiv e_F - g_\omega \langle V_0 \rangle$ everywhere on the boundary of the integration region. The vanishing of the baryon current, that could have been anticipated, as we are dealing with uniform matter in its ground state, implies that the mean values of the space components of the vector field also vanish, i.e. that $\langle V_i \rangle = 0$. As a consequence, the energy eigenvalues depend upon the magnitude of the nucleon momentum only, according to

$$e_{\mathbf{k}} = e_k = \sqrt{|\mathbf{k}|^2 + (m - g_\sigma \langle \phi \rangle)^2} + g_\omega \langle V_0 \rangle \ , \tag{4.115}$$

and the occupied region of momentum space is sphere. Eq. (4.112) then shows that in symmetric nuclear matter, with Z=(A−Z)=A/2, the baryon density takes the familiar form $n_B = 2k_F^3/(3\pi^2)$, k_F being the Fermi momentum.

Finally, the scalar density $n_s = \langle\overline{\psi}\psi\rangle$ can be evaluated from the derivative of $\langle\psi^\dagger k_0 \psi\rangle_{\mathbf{k}\alpha}$ with respect to m:

$$\frac{\partial}{\partial m}\langle\psi^\dagger k_0 \psi\rangle_{\mathbf{k}\alpha} = \frac{\partial e_{\mathbf{k}}}{\partial m} = \langle\psi^\dagger \frac{\partial k_0}{\partial m}\psi\rangle_{\mathbf{k}\alpha} = \langle\psi^\dagger\gamma_0\psi\rangle_{\mathbf{k}\alpha} = \langle\overline{\psi}\psi\rangle_{\mathbf{k}\alpha} \ , \tag{4.116}$$

yielding

$$\langle\overline{\psi}\psi\rangle_{\mathbf{k}\alpha} = \frac{(m - g_\sigma\langle\phi\rangle)}{\sqrt{|\mathbf{k}|^2 + (m - g_\sigma\langle\phi\rangle)^2}} \tag{4.117}$$

and

$$\langle\overline{\psi}\psi\rangle = \frac{\nu}{2\pi^2}\int_0^{k_F} k^2 dk \ \frac{(m - g_\sigma\langle\phi\rangle)}{\sqrt{|\mathbf{k}|^2 + (m - g_\sigma\langle\phi\rangle)^2}} \tag{4.118}$$

Collecting together the results of Eqs. (4.112), (4.114) and (4.118) we can rewrite the equations of motion (4.88)-(4.90) in the form:

$$g_\sigma\langle\phi\rangle = \left(\frac{g_\sigma}{m_\sigma}\right)^2 \frac{\nu}{2\pi^2}\int_0^{k_F} |\mathbf{k}|^2 d|\mathbf{k}| \ \frac{(m - g_\sigma\langle\phi\rangle)}{\sqrt{|\mathbf{k}|^2 + (m - g_\sigma\langle\phi\rangle)^2}} \tag{4.119}$$

$$g_\omega\langle V_0\rangle = \left(\frac{g_\omega}{m_\omega}\right)^2 \nu \ \frac{k_F^3}{6\pi^2} \tag{4.120}$$

$$m_\omega^2\langle V_i\rangle = 0, \quad i = 1,2,3 \ . \tag{4.121}$$

Note that, while Eqs. (4.120) and (4.121) are trivial, Eq. (4.119) implies a self-consistency requirement on the mean value of the scalar field, whose value has to satisfy a transcendental equation.

To obtain the equation of state, i.e. the relation between pressure and density (or energy density) of matter, in quantum field theory we start from the energy-momentum tensor, that for a generic Lagrangian $\mathcal{L} = \mathcal{L}(\phi, \partial_\mu\phi)$ can be written

$$T^{\mu\nu} = \frac{\partial\mathcal{L}}{\partial(\partial_\mu\phi)}\partial^\nu\phi - g^{\mu\nu}\mathcal{L} \ , \tag{4.122}$$

$g^{\mu\nu}$ being the metric tensor.

In a uniform system the expectation value of $T^{\mu\nu}$, is directly related to the energy density, ϵ, and pressure, P, through

$$\langle T_{\mu\nu}\rangle = u_\mu u_\nu\,(\epsilon + P) - g_{\mu\nu}P \ , \tag{4.123}$$

where u denotes the four velocity of the system, satisfying $u_\mu u^\mu = 1$. It follows that in the reference frame in which matter is at rest $\langle T_{\mu\nu} \rangle$ is diagonal and

$$\epsilon = \langle T_{00} \rangle = -\langle \mathcal{L} \rangle + \langle \overline{\psi} \gamma_0 k_0 \psi \rangle \tag{4.124}$$

$$P = \frac{1}{3} \langle T_{ii} \rangle = \langle \mathcal{L} \rangle + \frac{1}{3} \langle \overline{\psi} \gamma_i k_i \psi \rangle. \tag{4.125}$$

Within the mean field approximation, the lagrangian density of the σ-ω model reduces to

$$\mathcal{L}_{MF} = \overline{\psi} \left[i \partial\!\!\!/ - g_\omega \gamma^0 \langle V_0 \rangle - (m - g_\sigma \langle \phi \rangle) \right] \psi - \frac{1}{2} m_\sigma^2 \langle \phi \rangle^2 + \frac{1}{2} m_\omega^2 \langle V_0 \rangle^2 \ , \tag{4.126}$$

implying

$$T^{\mu\nu}_{MF} = i \overline{\psi} \gamma^\mu \partial^\nu \psi - g^{\mu\nu} \left[-\frac{1}{2} m_\sigma^2 \langle \phi \rangle^2 - \frac{1}{2} m_\omega^2 \langle V_0 \rangle^2 \right] \ . \tag{4.127}$$

As a consequence, Eqs. (4.124) and (4.125) become

$$\epsilon = -\langle \mathcal{L}_{MF} \rangle + \langle \overline{\psi} \gamma_0 k_0 \psi \rangle \tag{4.128}$$

$$P = \langle \mathcal{L}_{MF} \rangle + \frac{1}{3} \langle \overline{\psi} \gamma_i k_i \psi \rangle, \tag{4.129}$$

where (use Eqs. (4.109), (4.115) and (4.120))

$$\begin{aligned} \langle \overline{\psi} \gamma_0 k_0 \psi \rangle &= \frac{\nu}{2\pi^2} \int_0^{k_F} |\mathbf{k}|^2 d|\mathbf{k}| \left[\sqrt{|\mathbf{k}|^2 + (m - g_\sigma \langle \phi \rangle)^2} + g_\omega \langle V_0 \rangle \right] \\ &= g_\omega \langle V_0 \rangle n_B + \frac{\nu}{2\pi^2} \int_0^{k_F} |\mathbf{k}|^2 d|\mathbf{k}| \ \sqrt{|\mathbf{k}|^2 + (m - g_\sigma \langle \phi \rangle)^2} \\ &= \frac{g_\omega^2}{m_\omega^2} n_B^2 + \frac{\nu}{2\pi^2} \int_0^{k_F} |\mathbf{k}|^2 d|\mathbf{k}| \ \sqrt{|\mathbf{k}|^2 + (m - g_\sigma \langle \phi \rangle)^2} \end{aligned} \tag{4.130}$$

and (use eq.(4.114))

$$\langle \overline{\psi} \gamma_i k_i \psi \rangle = \langle \overline{\psi} (\boldsymbol{\gamma} \cdot \mathbf{k}) \psi \rangle = \frac{\nu}{2\pi^2} \int_0^{k_F} d|\mathbf{k}| \ \frac{|\mathbf{k}|^4}{\sqrt{|\mathbf{k}|^2 + (m - g_\sigma \langle \phi \rangle)^2}} \ . \tag{4.131}$$

Substitution of the above equations into Eqs. (4.128)-(4.129) finally yields (use Eq. (4.126) and the equation of motion for the nucleon field)

$$\epsilon = \frac{1}{2} \frac{m_\sigma^2}{g_\sigma^2} (m - m^*)^2 + \frac{1}{2} \frac{g_\omega^2}{m_\omega^2} n_B^2 + \frac{\nu}{2\pi^2} \int_0^{k_F} |\mathbf{k}|^2 d|\mathbf{k}| \ \sqrt{|\mathbf{k}|^2 + m^{*2}} \tag{4.132}$$

$$P = -\frac{1}{2}\frac{m_\sigma^2}{g_\sigma^2}(m - m^*)^2 + \frac{1}{2}\frac{g_\omega^2}{m_\omega^2}n_B^2 + \frac{1}{3}\ \frac{\nu}{2\pi^2}\int_0^{k_F} d|\mathbf{k}|\ \frac{|\mathbf{k}|^4}{\sqrt{|\mathbf{k}|^2 + m^{*2}}} \quad (4.133)$$

The first two contributions to the right hand side of the above equations arise from the mass terms associated with the vector and scalar fields, while the remaining term gives the energy density and pressure of a relativistic Fermi gas of nucleons of mass m^* given by (see Eq. (4.119))

$$\begin{aligned} m^* &= m - \frac{g_\sigma^2}{m_\sigma^2}\frac{\nu}{2\pi^2}\int_0^{k_F} |\mathbf{k}|^2 d|\mathbf{k}|\ \frac{m^*}{\sqrt{|\mathbf{k}|^2 + m^{*2}}} \\ &= m - \frac{g_\sigma^2}{m_\sigma^2}\frac{m^*}{\pi^2}\left[k_F e_F^* - m^{*2}\ln\left(\frac{k_F + e_F^*}{m^*}\right)\right] \ , \end{aligned} \quad (4.134)$$

with $e_F^* = \sqrt{k_F^2 + m^{*2}}$. Equations (4.132)-(4.134) yield energy density and pressure of nuclear matter as a function of the baryon number density n_B (recall: $k_F = (6\pi^2 n_B/\nu)^{(1/3)}$). The values of the unknown coefficients (m_σ^2/g_σ^2) and (m_ω^2/g_ω^2) can be determined by a fit to the empirical saturation properties of nuclear matter, i.e. requiring

$$\frac{B}{A} = \frac{\epsilon(n_0)}{n_0} - m = -16 \text{ MeV} \quad (4.135)$$

with $n_0 = .16$ fm^{-3}. This procedure leads to the result

$$\frac{g_\sigma^2}{m_\sigma^2}\ m^2 = 267.1 \quad , \quad \frac{g_\omega^2}{m_\omega^2}\ m^2 = 195.9\ . \quad (4.136)$$

Fig. 4.8 shows the binding energies of symmetric nuclear matter (solid line) and pure neutron matter (dashed line) predicted by the $\sigma - \omega$ model, plotted against the Fermi momentum k_F. Note that pure neutron matter is always unbound.

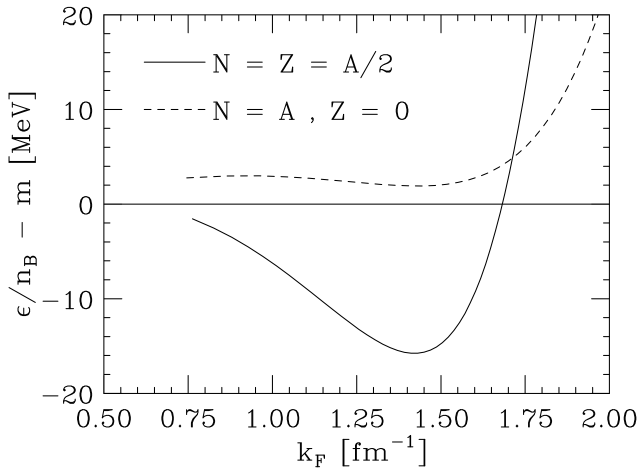

Figure 4.8: Fermi momentum dependence of the binding energy per nucleon of symmetric nuclear matter (solid line) and pure neutron matter (dashed line) evaluated using the $\sigma - \omega$ model and the mean field approximation.

Chapter 5

Matter at supranuclear densities

5.1 Strange hadronic matter

5.2 Quark matter

Elastic and deep inelastic electron scattering experiments have shown that nucleons are extended systems whose constituents are spin 1/2 particles, called quarks. ...

5.2.1 The MIT bag model

In the MIT bag model the main features of QCD are implemented through the assumptions that: i) quarks occur in colour neutral clusters confined to a finite region of space (the bag), whose volume is limited by the pressure of the QCD vacuum (the bag constant B), and ii) residual interactions between quarks are weak, and can be treated using low order perturbation theory.

Neglecting as a first approximation the gluon contribution, the bag model lagrangian density can be written in the form

$$\mathcal{L}(x) = \left\{ \frac{i}{2}[\overline{\psi}\gamma^\mu\partial_\mu\psi - (\partial_\mu\overline{\psi})\gamma^\mu\psi] - B \right\} \theta_V(x) - \frac{1}{2}\overline{\psi}(x)\psi(x)\Delta_S(x) \tag{5.1}$$

where $\psi(x)$ is the Dirac field describing the quarks, assumed to be massless (color and flavor indices are omitted to simplify the notation),

$$\theta_V(x) = \begin{cases} 1 & \text{inside the bag} \\ 0 & \text{outside the bag} \end{cases} , \tag{5.2}$$

and $\Delta_S(x)$ is the surface delta function, satisfying

$$\frac{\partial \theta_V}{\partial x^\mu} = n_\mu \Delta_S , \tag{5.3}$$

n_μ being the spacelike unit vector perpendicular to the bag surface. In the simple case of a spherical cavity of radius R

$$\theta_V = \theta(R-r) \quad , \quad \Delta_S = \delta(R-r) \ . \tag{5.4}$$

The equations of motion

$$\frac{\partial \mathcal{L}}{\partial \overline{\psi}} - \partial_\mu \frac{\partial \mathcal{L}}{\partial(\partial_\mu \overline{\psi})} = 0 \tag{5.5}$$

can be obtained from the lagrangian of Eq. (5.1) through

$$\frac{\partial \mathcal{L}}{\partial \overline{\psi}} = \left(\frac{i}{2}\gamma^\mu \partial_\mu \psi\right)\theta_V - \frac{1}{2}\psi \Delta_S \ , \tag{5.6}$$

$$\partial_\mu \frac{\partial \mathcal{L}}{\partial(\partial_\mu \overline{\psi})} = \left(-\frac{i}{2}\gamma^\mu \partial_\mu \psi\right)\theta_V - \frac{i}{2}\gamma^\mu n_\mu \psi \Delta_S \ . \tag{5.7}$$

Substitution of Eqs. (5.6) and (5.7) into Eq. (5.5) leads to

$$i\gamma^\mu \partial_\mu \psi = 0 \tag{5.8}$$

inside the cavity and

$$i\gamma^\mu n_\mu \psi = \psi \tag{5.9}$$

on its surface.

The physical interpretation of the constant B can be easily understood considering the energy momentum tensor

$$\begin{aligned} T^{\mu\nu} &= -g^{\mu\nu}\mathcal{L} + \left(\frac{\partial \mathcal{L}}{\partial(\partial_\mu \psi)}\partial^\nu \psi + \partial^\nu \overline{\psi}\frac{\partial \mathcal{L}}{\partial(\partial_\mu \overline{\psi})}\right) \\ &= -g^{\mu\nu}\mathcal{L} + \frac{i}{2}(\overline{\psi}\gamma^\mu \partial^\nu \psi - \partial^\nu \overline{\psi}\gamma^\mu \psi)\theta_V \ , \end{aligned} \tag{5.10}$$

satisfying the conservation law

$$\partial_\mu T^{\mu\nu} = 0 \ . \tag{5.11}$$

From Eq. (5.11) it follows that

$$B\Delta_S n^\nu + \frac{i}{2}(\overline{\psi}\gamma^\mu \partial^\nu \psi - \partial^\nu \overline{\psi}\gamma^\mu \psi) n_\mu \Delta_S = 0 \tag{5.12}$$

and

$$\partial_\mu(\overline{\psi}\psi\Delta_S) = 0 \ . \tag{5.13}$$

Substitution of the boundary condition (5.9) into Eq. (5.12) finally yields

$$Bn^\nu = \frac{1}{2}\frac{\partial}{\partial x_\nu}(\overline{\psi}\psi) \ . \tag{5.14}$$

As the right hand side of the above equation is not vanishing, Eq. (5.14) shows that the inclusion of the constant B in the lagrangian density is needed to guarantee four momentum conservation. In fact, Eq. (5.14) is nothing but the pressure balance equation. Using $n^\nu n_\nu = -1$ we find the relation

$$B = -\frac{1}{2} n_\nu \partial^\nu (\overline{\psi}\psi) \ , \tag{5.15}$$

which, in the case of a static spherical cavity, corresponding to $n^\nu \equiv (0, \mathbf{r}/|\mathbf{r}|)$, reduces to

$$B = -\frac{1}{2}\frac{\partial}{\partial r}(\overline{\psi}\psi) \ . \tag{5.16}$$

Hence, B is the inward pressure of the QCD vacuum, needed to balance the outward pressure of the quarks.

5.2.2 The equation of state of quark matter

The thermodynamic functions describing a many-particle system at temperature $T = 1/\beta$ can be obtained from the grand partition function, defined as

$$Z = \mathrm{Tr}\left[\exp\left(-\beta(H - \sum_i \mu_i N_i)\right)\right] \ , \tag{5.17}$$

where H is the hamiltonian operator and μ_i and N_i are the chemical potential and the number operator associated with particles of species i, respectively.

For example, pressure (P) and energy density (ϵ) can be defined in terms of the Gibbs free energy, Ω, which is in turn related to Z through

$$\Omega = -\frac{1}{\beta}\ln Z \ , \tag{5.18}$$

according to

$$P = -\frac{\Omega}{V} \ , \tag{5.19}$$

and

$$\epsilon = \Omega - \sum_i \left(\frac{\partial \Omega}{\partial \mu_i}\right)_{T,V} \ , \tag{5.20}$$

where V is the volume occupied by the system.

In the case of quark matter, due to the properties of QCD described in Section XXXX, Ω consists of two contributions. One of them, that will be denoted Ω_{pert}, is tractable in perturbation theory, while the second one takes into acount nonperturbative effects induced by the properties of the QCD vacuum.

The relation (5.19) between pressure and Gibbs free energy and the interpretation of the bag constant discussed in Section 5.2.1 suggest that within the MIT bag model the difference between Ω and Ω_{pert} can be identified with the bag constant, i.e. that

$$\Omega = \Omega_{pert} + VB \ . \tag{5.21}$$

The perturbative contribution can be expanded according to

$$\Omega_{pert} = V \sum_f \sum_n \Omega_f^{(n)} \ , \tag{5.22}$$

where the index f specifies the quark flavor, while $\Omega_f^{(n)}$ is the n-th order term of the perturbative expansion in powers of the strong coupling constant, α_s.

The EOS of quark matter can be obtained from the relations linking pressure and energy density to Ω:

$$P = -\frac{\Omega}{V} = -B - \sum_f \sum_n \Omega_f^{(n)} \ . \tag{5.23}$$

$$\epsilon = \frac{\Omega}{V} - \sum_f \left(\frac{\partial \Omega}{\partial \mu_f} \right) = -P + \sum_f \mu_f n_f \ , \tag{5.24}$$

n_f and μ_f being the density and chemical potential of the quarks of flavor f.

The lowest order contribution at $T = 0$, reads (compare to Eqs. (1.28) and (1.29))

$$\begin{aligned} \Omega_f^{(0)} \ = \ & -\frac{1}{\pi^2} \left[\frac{1}{4} \mu_f \sqrt{\mu_f^2 - m_f^2} \left(\mu_f^2 - \frac{5}{2} m_f^2 \right) \right. \\ & \left. + \frac{3}{8} m_f^4 \log \frac{\mu_f + \sqrt{\mu_f^2 - m_f^2}}{m_f} \right] \ , \end{aligned} \tag{5.25}$$

where m_f is the quark mass.

Substituting Eq. (5.25) into Eqs. (5.23) and (5.24) and taking the limit of massless quarks one finds the EOS

$$P = \frac{\epsilon - 4B}{3} \ . \tag{5.26}$$

The contribution of first order in α_s, arising from the one-gluon exchange processes discussed in Appendix C, reads

$$\Omega_f^{(1)} = \frac{2\alpha_s}{\pi^3}\left[\frac{3}{4}\left(\mu_f\sqrt{\mu_f^2 - m_f^2} - m_f^2 \log\frac{\mu_f + \sqrt{\mu_f^2 - m_f^2}}{m_f} \right)^2 - \frac{1}{2}(\mu_f^2 - m_f^2)^2\right] . \tag{5.27}$$

The chemical potentials appearing in Eqs.(5.25) and (5.27) can be written

$$\mu_f = e_{F_f} + \delta\mu_f = \sqrt{m_f^2 + p_{F_f}^2} + \delta\mu_f, \tag{5.28}$$

where the first term is the Fermi energy of a gas of noninteracting quarks of mass m_f at density $n_f = p_{F_f}^3/\pi^2$, whereas the second term is a perturbative correction of order α_s, whose explicit expression is

$$\delta\mu_f = \frac{2\alpha_s}{3\pi^2}\left[p_{F_f} - 3\frac{m_{F_f}^2}{e_{F_f}} \log\left(\frac{e_{F_f} + p_{F_f}}{m_f}\right)\right] . \tag{5.29}$$

Including both $\Omega_f^{(0)}$ and $\Omega_f^{(1)}$ in Eqs. (5.23) and (5.24) and taking again the limit of vanishing quark masses one finds

$$P = \frac{1}{4\pi^2}\left(1 - \frac{2\alpha_s}{\pi}\right)\sum_f \mu_f^4 - B \tag{5.30}$$

$$\epsilon = \frac{3}{4\pi^2}\left(1 - \frac{2\alpha_s}{\pi}\right)\sum_f \mu_f^4 + B . \tag{5.31}$$

Comparison to Eq. (5.26) shows that the EOS of a system of massless quarks in unaffected by one-gluon exchange interactions.

For any baryon density, quark densities are dictated by the requirements of baryon number conservation, charge neutrality and weak equilibrium. In the case of two flavors, in which only the light up and down quarks are present, we have

$$n_B = \frac{1}{3}(n_u + n_d) , \tag{5.32}$$

$$\frac{2}{3}n_u - \frac{1}{3}n_d - n_e = 0 \tag{5.33}$$

$$\mu_d = \mu_u + \mu_e , \tag{5.34}$$

where n_e and μ_e denote the density and chemical potential of the electrons produced through

$$d \to u + e^- + \overline{\nu}_e \ . \tag{5.35}$$

Note that we have not taken into account the possible appearance of muons, as in the density region relevant to neutron stars μ_e never exceeds the muon mass.

As the baryon density increases, the d-quark chemical potential reaches the value $\mu_d = m_s$, m_s being the mass of the strange quark. The energy of quark matter can then be lowered turning d-quarks into s-quarks through

$$d + u \to u + s \ . \tag{5.36}$$

In presence of three flavors, Eqs. (5.32)-(5.34) become

$$n_B = \frac{1}{3}(n_u + n_d + n_s) \ , \tag{5.37}$$

$$\frac{2}{3}n_u - \frac{1}{3}n_d - \frac{1}{3}n_s - n_e = 0 \tag{5.38}$$

$$\mu_d = \mu_s = \mu_u + \mu_e \ . \tag{5.39}$$

Unfortunately, the parameters entering the bag model EOS are only loosely constrained by phenomenology and their choice is somewhat arbitrary.

As quarks are confined and not observable as individual particles, their masses are not directly measurable and must be inferred from hadron properties. The Particle Data Group reports masses of a few MeV for up and down quarks and 60 to 170 MeV for the strange quark. At typical neutron stars densities heavier quarks do not play a role.

The strong coupling constant α_s can be obtained from the renormalization group equation

$$\alpha_s = \frac{12\pi}{(33 - 2N_f)\ln(\overline{\mu}^2/\Lambda^2)} \ , \tag{5.40}$$

where $N_f = 3$ is the number of active flavors, Λ is the QCD scale parameter and $\overline{\mu}$ is an energy scale typical of the relevant density region (e.g. the average quark chemical potential). Using $\Lambda \sim 100 \div 200$ MeV and setting $\overline{\mu} = \mu_d \sim \mu_u$ at a typical baryon density $n_B \sim 4n_0$ one gets $\alpha_s \sim 0.4 \div 0.6$.

The values of the bag constant resulting from fits of the hadron spectrum range between ~ 57 MeV/fm^3, with $\Lambda = 220$ MeV, and ~ 350 MeV/fm^3 , with $\Lambda = 172$ MeV. However, the requirement that the deconfinement transition does not occur at density $\sim n_0$ constrains B to be larger than $\sim 120 - 150$ MeV/fm^3, and lattice results suggest a value of ~ 210 MeV/fm^3.

Figure 5.1 shows the energy density of neutral quark matter in weak equilibrium as a function of baryon density, for different values of B and α_s. Comparison between the dotdash line and those corresponding to $\alpha_s \neq 0$ shows that perturbative gluon exchange, whose inclusion produces a sizable change of slope, cannot be simulated by adjusting the value of the bag constant and must be explicitly taken into account.

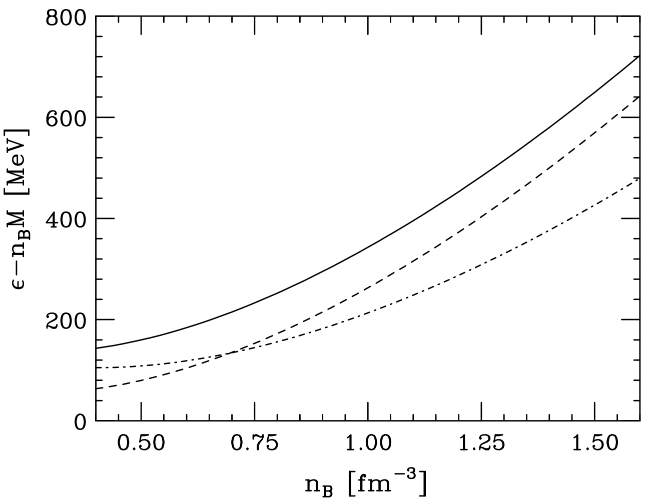

Figure 5.1: Energy density of neutral quark matter in weak equilibrium as a function of baryon number density. The solid and dashed lines have been obtained setting $\alpha_s = 0.5$ and $B = 200$ and 120 MeV/fm^3, respectively, while the dashdot line corresponds to $\alpha_s = 0$ and $B = 200$ MeV/fm^3. The quark masses are $m_u = m_d = 0$, $m_s = 150$ MeV.

The composition of charge neutral quark matter in weak equilibrium obtained from the MIT bag model is shown in Fig. 5.2. Note that at large densities quarks of the three different flavors are present in equal number, and leptons are no longer needed to guarantee charge neutrality.

5.2.3 Color superconductivity

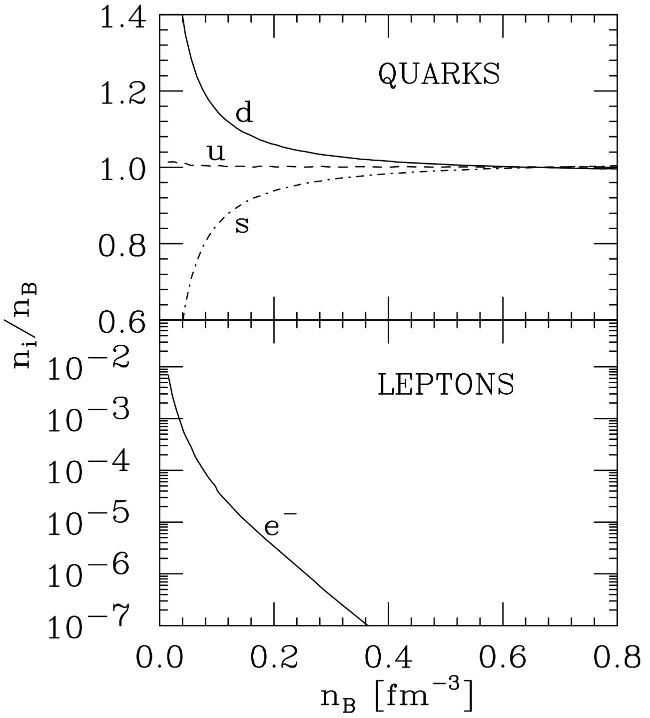

Figure 5.2: Composition of charge neutral matter of u, d and s quarks and electrons in weak equilibrium, obtained from the MIT bag model setting $m_u = m_d = 0$, $m_s = 150$ MeV, $B = 200$ MeV/fm^3 and $\alpha_s = 0.5$.

Chapter 6

Phase transitions in neutron stars

At large baryon number density, the energy density of nucleon matter predicted by theoretical calculations, carried out within either NMBT or RMFT, grows according to $\epsilon_{NM} \propto n^2$. On the ohter hand, the energy density of quark matter grows according to $\epsilon_{NM} \propto n^{4/3}$. Hence, at large enough density quark matter is expected to become the ground state of matter. If the density $\bar{n}_B$ corresponding to $\epsilon_{NM}(\bar{n}_B) = \epsilon_{QM}(\bar{n}_B)$ is reached in the inner core, the neutron star contains deconfined quark matter.

Early studies of the appearance of quark matter in neutron stars were based on the familiar Maxwell double tangent construction, which amounts to assuming that the transition occurs at constant pressure. Within this picture, charge-neutral nuclear matter at energy density ϵ_{NM} coexists with charge-neutral quark matter at energy density ϵ_{QM}, the two phases being separated by a sharp interface.

In the early 90s Glendenning first pointed out that the requirement that the two phases be individually charge-neutral is in fact too restrictive. In a more general scenario charged nuclear and quark matter may share a common lepton background, thus giving rise to a mixed phase extending in space over a sizable fraction of the star.

The two different descriptions of the phase transitions and their implications for neutron star structure are discussed in the following Sections.

6.1 Coexisting phases *vs* mixed phase

Equilibrium between charged phases of nuclear matter and quark matter at $T = 0$ requires the fulfillment of Gibbs conditions

$$P_{NM}(\mu^B_{NM}, \mu^Q_{NM}) = P_{QM}(\mu^B_{QM}, \mu^Q_{QM}) \ , \tag{6.1}$$

$$\mu^B_{NM} = \mu^B_{QM} \quad , \quad \mu^Q_{NM} = \mu^Q_{QM} \ , \tag{6.2}$$

where P denotes the pressure, while μ^B and μ^Q are the chemical potentials associated with the two conserved quantities, namely baryonic number B and electric charge Q.

The above equations imply that, for any pressure $\bar{P}$, the projection of the surfaces $P_{NM}(\mu^B, \mu^Q)$ and $P_{QM}(\mu^B, \mu^Q)$ onto the $P = \bar{P}$ plane defines two curves, whose intersection corresponds to the equilibrium values of the chemical potentials. As the chemical potentials determine the charge densities of the two phases, the volume fraction occupied by quark matter, χ, can then be obtained exploiting the requirement of *global* neutrality

$$\chi Q_{QM} + (1-\chi)Q_{NM} + \sum_\ell Q_\ell = 0 \ , \tag{6.3}$$

where Q_{QM}, Q_{NM} and Q_ℓ denote the electric charge carried by nuclear matter, quark matter and leptons, respectively. From Eq.(6.3) it follows that

$$\chi = \frac{Q_{NM} + \sum_\ell Q_\ell}{Q_{NM} - Q_{QM}} \ , \tag{6.4}$$

with $0 \leq \chi \leq 1$. Finally, the total energy density ϵ can be calculated using

$$\epsilon = \chi \epsilon_{QM} + (1-\chi)\epsilon_{NM} \ , \tag{6.5}$$

and the EOS of state of the mixed phase can be cast in the standard form $P = P(\epsilon)$.

Requiring that the two phases be individually neutral, as in the pioneering work of Baym & Chin, reduces the number of chemical potentials to one, thus leading to the equilibrium conditions

$$P_{NM}(\mu^B_{NM}) = P_{QM}(\mu^B_{QM}) \ , \tag{6.6}$$

$$\mu^B_{NM} = \mu^B_{QM} \ . \tag{6.7}$$

Within this scenario, charge-neutral nuclear matter at baryon number density n_B^{NM} coexists with charge-neutral quark matter at density n_B^{QM}, n_B^{NM} and n_B^{QM} being determined by the requirements

$$\mu_B = \left(\frac{\partial \epsilon_{NM}}{\partial n_B}\right)_{n_B = n_B^{NM}} = \left(\frac{\partial \epsilon_{QM}}{\partial n_B}\right)_{n_B = n_B^{QM}} \ . \tag{6.8}$$

At $n_B^{NM} < n_B < n_B^{QM}$ pressure and chemical potential remain constant, the energy density is given by

$$\epsilon = \mu_B n_B - P \ , \tag{6.9}$$

and the volume fraction occupied by quark matter grows linearly with density according to

$$\chi = \frac{\mu_B n_B - P - \epsilon_{NM}(n_{NM}^B)}{\epsilon_{QM}(n_B^{QM}) - \epsilon_{NM}(n_B^{NM})}. \tag{6.10}$$

Note that the above equation obviously implies that $0 \leq \chi \leq 1$, with $\chi(n_B^{NM}) = 0$ and $\chi(n_B^{QM}) = 1$.

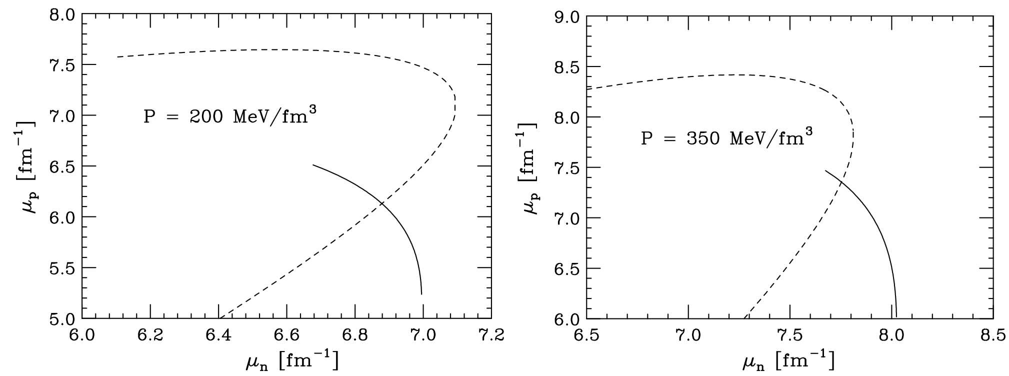

Figure 6.1: Isobars $P(\mu_n, \mu_p) = 200$ MeV/fm^3 (left panel) and 350 MeV/fm^3 (right panel) obtained using NMBT (solid lines) and the MIT bag model of quark matter, with $\alpha_s = 0.5$ and $B = 200$ MeV/fm^3 (dashed lines). The intersections determine the values of the chemical potentials corresponding to equilibrium of the two phases according to Gibbs rules.

The intersection between the surfaces describing the pressure of nuclear and quark matter is determined numerically, choosing as independent variables, instead of μ^B and μ^Q, the proton and neutron chemical potentials μ_p and μ_n. In nuclear matter they are simply related to the lepton chemical potential through the β-stability condition $\mu_n - \mu_p = \mu_\ell$. In quark matter the chemical potentials of up and down quarks can be obtained from μ_p and μ_n, inverting the relations

$$\mu_p = 2\mu_u + \mu_d \tag{6.11}$$

$$\mu_n = 2\mu_d + \mu_u \ , \tag{6.12}$$

while the strange quark and lepton chemical potentials are dictated by the conditions of weak equilibrium

$$\mu_s = \mu_d \ , \tag{6.13}$$

$$\mu_d - \mu_u = \mu_\ell \ . \tag{6.14}$$

Figure 6.1 illustrates the construction employed to determine the values of μ_p and μ_n corresponding to equilibrium between nuclear matter, described by NMBT, and quark matter, described by by the MIT bag model EOS with $\alpha_s = 0.5$ and $B = 200$ MeV/fm^3. The region $P_{min} < P < P_{max}$ in which the isobars of nuclear and quark matter intersect defines the range of densities $n_{min} < n_B < n_{max}$ in which the mixed phase is energetically favored. At $n_B < n_{min}$ and $n_B > n_{max}$ the ground state consists of pure nuclear and quark matter, respectively.

The phase transition between nuclear and quark matter, obtained with B = 200 MeV/fm^3 and $\alpha_s = 0.5$, is illustrated in Fig. 6.2. Dashed and dotdash lines show the dependence on n_B of the energy density of charge neutral nuclear and quark matter in weak equilibrium, respectively, while the solid line corresponds to the mixed phase. The latter turns out to be the ground state of neutron star matter at densities $.7 \lesssim n_B \lesssim 1.7$ fm^{-3}.

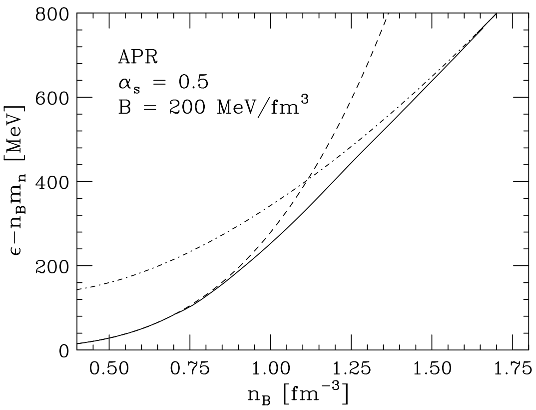

Figure 6.2: Dashed and dotdash lines show the energy density of charge neutral nuclear and quark matter in weak equilibrium, respectively. The bag model parameters have been set to B = 200 MeV/fm^3 and $\alpha_s = 0.5$. The solid line corresponds to the mixed phase, obtained from Gibbs equilibrium conditions.

The dependence of the results on the MIT bag model parameters can be gauged from the left panel of Fig. 6.3. A lower value of the bag constant, corresponding to a softer quark matter EOS, leads to the appearance of the mixed phase at lower density. Keeping $\alpha_s = 0.5$ and setting B = 120 MeV/fm^3 one finds that the mixed phase is energetically favored in the range $.6 \lesssim n_B \lesssim 1.4$ fm$^-3$. An even larger effect, illustrated by the right panel of Fig. 6.3 is obtained with B = 120 MeV/fm^3 and $\alpha_s = 0$, i.e. neglecting perturbative gluon exchange altogether. For this case the figure also shows the results obtained from the Maxwell construction, leading to the coexistence of charge-neutral nuclear matter at $n_B = .42$ fm^{-3} and charge-neutral quark matter at $n_B = .57$ fm^{-3}. This cohexistence region is to be compared to the region of stability of the mixed phase, corresponding to $0.22 \lesssim n_B \lesssim 0.75$ fm^{-3}.

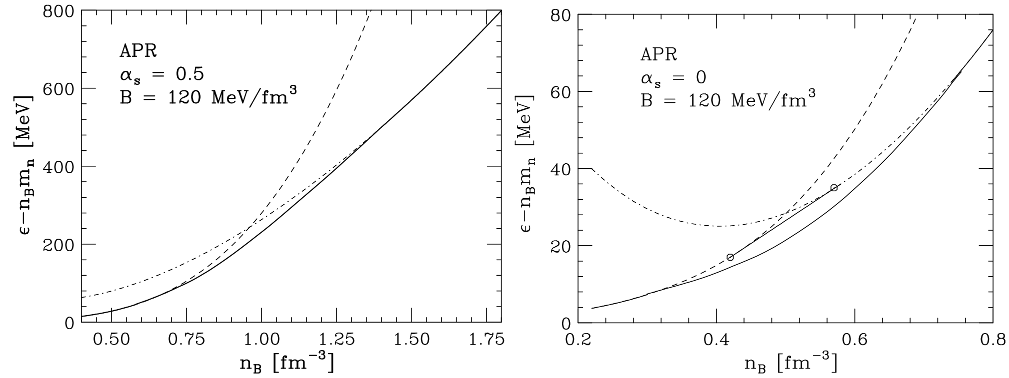

Figure 6.3: As in Fig. 6.2, but with the EOS of quark matter obtained using different values of the MIT bag model parameters. Left panel: B = 120 MeV/fm^3 and $\alpha_s = 0.5$; right panel B = 120 MeV/fm^3 and $\alpha_s = 0$. The straight line in the lower panel is the double tangent resulting from the Maxwell construction, while the open circles show the extrema of the coexistence region.

6.2 Stability of the mixed phase

The discussion of the previous Section suggests that, irrespective of the details of the EOS, the transition from nuclear to quark matter proceed through the formation of a mixed phase. However, two issues relevant to both the appearance and the stability of the mixed phase, not taken yet into account, need to be further analyzed.

Consider a mixed phase consisting of droplets of quark matter immersed in β-stable nuclear matter, global charge neutrality being guaranteed by a lepton background. This picture is obvioulsy based on the assumption that the appearance of the charged droplets do not significantly affect the space distribution of the leptons, i.e. that the Debye screening length λ_D is large compared to both the typical size of the droplets and their separation distance. If this condition is not satisfied the lepton background is distorted in such a way as to screen electrostastic interactions.

Estimates of λ_D reported by in the literature suggest that screening effects can be disregarded if the structures appearing in the mixed phase of quark and nuclear matters have typical size and separation distance of ~ 10 fm. The results of calculations, that will be discussed discussed later in this Section, show that this appears indeed to be the case.

The second issue deserving consideration is the stability of the mixed phase, i.e. the question of whether or not its energy is lower than the energy of the coexisting phases of nuclear and quark matter.

Formation of a spherical droplet of quark matter requires the energy

$$\mathcal{E}_D = \mathcal{E}_C + \mathcal{E}_S \ . \tag{6.15}$$

where the surface contribution $\mathcal{E}_S$ is parametrized in terms of the surface tension σ according to

$$\mathcal{E}_S = \sigma \ 4\pi R^2 \ , \tag{6.16}$$

R being the droplet radius. The electrostatic energy $\mathcal{E}_C$ can be cast in the form

$$\mathcal{E}_C = \frac{3}{5}\frac{Q^2}{R}\left(1 - \frac{3}{2}u^{1/3} + \frac{1}{2}u\right) \ , \tag{6.17}$$

with $u = (R/R_c)^3$, R_c being the radius of the Wigner-Seitz cell. Note that the first term on the right hand side of the above equation is the self energy of a droplet of radius R and charge Q obtained from Gauss law. The electric charge Q is given by

$$Q = \frac{4\pi R^3}{3} \left(\rho_{QM} - \rho_{NM}\right) \ , \tag{6.18}$$

ρ_{QM} and ρ_{NM} being the charge densities of quark matter and nuclear matter, respectively. Minimization of the energy density $\epsilon = 3\mathcal{E}_D/4\pi R_c^3$ with respect to the droplet radius yields

$$\mathcal{E}_S = 2\mathcal{E}_C \tag{6.19}$$

and

$$R = \left[\frac{4\pi(\rho_{QM} - \rho_{NM})^2}{3\sigma} \ f_3(u)\right]^{-1/3} \ , \tag{6.20}$$

where

$$f_3(u) = \frac{1}{5}\left(2 - 3u^{1/3} + u\right) \ . \tag{6.21}$$

As the density increases, the droplets begin to merge and give rise to structures of variable dimensionality, changing firts from spheres into rods and eventually into slabs [1]. At larger densities the volume fraction occupied by quark matter exceeds 1/2, and the role of the two phases is reversed. Nuclear matter, initially arranged in slabs, turns into rods and spheres that finally dissolve in uniform charge-neutral quark matter.

[1] In the literature, the rods and slabs that form in the mixed phase are often referred to as *spaghetti* and *lasagna*, respectively, or as *nuclear pasta*.

The energy density needed for the formation of the structures appearing in the mixed phase has been obtained by Ravenhall et al. in the context of a study of matter in the neutron star inner crust. It can be written in the concise form

$$\epsilon_C + \epsilon_S = 6\pi u \left[\frac{\alpha}{4\pi} \sigma^2 d^2 \left(n_B^{NM} - n_B^{QM} \right)^2 f_d(u) \right] , \tag{6.22}$$

where α is the fine structure constant, u is the volume fraction occupied by the less abundant phase (i.e. $u = \chi$ for $\chi < 1/2$, $u = 1 - \chi$ for $\chi \geq 1/2$) and

$$f_d(u) = \frac{1}{d+2} \left[\frac{1}{d-2} \left(2 - d u^{1-2/d} \right) + u \right] . \tag{6.23}$$

For $d = 1, 2$ and 3 Eqs.(6.22) and (6.23) provide the correct energy density for the case of slabs, rods and spheres, respectively.

For $\sigma = 0$ both surface and Coulomb energies vanish, and the energy density of the mixed phase is given by Eq.(6.5), while for $\sigma \neq 0$

$$\epsilon(\sigma) = \epsilon(\sigma = 0) + \epsilon_C + \epsilon_S . \tag{6.24}$$

The mixed phase is energetically favorable if $\epsilon(\sigma)$ is less than the energy density obtained from the Maxwell construction, given by Eq.(6.9).

The value of the surface tension at the interface between nuclear and quark matter is not known. It has been estimated using the MIT bag model and ignoring gluon exchange. Assuming that a strange quark has mass of ~ 150 MeV, Berger & Jaffe predict $\sigma \sim 10$ MeV/fm^2. To quantitatively investigate the stability of the mixed phase, $\Delta_\epsilon = \epsilon(\sigma) - \epsilon(0)$ has been calculated for different values of σ, ranging from 2 MeV/fm^2 to 10 MeV/fm^2.

For any given value of the baryon number density n_B, the energy density of Eqs.(6.22)-(6.23) has been calculated using the nuclear and quark matter densities determined according to the procedure described in the previous Section and carrying out a numerical minimization with respect to the value of the dimensionality parameter d. As n_B increases, the resulting values of d change initially from ~ 3 to ~ 2 and ~ 1 and then again to ~ 2 and finally to ~ 3. For example, in the case illustrated by Fig. 6.4, and corresponding to $\sigma = 10$ MeV/fm^2, spherical droplets of quark matter ($d \sim 3$) appear at $n_B \sim .75$ fm^{-3} and turn into rods ($d \sim 2$) and slabs ($d \sim 1$) at $n_B \sim .95$ and ~ 1.2 fm^{-3}, respectively. For larger densities, quark matter becomes the dominant phase (i.e. $\chi > 1/2$): at $n_B \sim 1.5$ and ~ 1.7 fm^{-3} the mixed phase features rods ($d \sim 2$) and droplets ($d \sim 3$) of nuclear matter that eventually dissolve in the quark matter background.

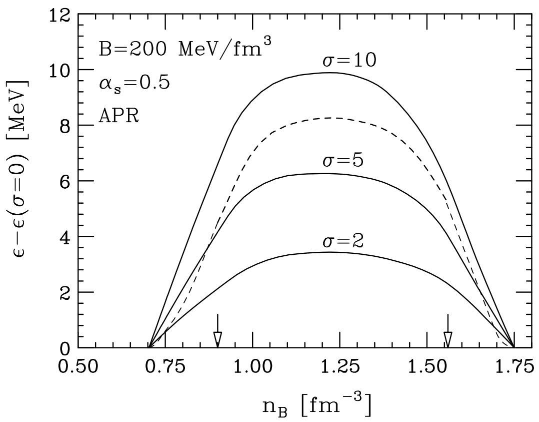

Figure 6.4: The solid lines correspond to the difference $\Delta_\epsilon = \epsilon(\sigma) - \epsilon(0)$ (see Eq.(6.24)), evaluated for $\sigma = 10$, 5 and 2 MeV/fm^3. The dashed line shows the difference $\widetilde{\Delta}$ between the energy density resulting from the Maxwell construction and $\epsilon(0)$. The arrows mark the limits of the cohexistence region. Nuclear and quark matter are described by the NMBT and the MIT bag model EOS, with $\alpha_s = 0.5$ and $B = 200$ MeV/fm^3, respectively.

These results are summarized in Figs. 6.4 and 6.5, that correspond to different choices of the MIT bag model parameters. The solid lines show the n_B dependence of the calculated Δ_ϵ for different values of the surface tension σ. The dashed line represents the difference $\widetilde{\Delta}_\epsilon = \epsilon_M - \epsilon(0)$, where ϵ_M is the energy density obtained from Maxwell construction. For any given value of the surface tension, the mixed phase is favorable if the corresponding solid line lies below the dashed line.

The results of Fig. 6.4, corresponding to $B = 200$ MeV/fm^3 and $\alpha_s = 0.5$, show that the mixed phase, while being always the lowest energy phase for $\sigma = 2$ MeV/fm^2, becomes energetically unfavorable at some densities for $\sigma \gtrsim 5$ MeV/fm^2. For $\sigma = 10$ MeV/fm^2 coexistence of charge neutral phases of nuclear and quark matter turns out to be favorable over the whole density range.

To gauge the dependence upon the MIT bag model parameters we have repeated the calculations setting $B = 120$ MeV/fm^3 and $\alpha_s = 0$. The results of Fig. 6.5 show that for σ in the range $2 - 5$ MeV/fm^2 the mixed phase is energetically favorable over a density region larger than the coexistence region predicted by the Maxwell construction.

Finally, we return to the problem of the comparison between the Debye screening length and the typical size of the structures appearing in the mixed phase. The results of theoretical calculations suggest that the conditions outlined in the work of Heiselberg et al. are indeed fulfilled. For example,

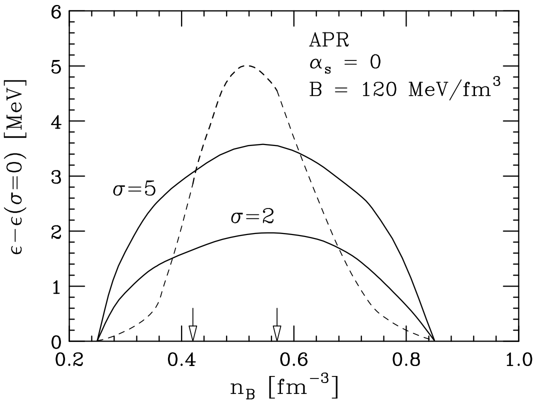

Figure 6.5: Same as in Fig. 6.4, but with $\alpha_s = 0$ and $B = 120$ MeV/fm^3. The solid lines show to the difference $\Delta_\epsilon = \epsilon(\sigma) - \epsilon(0)$ (see Eq.(6.24)), evaluated for $\sigma = 5$ and 2 MeV/fm^3, respectively.

in the case $B = 200$ MeV/fm^3 and $\alpha_s = 0.5$, in the region of $\chi \ll 1$, corresponding to formation of droplets of quark matter, the droplets radius given by Eq. (6.20) is $\sim 2 - 3$ fm.

6.3 Implications for neutron star structure

Plugging the EOS $P = P(\epsilon)$ into the Tolman Oppenheimer Volkoff (TOV) equations

$$\frac{dP(r)}{dr} = -G \; \frac{[\epsilon(r) + P(r)]\,[M(r) + 4\pi r^2 P(r)]}{r^2\,[1 - 2GM(r)/r]} \ , \tag{6.25}$$

where G denotes the gravitational constant, and

$$M(r) = 4\pi \int_0^r r'^2 dr' \epsilon(r') \ , \tag{6.26}$$

one can obtain the properties of the stable configurations of a nonrotating neutron star. Eqs.(6.25) and (6.26) are solved by integrating outwards with the initial condition $\epsilon(r = 0) = \epsilon_c$. For any given value of the central density, ϵ_c, the star radius R is determined by the condition $P(R) = 0$ and its mass $M = M(R)$ is given by Eq.(6.26).

The occurrence of the transition to quark matter makes the EOS softer, thus leading to a lower value of the maximum mass. In Fig. 6.6 the mass-central energy density relations obtained using the NMBT nuclear matter EOS only is compared to that obtained allowing for a transition to quark matter with $\alpha_s = 0.5$ and $B = 120$ and 200 MeV/fm^3. The transition is described according to Gibbs conditions, neglecting surface and Coulomb effects. Calculations yield $M_{max} = 2.20\ M_\odot$ for the star made of nuclear matter only and $M_{max} = 1.89$ and 2.03 $M_\odot$ for the hybrid stars corresponding to $B = 120$ and 200 MeV/fm^3, respectively.

In Fig. 6.6 the $M(\epsilon_c)$ curves obtained setting $B = 120$ MeV/fm^3 and $\alpha_s = 0$ and adopting either the Gibbs or Maxwell picture are also compared. Whether the phase transition proceeds through the appearance of a mixed phase or through coexistence of charge-neutral phases does not appear to significantly affect the mass-central energy density relation. On the other hand, neglecting perturbative gluon exchange results in a rather low maximum mass, $M_{max} \sim 1.4\ M_\odot$, barely compatible with the measured neutron star masses.

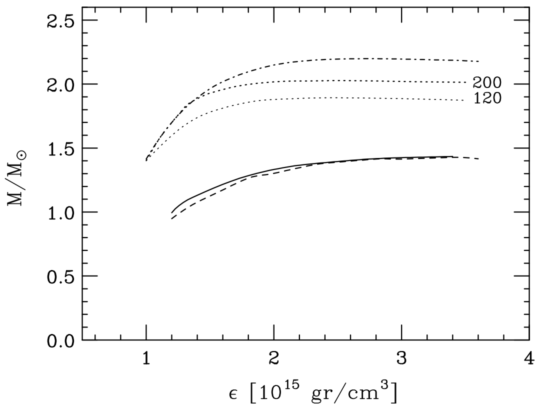

Figure 6.6: Relation between neutron star mass and central energy density for different EOS. Dotdash line: pure nuclear matter (NMBT); dotted lines: nuclear matter (NMBT) and quark matter (MIT bag model with $B = 120$ and 200 MeV/fm^3 and $\alpha_s = 0.5$). The phase transition is described according to Gibbs rules; solid line: same as the dotted line, but with $B = 120$ MeV/fm^3 and $\alpha_s = 0.5$; dashed line: same as the solid line, but with the phase transition described using Maxwell construction.

The neutron star mass-radius relations associated with the $M(\epsilon_c)$ curves of Fig. 6.6, displayed in Fig. 6.7, show that in this case using the Maxwell construction instead of Gibbs rules produces a visible effect. However, all EOS predict the existence of stable star configurations with masses in the range allowed by observation, as well as a $M(R)$ relation compatible with that resulting from the gravitational red shift measurement of Cottam et al..

Fig 6.8 shows that different descriptions of the phase transition lead to remarkably different star density profiles. While in the presence of the mixed

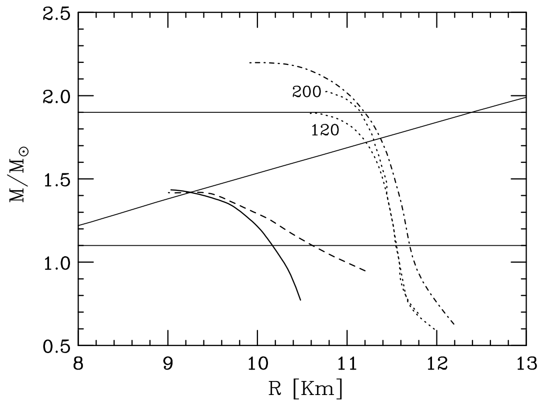

Figure 6.7: Mass radius relation for different EOS. The meaning of the curves is the same as in Fig. 6.6. The horizontal lines correspond to the observational limits on neutron star mass, whereas the third straight line is the mass-radius relation resulting from the gravitational redshift measurement of Cottam et al.

phase the density is a smooth function of the distance from the star center, the Maxwell construction leads to the appearance of a disontinuity. For comparison, the profile of a star of the same mass, $\sim 1.4\ M_\odot$, made of pure nuclear matter described by the NMBT EOS is also shown.

The discontinuous behavior can be easily understood noting that TOV equations (6.25) and (6.26) require that the pressure $P(r)$ be a monotonically decreasing function. It follows that if the pressure is the same for two different values of density, as in the phase transition in the Maxwell construction, they must necessarily correspond to the same value of r.

In the coexisting phases scenario, the transition only takes place in stars whose central density exceeds the density of the quark matter phase. These star configurations turn out to be marginally stable, their mass being close to the maximum mass. For example, setting $B = 200$ MeV/fm^3 and $\alpha_s = 0.5$ the transition only occurs in stars having mass $\sim 2.0 M_\odot$. The radius of the quark matter core is small (~ 1 Km), while the density jump is large, going from 1.8×10^{15} g/cm^3 to 3.9×10^{15} g/cm^3. These results are to be compared with those obtained in the mixed phase scenario when Coulomb and surface effects are neglected. In this case there is no jump and the density varies smoothly. At the center of a star of mass $\sim 2.0 M_\odot$, corresponding to energy-density $\sim 2.4 \times 10^{15}$ g/cm^3 the volume fraction occupied by quark matter reaches $\chi \sim 30$ %.

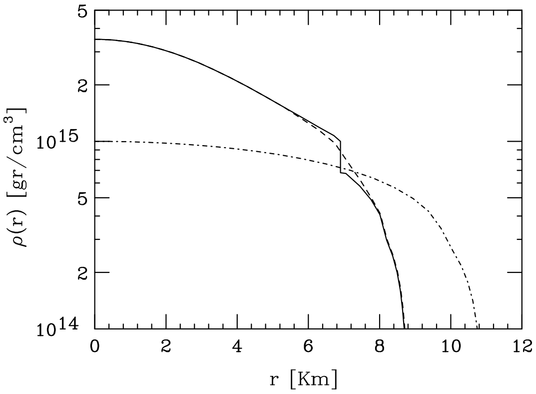

Figure 6.8: Density profiles of a neutron star of mass $\sim 1.4\ M_\odot$ resulting from different models. Dashed line: APR EOS and MIT bag model EOS with $\alpha_s = 0$ and $B = 120$ MeV/fm^3. Phase transition described allowing for the presence of the mixed phase. Solid line: same as the solid line, but with the phase transition described according to Maxwell construction. Dotdash line: pure nuclear matter with APR EOS.

Appendix A

Many-body perturbation theory

Let us consider N spin 1/2 particles whose dynamics is described by the hamiltonian

$$H = \sum_{i=1}^{N} K_i + \sum_{j>i=1}^{N} v_{ij} \ , \tag{A.1}$$

where K_i and v_{ij} are the kinetic energy operator and the interaction potential, respectively.

The above equation can be rewritten introducing a single particle potential U providing a reasonable independent particle model description of the system (for example the nuclear shell model). The new expression reads

$$H = H_0 + H_1 \tag{A.2}$$

with

$$H_0 = \sum_{i=1}^{N} (K_i + U_i) = \sum_{i=1}^{N} h_i \ , \tag{A.3}$$

and

$$H_1 = \sum_{j>i=1}^{N} v_{ij} - \sum_{i=1}^{N} U_i \ . \tag{A.4}$$

Let us define the matrix elements

$$\langle r|U|m\rangle = \int dx_1 \ \phi_r^\dagger(x_1) U_1 \phi_m(x_1) \tag{A.5}$$

$$\langle rs|v|mn\rangle = \int dx_1 dx_2 \ \phi_r^\dagger(x_1)\phi_s^\dagger(x_2) v_{12} \phi_m(x_1)\phi_n(x_2) \ , \tag{A.6}$$

where $x_i \equiv (\mathbf{r}_1, \boldsymbol{\sigma}_i)$, the integration includes the sum over the spins and the ϕ_i's are solutions of the one-body Schrödinger equation

$$h|\phi_i\rangle = \epsilon_i|\phi_i\rangle \ . \tag{A.7}$$

We can rewrite the hamiltonian of Eq. (A.1) as an operator acting in the hilbert space whose state vectors are specified by the set of the occupation number of the eigenstates of h. Denoting $a_i^\dagger$ and a_i the fermion operators that create and annihilate a particle in the state i we find

$$H_0 = \sum_{rm} \langle r|h|m\rangle \; a_r^\dagger a_m = \sum_m \; \epsilon_m a_m^\dagger a_m \tag{A.8}$$

and

$$H_1 = \sum_{rsmn} \langle rs|v|mn\rangle \; a_r^\dagger a_s^\dagger a_n a_m - \sum_{rm} \langle r|U|m\rangle \; a_r^\dagger a_m \; . \tag{A.9}$$

Note the first sum in Eq. (A.8) includes all *distinct* matrix elements [1]

$$G_0 = a_{\mathbf{p}}^\dagger a_{\mathbf{p}} \tag{A.10}$$

[1]The matrix element $\langle rs|v|mn\rangle$ is distinct from $\langle rs|v|nm\rangle$ but *not* from $\langle sr|v|nm\rangle$

Appendix B

The one pion exchange potential

Let us consider the process depicted in Fig. 4.2. The corresponding S-matrix element reads

$$\begin{aligned} S_{fi} &= (-ig)^2 \frac{m^2}{(E_1 E_2 E_{1'} E_{2'})^{1/2}} (2\pi)^4 \delta^{(4)}(p_1 + p_2 - p_{1'} - p_{2'}) \\ &\times \eta_{1'}^{\dagger} \boldsymbol{\tau} \eta_1 \; \bar{u}_{1'} i\gamma_5 u_1 \frac{i}{k^2 - m_\pi^2} \eta_{2'}^{\dagger} \boldsymbol{\tau} \eta_2 \; \bar{u}_{2'} i\gamma_5 u_2 \end{aligned} \tag{B.1}$$

where m_π is the pion mass, $k = p_2 - p_{2'}$ and η_i denotes the two-component Pauli spinor describing the isospin state of particle i. Equation (B.1) can be rewritten in the form

$$\begin{aligned} S_{fi} &= ig^2 \frac{m^2}{(E_1 E_2 E_{1'} E_{2'})^{1/2}} (2\pi)^4 \delta^{(4)}(p_1 + p_2 - p_{1'} - p_{2'}) \\ &\times \langle \boldsymbol{\tau}_1 \cdot \boldsymbol{\tau}_2 \rangle \; \bar{u}_{2'} \gamma_5 u_2 \bar{u}_{1'} \gamma_5 u_1 \frac{1}{k^2 - m_\pi^2} \ , \end{aligned} \tag{B.2}$$

with $\langle \boldsymbol{\tau}_1 \cdot \boldsymbol{\tau}_2 \rangle = \eta_{2'}^{\dagger} \boldsymbol{\tau} \eta_2 \; \eta_{1'}^{\dagger} \boldsymbol{\tau} \eta_1$.

Substituting the nonrelativistic limit

$$\begin{aligned} \bar{u}_{2'} \gamma_5 u_2 &= \frac{(E_{2'} + m)^{1/2} (E_2 + m)^{1/2}}{2m} \left[\chi_{s'}^{\dagger} \frac{\boldsymbol{\sigma} \cdot \mathbf{p}_2}{E_2 + m} \chi_s - \chi_{s'}^{\dagger} \frac{\boldsymbol{\sigma} \cdot \mathbf{p}_{2'}}{E_{2'} + m} \chi_s \right] \\ &\approx \chi_{s'}^{\dagger} \frac{\boldsymbol{\sigma}(\mathbf{p}_2 - \mathbf{p}_{2'})}{2m} \chi_s = \chi_{s'}^{\dagger} \frac{(\boldsymbol{\sigma} \cdot \mathbf{k})}{2m} \chi_s \end{aligned} \tag{B.3}$$

and the similar expression for $\bar{u}_{1'} \gamma_5 u_1$ in the definition of S_{fi} and replacing (use $E_i \approx E_{i'} \approx m_\pi$ and $k^2 = (E_i - E_{i'})^2 - |\mathbf{k}|^2 \approx -|\mathbf{k}|^2$)

$$\frac{1}{k^2 - m_\pi^2} \approx -\frac{1}{|\mathbf{k}|^2 + m_\pi^2} \tag{B.4}$$

we obtain

$$S_{fi} \approx -i\frac{g^2}{4m^2}(2\pi)^4\delta^{(4)}(p_1+p_2-p_{1'}-p_{2'})\ \langle\boldsymbol{\tau}_1\cdot\boldsymbol{\tau}_2\rangle \times \chi^\dagger_{1'}\chi^\dagger_{2'}\frac{(\boldsymbol{\sigma}_1\cdot\mathbf{k})(\boldsymbol{\sigma}_2\cdot\mathbf{k})}{|\mathbf{k}|^2+m_\pi^2}\chi_2\chi_1 \tag{B.5}$$

The corresponding potential in momentum space is

$$\begin{aligned} v^\pi(\mathbf{k}) &= -\frac{g^2}{4m^2}\frac{(\boldsymbol{\sigma}_1\cdot\mathbf{k})(\boldsymbol{\sigma}_2\cdot\mathbf{k})}{\mathbf{k}^2+m_\pi^2}\ \boldsymbol{\tau}_1\cdot\boldsymbol{\tau}_2 \\ &= \left(\frac{f_\pi}{m_\pi}\right)^2\frac{(\boldsymbol{\sigma}_1\cdot\mathbf{k})(\boldsymbol{\sigma}_2\cdot\mathbf{k})}{\mathbf{k}^2+m_\pi^2}\ \boldsymbol{\tau}_1\cdot\boldsymbol{\tau}_2 \end{aligned} \tag{B.6}$$

with $g^2/4\pi = 14$ and

$$f_\pi^2 = g^2\frac{m_\pi^2}{4m^2} \approx 4\pi\times 14\frac{(140)^2}{4\times(939)^2} \approx 4\pi\times 0.08 \approx 1 \tag{B.7}$$

The configuration space $v^\pi(\mathbf{r})$ is obtained from the Fourier transform:

$$\begin{aligned} v^\pi(\mathbf{r}) &= -\frac{f_\pi^2}{m_\pi^2}\int\frac{d^3k}{(2\pi)^3}\ \boldsymbol{\tau}_1\cdot\boldsymbol{\tau}_2\ \boldsymbol{\sigma}_1\cdot\mathbf{k}\ \boldsymbol{\sigma}_2\cdot\mathbf{k}\ \frac{1}{(|\mathbf{k}|^2+m_\pi^2)}\ e^{-i\mathbf{k}\cdot\mathbf{r}} \\ &= \frac{f_\pi^2}{m_\pi^2}\ \boldsymbol{\tau}_1\cdot\boldsymbol{\tau}_2\ \boldsymbol{\sigma}_1\cdot\boldsymbol{\nabla}\ \boldsymbol{\sigma}_2\cdot\boldsymbol{\nabla}\int\frac{d^3k}{(2\pi)^3}\frac{1}{(|\mathbf{k}|^2+m_\pi^2)}e^{-i\mathbf{k}\cdot\mathbf{r}} \\ &= \frac{1}{4\pi}\ \frac{f_\pi^2}{m_\pi^2}\ \boldsymbol{\tau}_1\cdot\boldsymbol{\tau}_2\ \boldsymbol{\sigma}_1\cdot\boldsymbol{\nabla}\ \boldsymbol{\sigma}_2\cdot\boldsymbol{\nabla}\ \frac{e^{-m_\pi r}}{r}. \end{aligned} \tag{B.8}$$

The Laplacian of the Yukawa function,

$$y_\pi(r) = \frac{e^{-m_\pi r}}{r} = 4\pi\int\frac{d^3k}{(2\pi)^3}\frac{1}{(|\mathbf{k}|^2+m_\pi^2)}e^{i\mathbf{k}\cdot\mathbf{r}}, \tag{B.9}$$

involves a δ-function singularity at the origin, as can be easily seen from

$$(-\nabla^2+m_\pi^2)\ y_\pi(r) = 4\pi\delta(\mathbf{r})\ . \tag{B.10}$$

Gradients in Eq. (B.8) have to be evaluated taking this singularity into account. For this purpose it is convenient to rewrite

$$\begin{aligned} \boldsymbol{\sigma}_1\cdot\boldsymbol{\nabla}\ \boldsymbol{\sigma}_2\cdot\boldsymbol{\nabla}y_\pi(r) &= \left(\boldsymbol{\sigma}_1\cdot\boldsymbol{\nabla}\ \boldsymbol{\sigma}_2\cdot\boldsymbol{\nabla} - \frac{1}{3}\boldsymbol{\sigma}_1\cdot\boldsymbol{\sigma}_2\ \nabla^2\right)y_\pi(r) \\ &+ \frac{1}{3}\boldsymbol{\sigma}_1\cdot\boldsymbol{\sigma}_2\ \nabla^2\ y_\pi(r)\ , \end{aligned} \tag{B.11}$$

as the δ-function contribution to $\nabla^2 y_\pi(r)$ does not appear in the first term, yielding

$$\left(\boldsymbol{\sigma}_1\cdot\boldsymbol{\nabla}\boldsymbol{\sigma}_2\cdot\boldsymbol{\nabla}-\frac{1}{3}\,\boldsymbol{\sigma}_1\cdot\boldsymbol{\sigma}_2\nabla^2\right)y_\pi(r) \qquad \text{(B.12)}$$
$$=\left(\boldsymbol{\sigma}_1\cdot\hat{\mathbf{r}}\;\boldsymbol{\sigma}_2\cdot\hat{\mathbf{r}}-\frac{1}{3}\,\boldsymbol{\sigma}_1\cdot\boldsymbol{\sigma}_2\right)\left(m_\pi^2+\frac{3m_\pi}{r}+\frac{3}{r^2}\right)y_\pi(r),$$

where $\hat{\mathbf{r}}=\mathbf{r}/|\mathbf{r}|$. The laplacian $\nabla^2 y_\pi(r)$ in the second term of Eq. (B.11) can be replaced with $m_\pi^2 y_\pi(r)\;-\;4\pi\;\delta(r)$ using Eq. (B.10).

Carrying out the calculation of the derivatives in Eq. (B.8) in this way we find

$$\begin{aligned} v^\pi(\mathbf{r}) \;=\; & \frac{1}{3}\frac{1}{4\pi}\,f_\pi^2\;m_\pi\;\boldsymbol{\tau}_1\cdot\boldsymbol{\tau}_2\;\Big[\,T_\pi(r)S_{12} \\ & +\left(Y_\pi(r)-\frac{4\pi}{m_\pi^3}\delta(\mathbf{r})\right)\boldsymbol{\sigma}_1\cdot\boldsymbol{\sigma}_2\Big]\;, \end{aligned} \qquad \text{(B.13)}$$

with

$$Y_\pi(r)=\frac{e^{-m_\pi r}}{m_\pi r}\;, \qquad \text{(B.14)}$$

and

$$T_\pi(r)=\left(1+\frac{3}{m_\pi r}+\frac{3}{m_\pi^2 r^2}\right)Y_\pi(r)\;, \qquad \text{(B.15)}$$

i.e. Eqs. (4.30) and (4.31).

Appendix C

The one gluon exchange

Let us consider